The Development of Spiral Structure in a Galaxy Approached by Numerical Computations

BY

PER OLOF LINDBLAD

Contents

Abstract

The behaviour of numerical mass-point models of ring shaped configurations in the central layer of a galaxy is integrated with an electronic computer. Initial deviations from rotational symmetry are realized in two different ways:

1. A slightly elongated massive ring, the apsidal line of which proceeds with the angular velocity of the apsidal line of a dispersion orbit, is introduced. This ring, that we call a dispersion ring, will have a considerable degree of stability (Chapter II), dispersion of matter being mainly along the ring. Its disturbing influence on circular motions in a surrounding, not very massive central layer is treated in Chapter III and summarized in Fig. 18. It is suggested that the action from a potential wave of this kind is responsible for the extended outer rings common in spiral galaxies of early type. The interactions between a dispersion ring and outer massive rings are discussed in Chapter IV. They first result in the development of a tightly wound spiral structure with leading arms that, at a later stage, tend to shift over into trailing ones.

2. In the second case a circular ring is given a bisymmetrical density variation along its circumference which proceeds with approximately the angular velocity of circular motion. This density wave is intimately related to the structure of a "bar" in the system. This case is treated in Chapter V. A central layer of circular motions proves to be unstable for a rather small initial amplitude of the density varia-

tion, and breaks up under the formation of a spiral pattern. The developments of the most important models are shown in Figs. 30–32. Also, in this case, the spiral arms come into being as leading ones, and a bar grows out of the initial density wave. The arms are drawn into the ends of the bar and generally, at a later stage, tend to change over into trailing ones.

In all figures illustrating the computations, the direction of rotation is clockwise. The time counted from the start of the computations is given in millions of years for each configuration.

I. The galactic model

Introduction

The theoretical foundations of the present work are the investigations of the dynamics of a flattened galactic subsystem by B. LINDBLAD *et al.* during the last decade. These investigations have proceeded along two different lines.

The earlier approach is exposed in works by LINDBLAD, R. COUTREZ and R. G. LANGEBARTEL on the existence of density waves or waves of deformation in a quasi-spheroidal stellar system. A summarizing representation of this theory is given by LINDBLAD and LANGEBARTEL (1953). It is shown that in a region of a flattened subsystem, where the variation of angular rotation with the distance from the centre is slow, a certain series of density waves is possible. The angular velocities of the waves are close to the velocities of circular motion in the same region. The most important one in this series is a bisymmetrical wave with two maxima of density along a certain diameter in the system, and two minima along the diameter at right angles to this. The wave is unstable for a ratio of less than $\frac{1}{5}$ between the minor and major axes of the spheroid. This wave is of fundamental importance in the theory of barred spirals.

Along the second line of approach LINDBLAD introduces the conception of "dispersion orbits" as the orbits of particles that, in a certain rotating coordinate system, follow the configurations along which dissolving clouds or associations are drawn out by differential rotation (see Chapter II).

E. HUBBLE (1940) and G. RANDERS (1940) have emphasized the importance of the occurrence of ring structures for the development of a spiral structure. RANDERS showed that viscous forces in the matter in the galactic plane will cause a redistribution of this matter into circular rings placed in the regions where the circular angular velocity $\omega(R)$ has maximum. He supposed that such a ring structure would break down under the formation of a spiral pattern.

LINDBLAD assumes rather that fairly massive elliptical rings of interstellar gas may be formed in regions where the angular velocities of the apsidal lines of the dispersion orbits attain maximum or minimum. LINDBLAD (1958b) proves the possible existence of sectorial harmonic waves of deformation in the very flattened central layer of a galaxy under certain restrictions in the central force field that seem to be fulfilled in the Galaxy. The wave proceeds with the angular velocity of the apsidal lines of the dispersion orbits. This wave

may be generated by a statistical combination and conglomeration of dispersion orbits, and it proves that the massive elliptical rings mentioned will be able to carry such a wave by their self-gravitational action. (For a summary of these considerations see LINDBLAD, 1959, p. 88.)

It appears that a massive ring can also maintain the density wave that proceeds with approximately circular angular velocity, and thus there is a connection here with the earlier theory of the barred spirals.

The aim of the present work is to test and follow up numerically the theoretical considerations, and the discussion is based most directly on the paper by LINDBLAD (1958b). By numerical computations of the motions in suitable galactic models, the behaviour of massive ring structures carrying the different types of waves and their gravitational influence on the development of the central layer will be investigated. The work by the Leiden astronomers on the 21-cm hydrogen line makes it possible to construct a model that rests to some extent on an observational basis and shares certain fundamental properties with the Galaxy. The basic principles of construction of the models are determined by the immediate object of the computations and by the computer available.

The computer

The electronic computer BESK was constructed and is run by the Swedish Board for Computing Machinery. It has been in operation since the end of 1953. BESK is a parallel-machine, and both programs and numerical data are stored in its memory and handled in the operations as binary numbers. A number consists of 40 binary digits (whole word) which corresponds to about 12 decimal digits. A whole word may also hold two instructions of the program. The memory consists of a ferrite-core memory with a capacity of 1024 whole words, to which the computing element has immediate access, and two magnetic drums of 8192 whole words altogether, from which blocks of data or instructions may be transferred to the ferrite-core memory or vice versa at a speed of about 1 msec per whole word. The operation time for an addition is 41 μsec. For multiplication the operation time is 266 μsec and for division 512 μsec.

The input in the machine is done with punched tape via a dielectric reader which reads 400 characters a second, where one character is 4 binary or one decimal digit. The output is done via a high speed punch which punches 145 characters a second on paper tape.

Since 1959 the machine has a "built-in" fluid binary point. However, all calculations in the present work were carried out with fixed binary point.

Some of the later computations were carried out on the new machine FACIT EDB installed in the summer of 1959. The main difference between this machine and BESK in their present states is the greater capacity of the new machine. Its ferrite-core memory is twice as large, and it has a magnetic tape memory with two tape stations (shortly to be increased to five) each holding 8192 blocks of 64 whole words. FACIT EDB has as yet no built-in fluid binary point.

Choice of model

As the most suitable model for the present investigation a mass-point model is chosen where the configurations, whose behaviour is to be studied, are represented by a number of gravitating particles of equal mass moving in a central field of force $F(R)$. As in the present work we shall limit our investigation to the central layer of the galaxy, all particles are brought to move strictly in the principal plane, and the whole problem is treated as two-dimensional. The field of force $F(R)$ then represents the force in the galactic plane exerted by the main bulk of the mass of the system that will be supposed to remain in an unperturbed, stationary condition with axial symmetry. This main bulk of the mass may be considered mainly to represent the population II and the disk population. In the Galaxy these two populations together hold about 90 % of the mass, have a smooth density distribution with strong concentration towards the centre and show a moderate flattening (J. H. Oort, 1958, Table 2).

A practical limit to the number of free mass-points is set, not by the limited storage-capacity of the computer but by the necessity of keeping the computing time within reasonable bounds. The number must be taken sufficiently large to give a fairly continuous representation of the configurations studied. Nevertheless, owing to the long computing times, the number had to be restricted in the present computations to such a degree that the individual masses would be of the order of $10^7 M_\odot$ to give large enough masses to the configurations deviating from rotational symmetry. Thus the particles do not represent single stars, but fairly large clouds of stars, dust, and gas. In the case of a close encounter between such mass points the Newtonian force of attraction has to be replaced by some other force function, or the forces will grow beyond all limits. Considering the cloud-character of the particles it is thought not unreasonable to surround the mass-points by circles with certain radii Δ_{min}, inside which the force of attraction increases proportionally to the mutual distance Δ between the points, and with such a rate that for $\Delta = \Delta_{min}$ the force is equal to the Newtonian gravitational force. A fairly large value of Δ_{min} will enhance the continuity of mass-distribution along the configurations, and will reduce the rate of increase of the velocity dispersion due to close encounters between clouds.

As a suitable, consistent representation of the force in the principal plane the force given by the model of the distribution of mass in the Galactic System, deduced by M. Schmidt (1956), has been adopted. Schmidt's final model consists of four non-homogeneous and nine homogeneous spheroids. A distance $R_\odot = 8.2$ kpc from the Sun to the galactic centre is assumed, and the density law of the non-homogeneous spheroids and the parameters of the homogeneous ones are chosen so as to reproduce the constants $A = +19.5$ km/sec·kpc and $B = -6.9$ km/sec·kpc of differential galactic rotation, the mass density $0.093\ M_\odot/pc^3$ in the solar neighbourhood, and the run of the force in the galactic plane for 0.84 kpc $\leqslant R \leqslant 8.2$ kpc as deduced from 21-cm observations of hydrogen velocities by K. K. Kwee, C. A. Muller, and G. Westerhout (1954). The manner of constructing the model implies that gravitation alone is responsible for this force. The total mass of the model is $7.02 \cdot 10^{10}\ M_\odot$.

TABLE 1.

R kpc	F 100 km²/sec² kpc	R kpc	F 100 km²/sec² kpc	R kpc	F 100 km²/sec² kpc	R kpc	F 100 km²/sec² kpc
0.0	0	5.5	89.4	11	30.8	22	6.5
0.5	215	6.0	84.0	12	25.2	24	5.4
1.0	207	6.5	78.7	13	20.8	25	5.0
1.5	175.3	7.0	72.7	14	17.4	26	4.6
2.0	155.5	7.5	66.2	15	14.9	28	3.9
2.5	141.0	8.0	59.5	16	12.9	30	3.4
3.0	129.6	8.5	52.9	17	11.3	32	3.0
3.5	119.2	9.0	46.9	18	10.0	35	2.5
4.0	110.3	9.5	41.9	19	8.9	40	1.9
4.5	102.6	10.0	37.6	20	8.0	45	1.5
5.0	95.6	10.5	34.0	21	7.2		

The reduction of the 21-cm observations involves the assumption of circular velocities, an assumption that is not exactly correct. However, deviations may not have a large influence on the deduced $F(R)$. The picture of the hydrogen arms as dispersion orbits proposed by B. LINDBLAD (1958a) would give an increase of $F(R)$ of about 4 per cent. The value of the assumed mass density near the Sun is somewhat smaller than the recent figure 0.15 $M_\odot$/pc³ given by OORT (1960). Some further doubt as to the correctness of the fundamental constants on which the model is founded, is caused by the necessity to introduce a large class of unknown objects with a steep density gradient near the Sun. SCHMIDT (1958) estimates that the values $A = 15$ km/sec·kpc, $B = -10$ km/sec·kpc and $R_\odot = 10$ kpc would obviate this drawback. However, the exact form of $F(R)$ is not crucial for the present problem, as the aim is not to reproduce the Galaxy but rather conditions prevailing in a typical spiral system. A slight revision of this force will not change the main results of the computations.

The force $F(R)$ as used in the present work is deduced by differentiation of SCHMIDT's Table 10 and is given in Table 1 and Fig. 1. Table 1 is stored in the machine, and $F(R)$ is interpolated to the second order by the computer. For $R \geqslant 40$ kpc the force is given by

$$F(R) = \frac{3012}{R^2} \quad (100 \text{ km}^2/\text{sec}^2 \cdot \text{kpc})$$

in accordance with SCHMIDT. The mass-points to be added will, of course, slightly modify this force. Finally, Table 1 stored in the machine may easily be changed into any other function that can suitably be interpolated between the same arguments, and the table has actually been thus modified in some computations.

No attempts to apply magneto-hydrodynamic forces have been made in the present work. Some experiments have been made to account for gas-dynamical friction by letting particles at close encounters share their velocities in a special way, but the results were not very satisfactory. Magneto-hydrodynamic forces have been introduced in a special case,
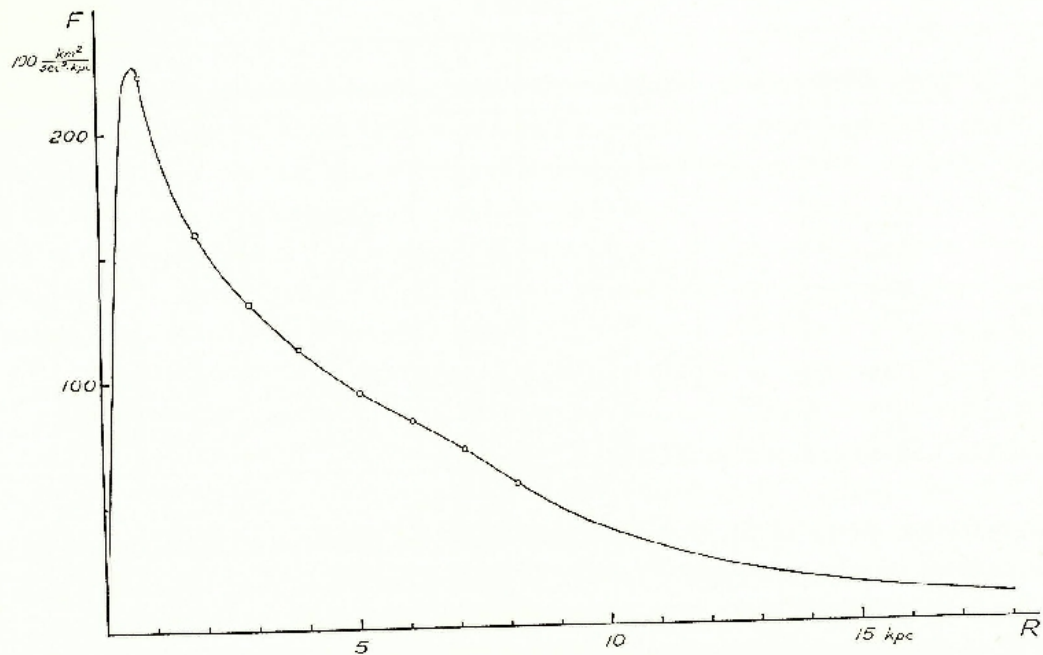
Fig. 1. The force F in the galactic plane as a function of the distance R from the centre according to the Schmidt model. Open circles refer to observations of the 21-cm line (SCHMIDT, 1956, Table 1).

according to ideas developed by AINA ELVIUS, in a recent paper by AINA ELVIUS and P. O. LINDBLAD (1959) where computations were made with the programs of the present work.

A different possibility to that of the mass-point model would be to use a model corresponding to a gravitating continuum. The galactic plane would in that case be divided into a grating of small squares with fixed positions, the velocities and densities of matter in these cells being the variables. As the computation of distances between the particles is by far the most time-consuming operation in the mass-point model, the advantage with the cell model would be the use of fixed distances. However, the number of elements would have to be very large in order to provide a fine enough grating, and the capacity of the computer would not nearly suffice. Further, if the velocity should not be a single-valued function of position, it would be necessary to take into consideration the distribution of velocities within each cell and thus to introduce a four-dimensional phase space with even higher claims for storage capacity.

Computing programs

The numerical integrations of the equations of motion for the mass-point models have been performed at the electronic computer by means of two programs, here called E and F. They treat two different versions of the present problem. Program E computes the motions of a number of massive mutually attracting particles in the central force field $F(R)$, and program F the motions in a rotating coordinate system of particles of infinitely small mass under the combined influence of the force $F(R)$ and a system of fixed mass-points. In

addition there is a series of auxiliary programs for a number of shorter computations, necessary when deriving initial positions and velocities for the different models. A punched tape containing these initial positions and velocities can thus be produced more or less automatically once the parameters of the model are given. This makes a change of parameters very easy.

A description of the various programs is given in the Appendix.

II. Dispersion rings

Theory

The theory of dispersion orbits has been developed by B. LINDBLAD in a series of papers (B. LINDBLAD and F. NAHON, 1954; B. LINDBLAD, 1955–1958). Some formulae will be reproduced here in order to define some general notions.

We study the motions in the principal plane in a coordinate system centred at the centre of the galaxy and rotating with a certain constant angular velocity ω'. Let R and θ be the polar coordinates. For a particle, the orbit of which does not deviate much from a circle with radius R_0, we get, introducing the differential radial coordinate

$$\xi = R - R_0,$$

to the first order, the well known epicyclic motion

$$\xi = c_1 + c \cos \varkappa (t - t_0) \tag{1}$$

$$\theta - \theta_0 = (\omega - \omega')(t - t_0) - \frac{c}{R_0 + c_1} \cdot \frac{2\omega}{\varkappa} \sin \varkappa (t - t_0). \tag{2}$$

Here c_1, c, θ_0 and t_0 are the arbitrary constants. ω is the circular angular velocity defined by

$$\omega^2 = \frac{F(R)}{R}$$

and

$$\varkappa^2 = 3\omega^2 + \frac{dF}{dR}$$

both quantities valid for $R = R_0 - c_1$. Thus both ω and $\varkappa$ vary with c_1.

Assuming $\omega' \neq \omega$ we may put approximately, as c/R is supposed to be small,

$$\xi = c_1 + c \cos \frac{\varkappa}{\omega - \omega'} (\theta - \theta_0).$$

We introduce

$$n = \frac{\varkappa}{\omega - \omega'} \tag{3}$$

and obtain

$$\xi = c_1 + c \cos n (\theta - \theta_0). \tag{4}$$

This is the shape of the orbit in the coordinate system rotating with the angular velocity

$$\omega' = \omega - \frac{\varkappa}{n}.$$

TABLE 2.

R kpc	ω km/sec $\cdot$ kpc	$\varkappa$ km/sec $\cdot$ kpc	$\omega - \dfrac{\varkappa}{2}$ km/sec $\cdot$ kpc	R kpc	ω km/sec $\cdot$ kpc	$\varkappa$ km/sec $\cdot$ kpc	$\omega - \dfrac{\varkappa}{2}$ km/sec $\cdot$ kpc
2.0	88.2	141.7	17.3	12.0	14.5	11.5	8.8
.5	74.1	120.0	14.1	.5	13.5	10.2	8.4
3.0	65.7	103.9	13.8	13.0	12.6	9.6	7.9
.5	58.4	91.0	12.8	.5	11.8	9.3	7.2
4.0	52.5	81.4	11.8	14.0	11.2	9.2	6.6
.5	47.7	73.3	11.1	.5	10.5	9.2	5.9
5.0	43.7	66.4	10.5	15.0	10.0	8.9	5.5
.5	40.3	61.1	9.8	.5	9.4	8.5	5.2
6.0	37.4	56.2	9.3	16.0	9.0	8.0	5.0
.5	34.8	50.1	9.8	.5	8.6	7.4	4.8
7.0	32.2	43.2	10.6	17.0	8.2	7.1	4.6
.5	29.7	36.3	11.6	.5	7.8	6.9	4.3
8.0	27.3	29.7	12.4	18.0	7.4	6.7	4.1
.5	25.0	24.5	12.7	.5	7.1	6.6	3.8
9.0	22.8	21.3	12.2	19.0	6.8	6.5	3.6
.5	21.0	19.8	11.1	.5	6.6	6.4	3.4
10.0	19.4	18.5	10.2	20.0	6.3	6.0	3.3
.5	18.0	17.1	9.4				
11.0	16.7	15.2	9.1				
.5	15.6	13.0	9.0				

Now, a cloud of particles with somewhat differing values of c_1 will disperse along a certain configuration due to the differential rotation. If we choose ω' such that n does not vary with the first order variations of c_1, i.e., according to eq. (3), such that

$$n = \frac{d\varkappa}{d\omega},$$

then (4) gives the shape of that very configuration. The orbit of the particle is then called a *dispersion orbit*. As the coefficient $\omega - \omega'$ of t in eq. (2) varies with c_1, there will be a considerable dispersion of particles along the dispersion orbit. Important cases are when the dispersion orbit is closed, i.e. when n is an integer.

Table 2 and Fig. 2 show how ω and $\varkappa$ vary with R in the present model of the force $F(R)$. The relation between $\varkappa$ and ω is illustrated in Fig. 3. In this figure the lines $\omega - \varkappa = 0$ and $\omega - \frac{1}{2}\varkappa = 11.2$ km/sec $\cdot$ kpc are drawn. As is pointed out by B. LINDBLAD (1956), the points from the inner region of the Galaxy adhere in a remarkable way to the line $\omega - \frac{1}{2}\varkappa =$ const., whereas points from the outer regions approach the line $\omega = \varkappa$. Thus, in the inner regions the average value of $n = d\varkappa/d\omega = 2$, the closed dispersion orbits are ellipses with their centres in the centre of the Galaxy and with their apsidal lines turning approximately with the angular velocity $\omega' = \omega - \frac{1}{2}\varkappa = 11.2$ km/sec $\cdot$ kpc. In the outer regions $n = 1$, and the dispersion orbits are Keplerian ellipses with apsidal lines fixed in space.
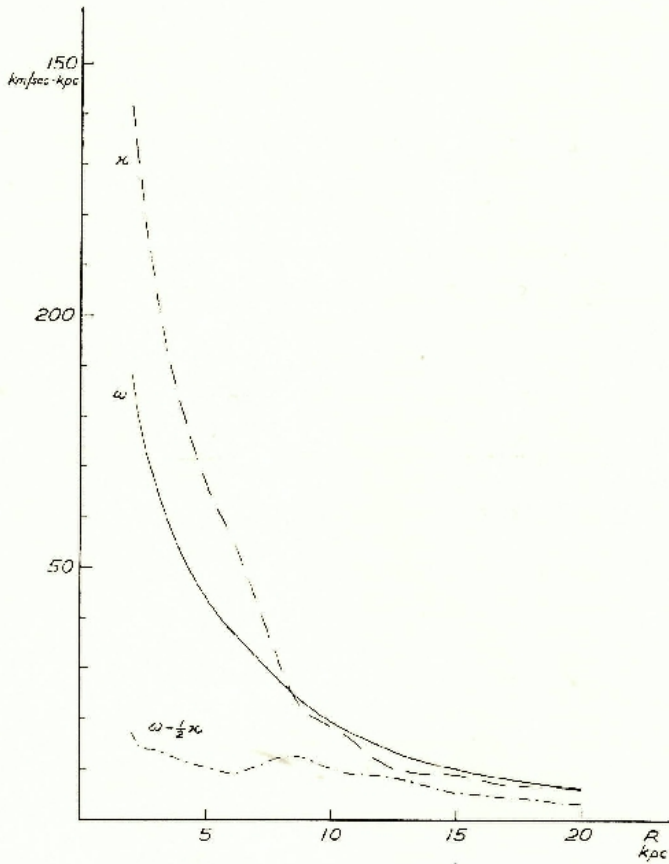
Fig. 2.

Fig. 3.

Fig. 2. The variation of the circular angular velocity ω and the frequency $\varkappa$ of radial oscillation as a function of R in the Schmidt model. In addition the angular velocity $\omega - \frac{1}{2}\varkappa$ of the apsidal line of a "special orbit" with two maxima of radius vector is given.
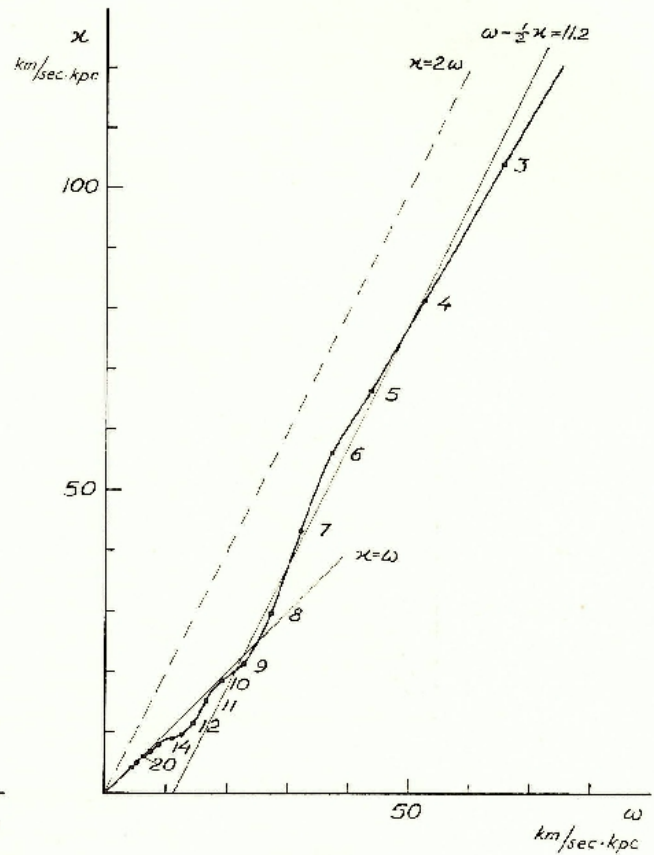
Fig. 3. Relation between ω and $\varkappa$ in Schmidt's model.

As a comparison Fig. 4 gives the relation between $\varkappa$ and ω in the Andromeda Nebula as derived from observations of the 21-cm hydrogen line by H. C. van de Hulst, E. Raimond and H. van Woerden (1957), and for M 81 as derived from the velocity curve given by G. Münch (1959). For the Andromeda Nebula a distance of 630 kpc is assumed. The lines $\omega - \varkappa$, and $\omega - \frac{1}{2}\varkappa - 10.0$ and 14.6 km/sec·kpc respectively are drawn as full lines in the figure.

B. Lindblad (1958b) has proved the possible existence of sectorial harmonic waves in very flattened subsystems in a galaxy where the relation between ω and $\varkappa$ has the same character as in Figs. 3 and 4. As long as $\varkappa$ is fairly large the angular velocity of the wave is approximately $\omega - \frac{1}{2}\varkappa$.

Also for a particle that moves in an orbit where $d\varkappa/d\omega \doteq 2$ we will always get a closed orbit with two maxima of the radius vector in a coordinate system rotating with the velocity $\omega_s' - \omega - \frac{1}{2}\varkappa$. This orbit is called a "special orbit". Due to the variation of ω and $\varkappa$ with the mean radius of the orbit, different special orbits will have different angular velocities ω_s' of

Fig. 4. Relation between ω and $\varkappa$ in M 31 and M 81.
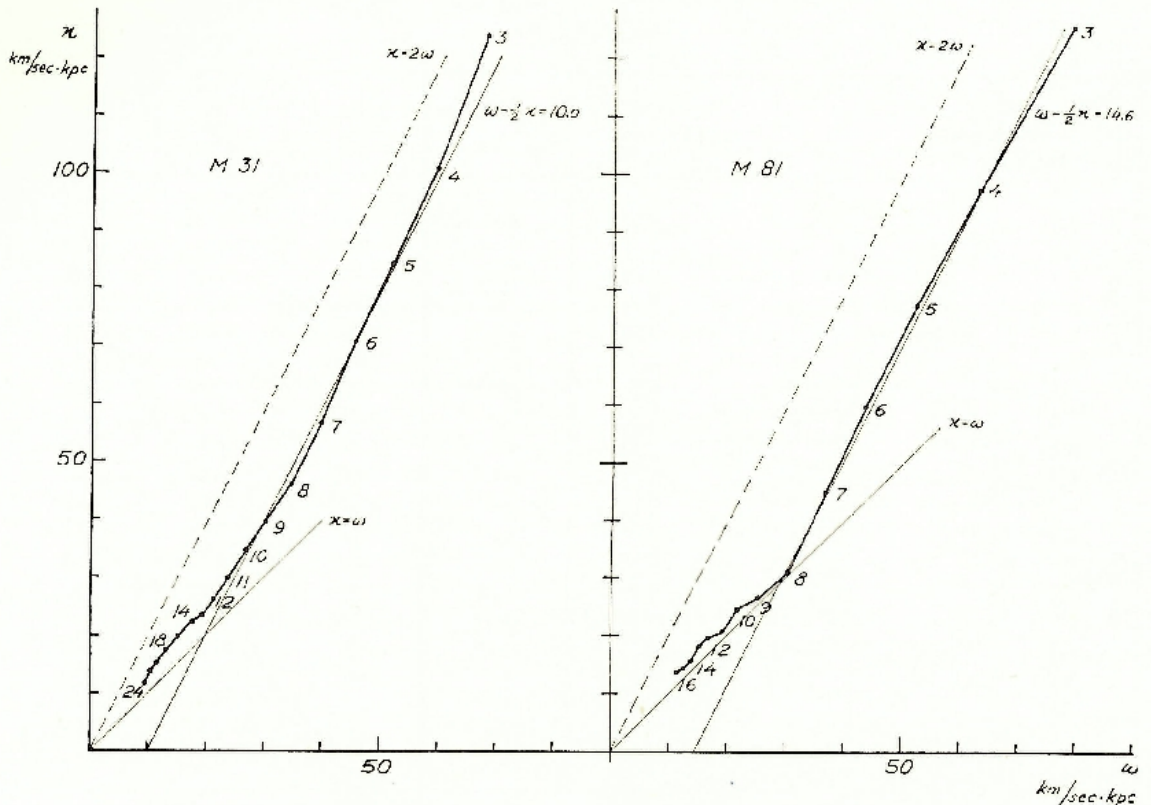
their apsidal lines. However, as the curves in Figs. 3 and 4 adhere rather closely to a line $\omega - \frac{1}{2}\varkappa = $ const., the variation of ω'_s will be small within large intervals of R. In fact, in the present model ω'_s keeps within the limits 9.3 and 12.8 km/sec·kpc for the entire range of R from 3.5 to 10.5 kpc. LINDBLAD suggests that this multitude of special orbits with only slightly differing angular velocities of their apsidal lines will amalgamate due to gravitational, viscous, and maybe magneto-hydrodynamic forces, and form massive elongated rings in the regions where $\omega - \frac{1}{2}\varkappa$ attains maximum or minimum, i.e. where $d\varkappa/d\omega = 2$ and the special orbits are dispersion orbits as well. The deformation of the rings would then proceed as harmonic waves with nearly the angular velocity $\omega - \frac{1}{2}\varkappa$. We will here call these massive configurations "dispersion rings".

In the next section we will investigate with the aid of numerical models the temporary stability of such dispersion rings. Then in Chapter III we shall study the perturbing influence of the rings on motions in the galactic plane and in Chapter IV the mutual interaction between several massive rings.

Construction of a model dispersion ring

The making of a numerical model of an idealized dispersion ring involves three steps.

1. The orbit of a particle in the field $F(R)$ is computed by means of program C (see the

TABLE 3.

Orbit	a kpc	b kpc	b/a	T' 10^6 years	θ	ω_s' km/sec · kpc	h 10^6 years	N	$\bar{R}$ kpc
I	9.3	7.4638	0.8	117.4869	173°9260	12.1855	0.25	64	8.4553
II	6.7	5.3468	0.8	55.4276	120.5580	9.4045	0.125	48	6.0576
III	5.0	3.5178	0.7	40.0355	116.3100	11.2101	0.125	48	4.31

TABLE 4. *Positions and velocities along the first quadrant of dispersion orbits I–III.*

|	x kpc	y kpc	$\dot{x}$ kpc/32 · 10^6 years	$\dot{y}$ kpc/32 · 10^6 years
I	0.2907	9.2921	2.5337	0.1370
	0.8724	9.2291	2.5375	− 0.4128
	1.4554	9.1023	2.5439	− 0.6944
	2.0399	8.9098	2.5504	− 0.9854
	2.6256	8.6491	2.5534	− 1.2893
	3.2111	8.3168	2.5476	− 1.6092
	3.7936	7.9091	2.5259	− 1.9479
	4.3685	7.4214	2.4800	− 2.3057
	4.9291	6.8496	2.3999	− 2.6811
	5.4664	6.1900	2.2749	− 3.0687
	5.9689	5.4410	2.0944	− 3.4586
	6.4227	4.6037	1.8498	− 3.8357
	6.8126	3.6832	1.5363	− 4.1802
	7.1227	2.6896	1.1561	− 4.4688
	7.3388	1.6384	0.7192	− 4.6777
	7.4498	0.5504	0.2442	− 4.7877
II	0.3221	6.6875	4.4596	− 0.3465
	0.9632	6.5874	4.4157	− 1.0400
	1.5946	6.3872	4.3253	− 1.7347
	2.2094	6.0867	4.1829	− 2.4294
	2.7993	5.6861	3.9812	− 3.1193
	3.3554	5.1868	3.7114	− 3.7960
	3.8670	4.5915	3.3642	− 4.4465
	4.3225	3.9053	2.9318	− 5.0524
	4.7091	3.1362	2.4096	− 5.5900
	5.0139	2.2962	1.7999	− 6.0314
	5.2250	1.4011	1.1148	− 6.3474
	5.3332	0.4710	0.3778	− 6.5127
III	0.2045	4.9909	3.9213	− 0.3488
	0.6121	4.9181	3.8924	− 1.0473
	1.0151	4.7725	3.8320	− 1.7480
	1.4099	4.5536	3.7342	− 2.4514
	1.7922	4.2612	3.5907	− 3.1558
	2.1566	3.8956	3.3901	− 3.8562
	2.4966	3.4576	3.1188	− 4.5425
	2.8040	2.9495	2.7623	− 5.1975
	3.0692	2.3758	2.3082	− 5.7954
	3.2817	1.7443	1.7506	− 6.3008
	3.4309	1.0667	1.0972	− 6.6723
	3.5080	0.3590	0.3743	− 6.8705
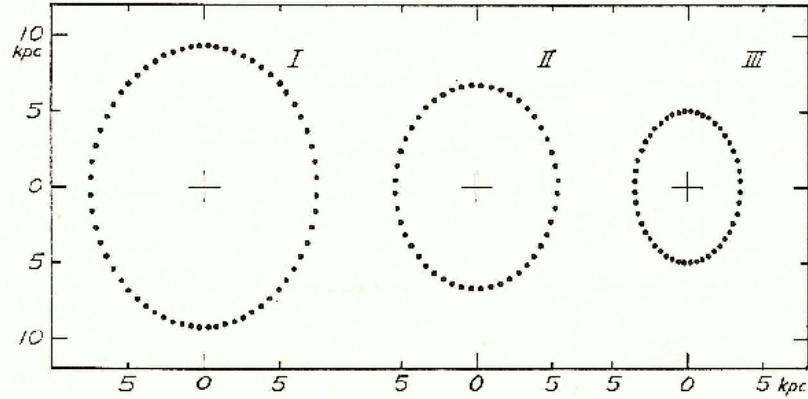
Fig. 5. The shapes of dispersion rings I–III.

Appendix). The particle is supposed to start in the apocentre, and the program locates the pericentre and evaluates the time T spent in the orbit between these two points. The initial velocity of the particle is chosen by trial and error so as to give a desired ratio between the largest and smallest radius vector. Three such orbits were computed, and the data are given in Table 3. a and b are the extremum values of the radius vector and θ the angle between the apocentre and the pericentre as seen from the centre of the galaxy. h is the original integration step. The angular velocity ω_s' of the coordinate system, in which the orbit is closed with two maxima of the radius vector, i.e. is a "special orbit", is given by

$$\omega_s' = \frac{1}{T}\left(\theta - \frac{\pi}{2}\right).$$

ω_s' will be a certain mean value of $\omega - \frac{1}{2}\varkappa$ over the orbit. As may be seen by a comparison with Fig. 3, orbit I is chosen to cover a region where $\omega - \frac{1}{2}\varkappa$ has a maximum and $d\varkappa/d\omega$ a mean value 2. Orbit II covers a region where $\omega - \frac{1}{2}\varkappa$ has a minimum and $d\varkappa/d\omega$ again averages 2. The innermost orbit III is more elongated than the other two, and $\omega - \frac{1}{2}\varkappa$ averages the mean for the whole inner part of the system.

2. The same orbits are now computed with program D in a Cartesian coordinate system turning with the angular speed ω_s'. Positions and velocities in the first quadrant of the now closed orbit are printed at equal intervals of time and the remaining quadrants may be formed by symmetry. The numbers of points N that are to compose the dispersion rings are given in Table 3 and the results are shown in Table 4 and Fig. 5. If the dots in the figure are thought to represent particles of equal mass, they reproduce the shape of and the distribution of mass along an idealized dispersion ring, where matter has been smoothed out along the ring during an infinitely long time. The mean radii $\bar{R}$ of the orbits, defined as the average of the radii vectores for all N particles, are given in Table 3.

3. In a coordinate system at rest the angular speed ω_s' has to be added to the velocity vectors of Table 4. Further, when finite masses are assigned to the particles, we have to balance the ring against self-gravitation by a small increase of the velocities. Both these

adjustments are made by program H. The compensation for self-gravitation is made by "individual balancing" (see the Appendix), and as the radius of curvature $\bar{\varrho}$ of the individual orbit the average radius R of the dispersion orbit is inserted. The dispersion rings are now ready to be studied by means of program E.

Integration of the motions

The aim of integrating the motions of the dispersion rings, formed in the way just described, is at first hand to check whether these rings are reasonably stable during a time sufficiently long to make them of importance for the development of the structure of the central layer. If the configurations are found to be thus stable, the rate of advance of the apsidal lines, to be used in future applications, will be determined from the computations.

It is a natural aspiration to keep the mass of a perturbing configuration or wave as low as possible from the start. On the other hand the perturbative effects must be able to develop within reasonable time. As an appropriate order of size of the mass of a single particle $m = 16 \cdot 10^6 \, M_\odot$ was chosen, or more exactly defined, if G is the constant of gravitation, $Gm = 68.965 \, \text{kpc} \cdot \text{km}^2/\text{sec}^2$. This m is here adopted as the unit of mass.

The motion of dispersion ring I was integrated in five different runs with program E (see Appendix), and the parameters are listed in Table A: 2. m was first given unit value, which gives the ring a total mass of about 1.5 % of the mass of the entire system. The limiting distance Δ_{min}, inside which the attractive force from a mass-point varies proportionally to the distance, was chosen at 0.8 kpc in the first run. The parameter D of the step-size control was given the value 0.15 kpc, which permitted the machine to keep the maximum integration step $32 \cdot 10^6$ years. The computation was carried on up to $768 \cdot 10^6$ years. The results are shown in Fig. 6, where the time with the unit 10^6 years is given for each configuration. The point that at the start is placed just in front of the apsidal line is marked with a cross. It is seen how the mass-points describe the circumference of the ring at the same time as the apsidal line turns clockwise. After some $300 \cdot 10^6$ years there appears a bend in the ring (not shown in the figure), and shortly afterwards a general dispersion of the particles sets in.

As it was thought that the bend in the ring might be caused by the discontinuity of the derivative of the force introduced by the limiting distance Δ_{min}, this distance was given a new value 1.133 kpc. With this value the two closest neighbours of each particle, but not more than two, fell inside that limiting circle in the initial configuration. This arrangement makes the particles more equivalent from the start and may reduce the appearance of bends. Although this particular distance does not retain this property in other configurations, it has, for the sake of uniformity, been kept in most computations. At this distance the attraction from a particle of unit mass is of the order of the attraction from the entire ring I, and 0.01 of the central force $F(R)$ at the average R of the ring.

With this value of Δ_{min}, and m equal to the unit, the motion of dispersion ring I was computed with three different step-sizes, 8, 16 and $32 \cdot 10^6$ years, and the results are shown in Fig. 7.
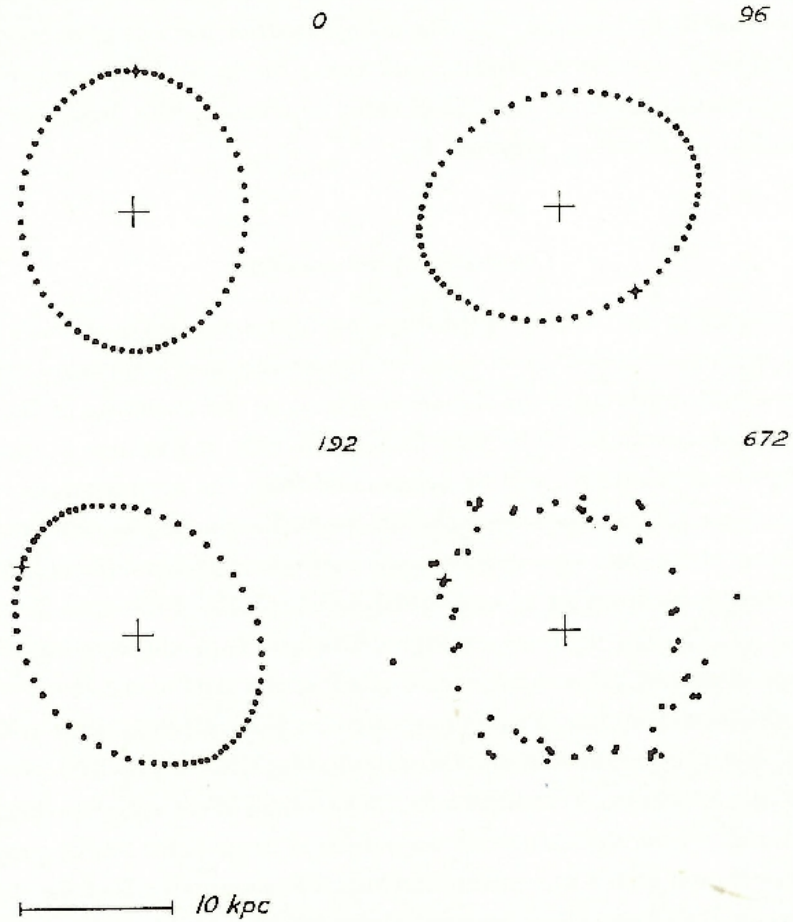
Fig. 6. Motion of dispersion ring I in the field $F(R)$. The mass of each mass-point $m = 1$ unit. $\Delta_{min} \sim 0.8$ kpc. For values of other parameters see Table A: 2. The time T in million years is given for each stage illustrated, and the mass-point that at the start just precedes the upper end of the apsidal line is marked with a cross.

Up to about $600 \cdot 10^6$ years the development is practically identical in the three cases. From there on the figure divides the sequence into three branches according to the three different step-sizes. The apsidal line turns in all three cases with an angular velocity ω' of 12.6 km/sec·kpc, which is exactly half the value of ω when account is taken of the selfgravitation of the ring. This is in agreement with the circumstance that $\omega \sim \varkappa$ in this region (Fig. 3). After some time the points disperse due to the effects of close encounters. However, the configuration being a dispersion ring, the dispersion mainly takes place along the ring, which seems to possess a fairly high degree of stability.

In the Appendix is described how these three runs with different step-sizes have been used for an estimate of the progressive errors of integration. The dispersion orbit shows the same fundamental behaviour in all three cases. Differences are due to different accuracy in computing close passages and to an increase of angular momentum reflected in the increase of areal velocities. In the choice of the proper step-size, one must remember that we are not interested here in computing close passages with high accuracy, but on the other hand it is
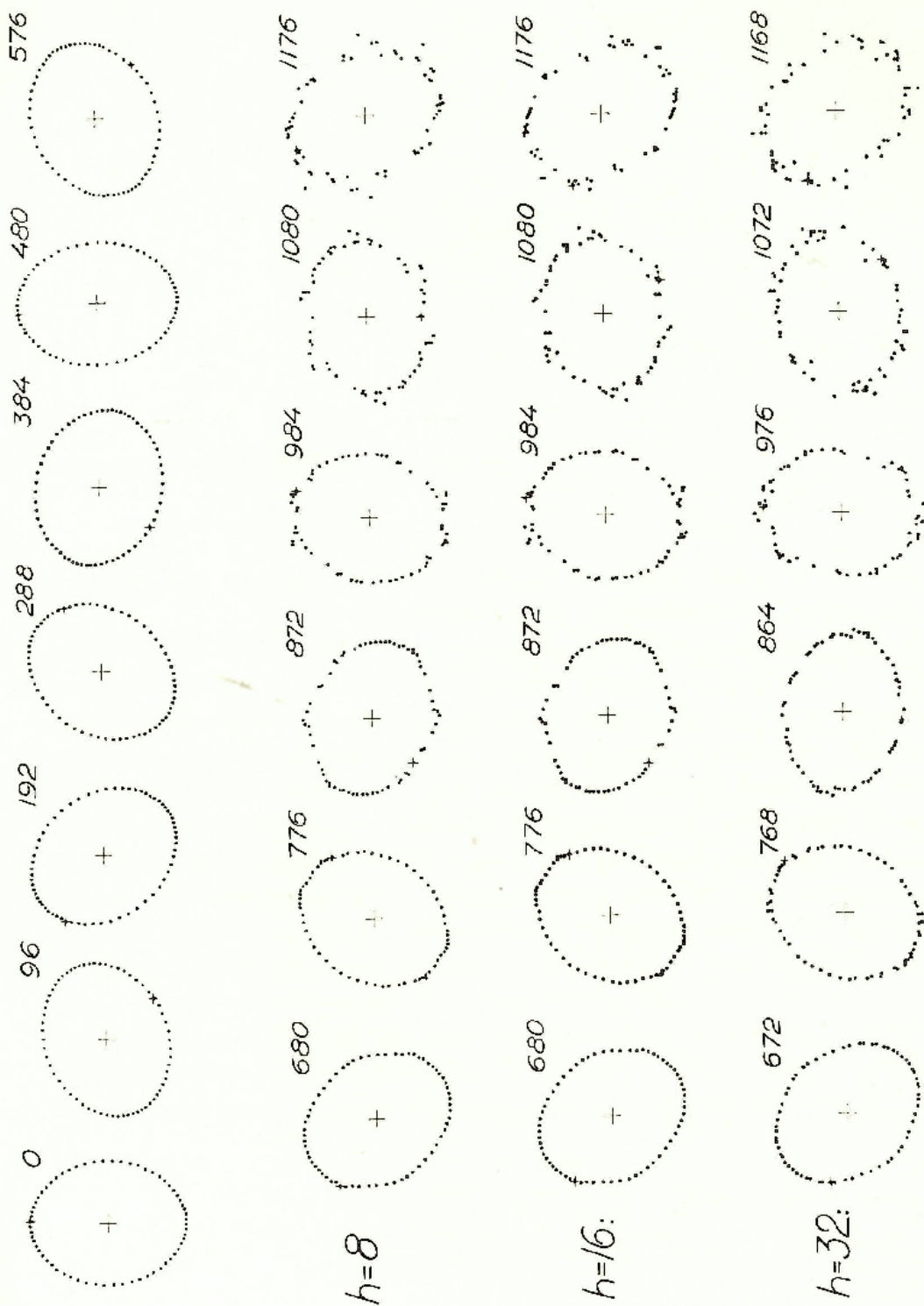
Fig. 7. Motion of dispersion ring I with $\Delta_{min} = 1.133$ kpc for three different sizes of the integration step h.
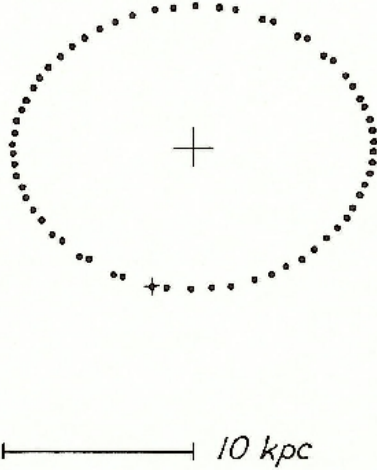
864

├─────────────────┤ *10 kpc*

Fig. 8. Dispersion ring I at $T = 864 \cdot 10^6$ years for a mass m of $\frac{1}{2}$ unit.

of course necessary to watch carefully for systematic effects, especially when resonance phenomena are at play or non-dispersion configurations involved.

The dispersion effects due to close encounters are much less for $\Delta_{min} = 1.133$ kpc than in the case $\Delta_{min} = 0.8$ kpc (Fig. 6), where the largest possible attraction between particles is about twice as large. In the case of the smaller Δ_{min} the dispersion becomes appreciable already after $600 \cdot 10^6$ years compared to about twice that time for the larger value. The computations were repeated with an m amounting only to half a unit, and the result after $864 \cdot 10^6$ years is shown in Fig. 8. It is seen that the scatter is much reduced. Figs. 6–8 give an idea of the influence of the masses and radii of stellar and interstellar clouds in dispersion configurations on the internal dispersion effects due to mutual encounters between such clouds. The masses and dimensions considered here are of one order of magnitude larger than the cloud complexes considered by L. SPITZER and M. SCHWARZSCHILD (1953).

For $m = \frac{1}{2}$ unit the angular velocity ω' of the apsidal line was decreased to 12.4 km/sec·kpc (Table 5). For infinitely small masses the ring is of course stable, and the apsidal line turns with the limiting velocity $\omega' = \omega'_s = 12.2$ km/sec·kpc (Table 3). It would perhaps be tempting to try larger and larger masses to find the limiting mass for which the ring is stable. However,

TABLE 5.

Disp. ring	m units	ω' km/sec · kpc
I	0.5	12.4
	1	12.6
II	1	9.6
	4	10.0
III	4	12.2

O   96
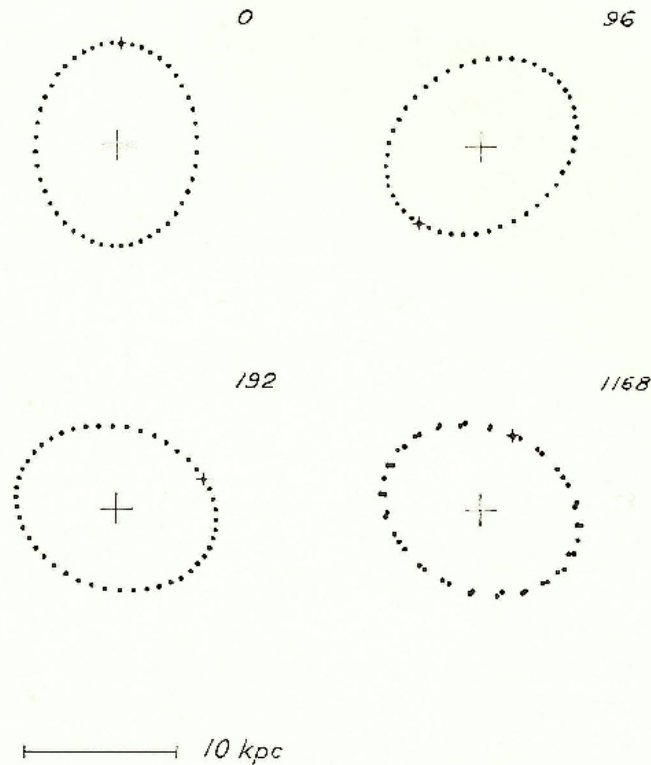
192   1168

Fig. 9. Motion of dispersion ring II in the
central field $F(R)$. |———————| 10 kpc

for large masses the choice of initial velocities and the value of Δ_{min} will be quite critical, and computations would not lead to conclusive results.

Parameters for the integrations of the motions of dispersion rings II and III are given in Table A: 2. Ring II was first computed with unit mass up to $T = 1168 \cdot 10^6$ years (Fig. 9). As will be seen in the next chapter, however, such a dispersion ring exerts only a very small influence on the rest of the system, and the computations were repeated with $m = 4$ and Δ_{min} increased to 1.9 kpc but now only up to $T = 352 \cdot 10^6$ years, which was sufficient to determine ω'. Ring III was computed with $m = 4$ up to $T = 1168 \cdot 10^6$ years (Fig. 10). The resulting values of ω' are given in Table 5.

It is seen from the figures that the inner dispersion rings II and III with their rapid circulation of matter around the circumference of the ellipses are much more resistant to the dissolving processes than is the outer dispersion ring I.

III. The influence of a stable dispersion ring on the surrounding field of motions

Theory

As the relatively high degree of stability of the dispersion rings has been demonstrated in the preceding chapter, it is now of interest to derive their perturbative influence on surrounding matter in the plane.

0   *96*

192   *1168*
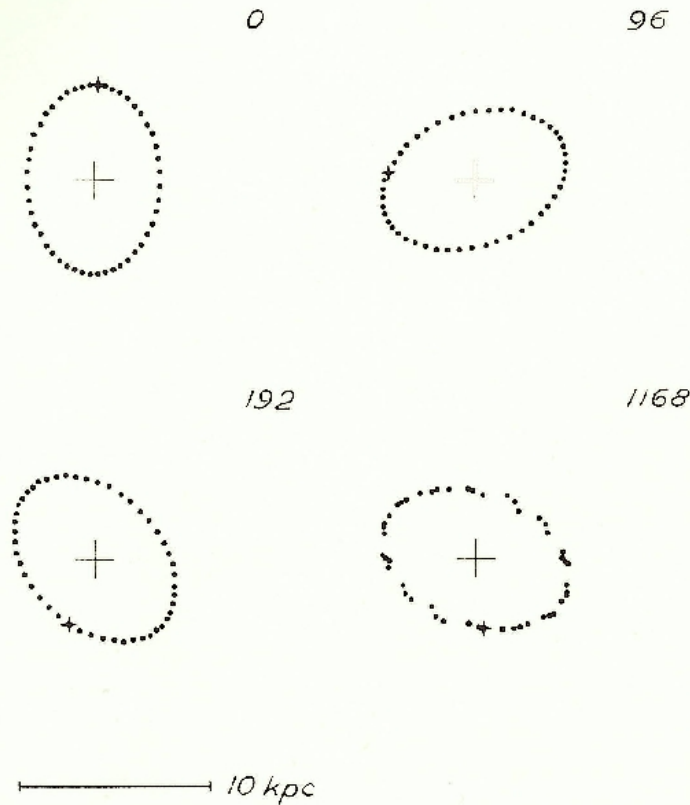
⊢————————————→ *10 kpc*

Fig. 10. Motion of dispersion ring III in the central field $F(R)$.

We develop the perturbing force due to the elongation of the ring and to the density variation along it in a Fourier series. For a distance $R = R_0 - \xi$ from the centre, where the constant R_0 so far is arbitrary, we write the components of the force along and perpendicular to the radius vector

$$
\left.
\begin{aligned}
f_\xi &= R_0 \cdot e^{\gamma t} \sum_{k=1}^{\infty} C_k \cos 2k\theta \\
f_\eta &= R_0 \cdot e^{\gamma t} \sum_{k=1}^{\infty} D_k \sin 2k\theta
\end{aligned}
\right\}
\tag{5}
$$

where C_k and D_k are functions of ξ, and θ is counted from the apsidal line of the perturbing ring. It is assumed that the ring develops slowly in such a way that the variation of the force with time takes an exponential form, and that γ is a small number. We now study the motions in a coordinate system that rotates with the same angular velocity ω' as the apsidal line of the dispersion ring, and introduce

$$
\frac{\sigma}{2} = \omega_0 - \omega',
$$

where ω_0 is the circular angular velocity at $R = R_0$. For particles that do not deviate much from the circular orbit with radius R_0 we may approximate

$$
\theta = \theta_0 + \frac{\sigma}{2} t
$$

in the expressions for f_ξ and f_η. Then the equations of motion will be (cp. for example B. LINDBLAD, 1959, eq. 17.7)

$$\frac{1}{R_0}\frac{d^2\xi}{dt^2} - 2\omega_0\frac{d\theta}{dt} + (\varkappa^2 - 4\omega_0^2)\frac{\xi}{R_0} + \omega_0\sigma = e^{\gamma t}\sum_k C_k \cos 2k\left(\frac{\sigma}{2}t + \theta_0\right)$$

$$\frac{d^2\theta}{dt^2} + 2\omega_0\frac{1}{R_0}\frac{d\xi}{dt} = e^{\gamma t}\sum_k D_k \sin 2k\left(\frac{\sigma}{2}t + \theta_0\right). \tag{6}$$

We neglect the variation of C_k and D_k with ξ in the present approximation. Thus for particles that at $t = -\infty$ describe circular orbits with radius R_0, the solutions for the general case $\gamma^2 \ll |\varkappa^2 - k^2\sigma^2|$ and $\gamma^2 \ll \sigma^2$ are

$$\frac{\xi}{R_0} = \sum_k \left\{\left[\frac{k\sigma}{\varkappa^2 - k^2\sigma^2}\left(C_k - \frac{2\omega_0}{k\sigma}D_k\right) + \frac{\omega_0}{k^2\sigma^2}D_k\right]\frac{2\gamma}{\varkappa^2 - k^2\sigma^2}e^{\gamma t}\sin 2k\left(\frac{\sigma}{2}t + \theta_0\right) + \right.$$
$$\left. + \left(C_k - \frac{2\omega_0}{k\sigma}D_k\right)\frac{1}{\varkappa^2 - k^2\sigma^2}e^{\gamma t}\cos 2k\left(\frac{\sigma}{2}t + \theta_0\right)\right\} \tag{7}$$

$$\theta - \theta_0 + \frac{\sigma}{2}t = \sum_k \left\{\left[\frac{2\omega_0}{\varkappa^2 - k^2\sigma^2}\left(C_k - \frac{2\omega_0}{k\sigma}D_k\right) + \frac{1}{k\sigma}D_k\right]\frac{1}{k\sigma}e^{\gamma t}\sin 2k\left(\frac{\sigma}{2}t + \theta_0\right)\right.$$
$$\left. - \left[\frac{\omega_0(3k^2\sigma^2 - \varkappa^2)}{\varkappa^2 - k^2\sigma^2}\left(C_k - \frac{2\omega_0}{k\sigma}D_k\right) + \frac{2\omega_0^2 - (\varkappa^2 - k^2\sigma^2)}{k\sigma}D_k\right]\frac{2\gamma}{k^2\sigma^2(\varkappa^2 - k^2\sigma^2)}e^{\gamma t}\cos 2k\left(\frac{\sigma}{2}t + \theta_0\right)\right\}. \tag{8}$$

These formulae correspond to eqs. (15) of B. LINDBLAD (1958 b).

Let all particles, that at $t = -\infty$ describe a circular orbit with radius R_0, form a ring of matter. For the density μ along this ring we have to first order

$$\frac{\mu}{\mu_0} = \frac{1}{\frac{\partial\theta}{\partial\theta_0}\left(1 + \frac{\xi}{R_0}\right)},$$

where μ_0 is the supposed uniform density of the initial circular ring. This gives

$$\frac{\mu}{\mu_0} = 1 - \sum_k \left\{\left[\frac{k^2\sigma^3 - 2\omega_0(3k^2\sigma^2 - \varkappa^2)}{\varkappa^2 - k^2\sigma^2}\left(C_k - \frac{2\omega_0}{k\sigma}D_k\right) - \frac{2(2\omega_0^2 - \varkappa^2 + k^2\sigma^2) - \omega_0\sigma}{k\sigma}D_k\right]\frac{2\gamma}{k\sigma^2(\varkappa^2 - k^2\sigma^2)} \cdot \right.$$
$$\left. \cdot e^{\gamma t}\sin 2k\left(\frac{\sigma}{2}t - \theta_0\right) + \left[\frac{\sigma - 4\omega_0}{\sigma(\varkappa^2 - k^2\sigma^2)}\left(C_k - \frac{2\omega_0}{k\sigma}D_k\right) - \frac{2}{k\sigma^2}D_k\right]e^{\gamma t}\cos 2k\left(\frac{\sigma}{2}t + \theta_0\right)\right\}. \tag{9}$$

If in the formulae (7)–(9) we change back $(\sigma/2)t - \theta_0$ into θ in the trigonometric expressions, then (7) gives the shape of and (9) the density variation along the perturbed ring of matter. From (7) we see that the position angles of the deformations of the ring are fixed in the rotating coordinate system, i.e. they proceed with the angular velocity of the perturbing wave.

It is evident that there are two cases of resonance when the coefficients become large, one when $\varkappa^2 - k^2\sigma^2 \to 0$ and one more general when $\sigma \to 0$.

$\varkappa^2 - k^2\sigma^2 \to 0$.

In this case we have resonance for a certain value of k. The terms with this value of k will dominate the solution, and we get for $\gamma^2 \ll k^2\sigma^2$, $\gamma^2 \ll \omega_0^2$ and $(\varkappa - k\sigma)^2 \ll \gamma^2$ the new solution

$$
\begin{aligned}
\frac{\xi}{R_0} &= \sum_k \left\{ \left(C_k - \frac{2\omega_0}{k\sigma} D_k \right) \frac{1}{2\gamma k\sigma} e^{\gamma t} \sin 2k\theta + \right. \\
&\quad + \left. \left[\frac{\gamma^2 + \varkappa^2 - k^2\sigma^2}{2\gamma^2} \left(C_k - \frac{2\omega_0}{k\sigma} D_k \right) - \frac{2\omega_0}{k\sigma} D_k \right] \frac{1}{2k^2\sigma^2} e^{\gamma t} \cos 2k\theta \right\} \\
\frac{\mu}{\mu_0} &= 1 + \sum_k \left\{ \left(\frac{4\omega_0}{\sigma} - 1 \right) \left(C_k - \frac{2\omega_0}{k\sigma} D_k \right) \frac{1}{2\gamma k\sigma} e^{\gamma t} \sin 2k\theta + \right. \\
&\quad + \left[\frac{8\omega_0\gamma^2 + (\gamma^2 + \varkappa^2 - k^2\sigma^2)(4\omega_0 - \sigma)}{4\gamma^2} \left(C_k - \frac{2\omega_0}{k\sigma} D_k \right) - \frac{4\omega_0^2 - 2k^2\sigma^2 - \omega_0\sigma}{k\sigma} D_k \right] \cdot \\
&\quad \left. \cdot \frac{1}{k^2\sigma^3} e^{\gamma t} \cos 2k\theta \right\}.
\end{aligned}
\tag{10}
$$

corresponding to eqs. (14) of the paper by B. LINDBLAD previously cited. If the angular velocity ω' of the perturbing wave is close to the average value of $\omega - \frac{1}{2}\varkappa$ for the inner part of the system, σ will be nearly equal to $\varkappa$ in the whole inner region where $R_0 < 10$ kpc, i.e. $k = 1$ in eqs. (10).

For γ small and $\varkappa + \sigma \approx 2\sigma$ we may approximate

$$
\begin{aligned}
\frac{\xi}{R_0} &= \left(C_1 - \frac{2\omega_0}{\sigma} D_1 \right) \frac{e^{\gamma t}}{2\gamma^2\sigma} [\gamma \sin 2\theta + (\varkappa - \sigma) \cos 2\theta] \\
\frac{\mu}{\mu_0} &= 1 + \left(\frac{4\omega_0}{\sigma} - 1 \right) \left(C_1 - \frac{2\omega_0}{\sigma} D_1 \right) \frac{e^{\gamma t}}{2\gamma^2\sigma} [\gamma \sin 2\theta + (\varkappa - \sigma) \cos 2\theta]
\end{aligned}
\tag{11}
$$

or

$$
\frac{\mu}{\mu_0} = 1 + \left(\frac{4\omega_0}{\sigma} - 1 \right) \frac{\xi}{R_0}.
\tag{12}
$$

As $(4\omega_0 - \sigma) \approx (4\omega_0 - \varkappa)$ which is always positive (Fig. 3), this means that the perturbed ring takes an elongated shape with density maxima at the ends of the major axes, the lines of apsides rotating with the angular velocity ω' of the perturbing wave. In other words it simulates a dispersion ring in the same region. As far as $|\varkappa - \sigma|$ is small compared to γ, the position angle of the apsidal line with respect to the wave oscillates around $\theta = +45°$ or $-45°$, depending upon whether $C_1 - (2\omega_0/\sigma) D_1$ is positive or negative.

$\sigma \to 0$.

This second case of resonance occurs where the circular angular velocity ω_0 is nearly equal to the angular velocity ω' of the perturbing wave. In this region also $|\varkappa^2 - k^2\sigma^2|$ may become small for higher values of the integer k. However, C_k and D_k are small too for such values of k, and we search for the solution for $k^2\sigma^2 \ll \varkappa^2$ and $\gamma^2 \ll \varkappa^2$

$$\frac{\xi}{R_0} = \sum_k \left[\left(\frac{k\,\sigma}{\varkappa^2} C_k + \frac{\omega_0}{\gamma^2 + k^2\,\sigma^2} D_k \right) \frac{2\,\gamma}{\varkappa^2} e^{\gamma t} \sin 2k\theta + \left(C_k - \frac{2\,\omega_0\,k\,\sigma}{\gamma^2 - k^2\,\sigma^2} D_k \right) \frac{1}{\varkappa^2} e^{\gamma t} \cos 2k\theta \right]$$

$$\frac{\mu}{\mu_0} = 1 - \sum_k \left\{ \frac{2\,\gamma}{\varkappa^2(\gamma^2 + k^2\,\sigma^2)} \left[\omega_0 D_k + 2k\,\omega_0\,C_k - (4\,\omega_0^2 - \varkappa^2) \frac{2k^2\,\sigma}{\gamma^2 + k^2\,\sigma^2} D_k \right] e^{\gamma t} \sin 2k\theta + \right.$$
$$\left. + \frac{1}{\varkappa^2} \left[C_k - \frac{2\,\omega_0\,k\,\sigma}{\gamma^2 + k^2\,\sigma^2} D_k - \frac{4\,\omega_0 k^2\,\sigma}{\gamma^2 + k^2\,\sigma^2} C_k - (4\,\omega_0^2 - \varkappa^2) \frac{\gamma^2 - k^2\,\sigma^2}{(\gamma^2 + k^2\,\sigma^2)^2} 2k\,D_k \right] e^{\gamma t} \cos 2k\theta \right\}.$$

(13)

As γ and σ are small, the terms with the higher power of $\gamma^2 + k^2\sigma^2$ in the denominator will dominate, and we may write, considering only terms with $k = 1$,

$$\frac{\xi}{R_0} = \frac{2\,\omega_0 D_1 e^{\gamma t}}{\varkappa^2(\gamma^2 + \sigma^2)} (\gamma \sin 2\theta - \sigma \cos 2\theta)$$

$$\frac{\mu}{\mu_0} = 1 + \frac{2(4\,\omega_0^2 - \varkappa^2) D_1 e^{\gamma t}}{\varkappa^2(\gamma^2 + \sigma^2)^2} [2\gamma\sigma \sin 2\theta - (\gamma^2 - \sigma^2) \cos 2\theta].$$

(14)

Introducing

$$\operatorname{tg}\varphi = \frac{\sigma}{\gamma} \qquad \left(-\frac{\pi}{2} < \varphi < +\frac{\pi}{2} \right)$$

(15)

we get

$$\frac{\xi}{R_0} = \frac{2\,\omega_0 D_1 e^{\gamma t}}{\varkappa^2 \sqrt{\gamma^2 + \sigma^2}} \sin(2\theta - \varphi)$$

$$\frac{\mu}{\mu_0} = 1 + \frac{2(4\,\omega_0^2 - \varkappa^2) D_1 e^{\gamma t}}{\varkappa^2(\gamma^2 + \sigma^2)} \cos(2\theta - 2\varphi).$$

(16)

D_1 as defined by eqs. (5) is obviously negative, and $4\omega_0^2 - \varkappa^2$ is always positive (Fig. 3). Thus we have the position angle for maximum ξ

$$\theta_{\xi\,\text{max}} = \frac{3\,\pi}{4} + \frac{\varphi}{2}$$

and for maximum μ

$$\theta_{\mu\,\text{max}} = \frac{\pi}{2} + \varphi.$$

We have

$$\left(\frac{d\left(\frac{\xi}{R_0} \right)}{d\theta} \right)_{\mu\,\text{max}} = -\frac{4\,\omega_0 D_1}{\varkappa^2 \sqrt{\gamma^2 + \sigma^2}} e^{\gamma t} \cos\varphi$$

which is always a positive quantity. Hence matter will concentrate along the parts of the elongated ring that are *outgoing* in the direction of rotation of the system. If ψ is the phase difference between maximum ξ and maximum μ we have

$$\psi = \theta_{\xi\,\text{max}} - \theta_{\mu\,\text{max}} = \frac{\pi}{4} - \frac{\varphi}{2}.$$

At maximum resonance when $\sigma = 0$, then $\theta_{\xi\,\text{max}} = 3\pi/4$ and $\theta_{\mu\,\text{max}} = \pi/2$. This case is sketched in Fig. 11. If we leave the resonance case $\sigma = 0$ through decreasing R_0, σ will increase through
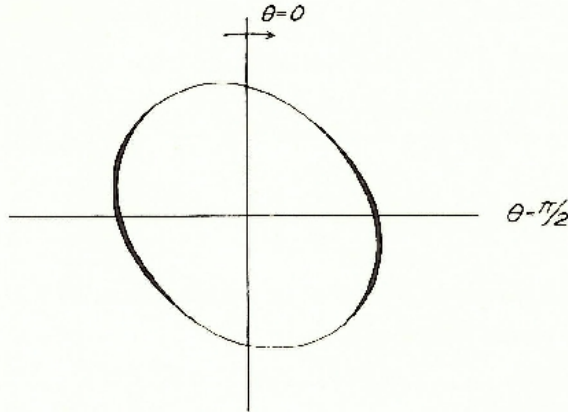
Fig. 11. Sketch of the first order deformations of a circular ring perturbed by a bisymmetrical potential wave. The ring is supposed to be situated at the resonance distance where $\sigma = 0$.

positive values, and $\theta_{\xi\,max}$ will increase from $3\pi/4$ to π, $\theta_{\mu\,max}$ from $\pi/2$ to π, and ψ decrease from $\pi/4$ to 0. Thus for large σ the apsidal line of the perturbed ring will coincide with the apsidal line of the perturbing wave with maxima of density situated at the major axes. If, on the other hand, we go outwards in the system from the case $\sigma - 0$, σ takes negative values, and $\theta_{\xi\,max}$ will decrease from $3\pi/4$ to $\pi/2$, $\theta_{\mu\,max}$ from $\pi/2$ to 0, and ψ increase from $\pi/4$ to $\pi/2$. Accordingly, for large negative values of σ the apsidal line will be at right angles to that of the perturbing wave and the density maxima placed at the ends of the minor axis. All these details are confirmed by the numerical computations.

Numerical computations

In the numerical illustrations of the perturbations by a sectorial harmonic wave, travelling with an angular velocity equal to a mean value of $\omega - \frac{1}{2}\varkappa$ in the region of the wave, on the field of circular motions in the principal plane we choose as the perturbing wave, in order, the dispersion rings I, II and III. The computations of the preceding chapter have shown these rings to be stable over a considerable period of time for masses m at least up to one unit. To get a fairly rapidly working program for investigations of first order disturbances, we place the dispersion ring as a fixed configuration of point-masses in a coordinate system rotating with the angular speed ω' of the apsidal line. The influence of this ring on circular rings composed of particles of negligible mass is then studied with program F (see the Appendix).

To avoid effects that might be a consequence of a sudden start, i.e. to ensure a small enough γ, the fixed massive configuration was not, from the beginning, given the shape of the elongated dispersion ring. At the start of the computations the massive points formed a circle of uniform density with a radius equal to the average radius of the dispersion ring. The points were then allowed to move in ten steps along straight lines until they reached their final positions in the dispersion ring given in Table 4 (Fig. 5). In this manner ten configurations were formed with successively increasing elongation. Now the computation with program F started with the first fixed configuration, which after a certain number of integra-

tion steps was changed into the next one and so on. When the final configuration of the dispersion ring was reached, it was kept throughout the continued computations.

The massless particles are given circular velocities from the start. These velocities are compensated for the general attraction of the massive dispersion ring by a small increase of the velocities, corresponding to the attraction from a circular ring of the same mass as the dispersion ring and with a radius equal to its mean radius. The force from such a massive circular ring was computed with program G, and the corresponding increase of the velocities made with program H.

Figs. 12–17 show the results of computations for dispersion ring I and outer circular rings of radii 11.25, 12, 13, 14, 15, and 16 kpc, each composed of 64 massless points. A further case with an outer ring of radius 10.5 kpc was computed (innermost of the outer rings in Fig. 18). Inside 10.5 kpc we can expect to meet distortions of the simple picture on account of close passages past the fixed points, and outside 16 kpc the mass density in the galactic plane has dropped to zero. The rate of development of the dispersion ring was such that it had acquired its final shape after $576 \cdot 10^6$ years. The masses of the fixed points were given unit values, and the angular velocity ω' of the coordinate system the value 12.6 km/sec·kpc in accordance with the computations of the preceding chapter (Table 5).

For this value of ω' the resonance case $\sigma = 0$ occurs at $R_0 = 13$ kpc, and the region studied is centred around this distance. The figures begin at the epoch $T = 576 \cdot 10^6$ years, and the computations are carried on to $896 \cdot 10^6$ years in most cases. The integration step was $16 \cdot 10^6$ years, and test runs showed the progressive error up to $T = 896 \cdot 10^6$ years to be of the order of 0.003 kpc.

The results reproduce fairly faithfully the features predicted in the theoretical discussion. The case $R_0 = 10.5$ kpc hardly shows any influence at all, except possibly a slight condensation that seems to follow the circular motion. The rings with $R_0 = 11.25$–15 kpc show an elongation and a bisymmetrical concentration of matter. The position angles of the apsidal line counted in the direction of the motion vary from about π for $R_0 = 11.25$ kpc over $3\pi/4$ for $R_0 = 13$ kpc to $\pi/2$ for $R_0 = 15$ kpc. The maximum density that in the case of $R_0 = 11.25$ kpc lies just behind the vertex, lags further and further behind, for $R_0 = 13$ kpc it lies in the position angle $\theta = \pi/2$ just between the major and minor axes, and for $R_0 = 15$ kpc it is situated on the minor axes in position angle $\theta = 0$. The case $R_0 = 16$ kpc, which is given in Fig. 17 only for $T = 1088 \cdot 10^6$ years, shows an extrapolation of these features.

The development is more rapid, the closer the ring comes to the resonance case $\sigma = 0$. The ring $R_0 = 13$ kpc is computed further than the other cases. It is seen that eventually the concentrations will become very strong until almost the entire ring is concentrated in two aggregates placed on the prolongation of the minor axis of the dispersion ring and subsequently drawn out owing to differential rotation. A case with an inner circular ring with a radius of 6 kpc was also computed up to $T = 768 \cdot 10^6$ years, but as could be expected, since the angular velocity is large and the effects of elongation and density variation of the dispersion ring counteract each other, there were no visible effects at all. This is to some extent
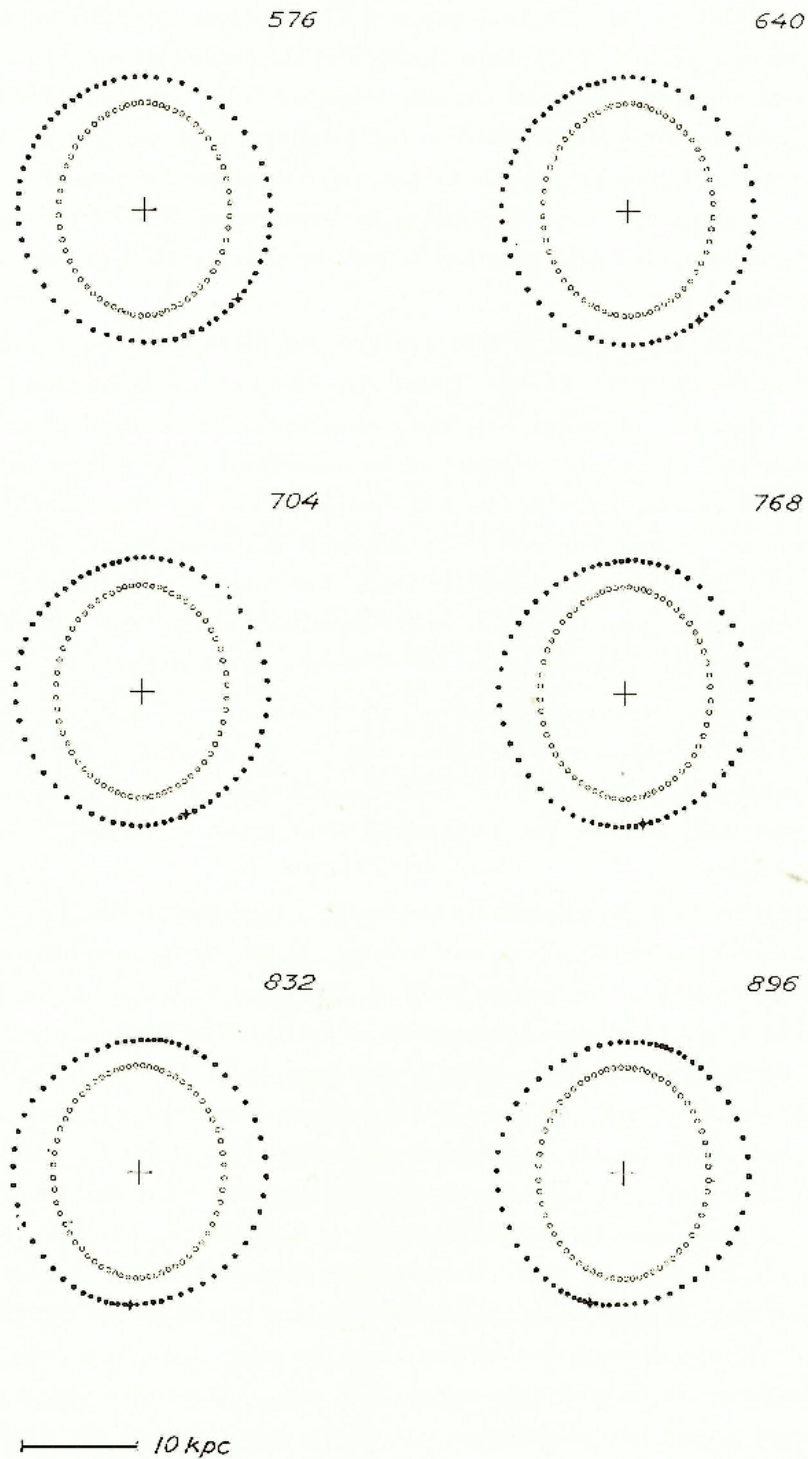
Fig. 12. Deformation of a circular ring of massless particles with a radius $R_0 = 11.25$ kpc due to the presence of dispersion ring I. The massive dispersion ring lies fixed in the coordinate system that rotates with the angular speed of its apsidal line. The dispersion ring has been successively developed from a circular ring as described in the text, and the illustration starts at $T = 576 \cdot 10^6$ years, when the dispersion ring is fully developed.
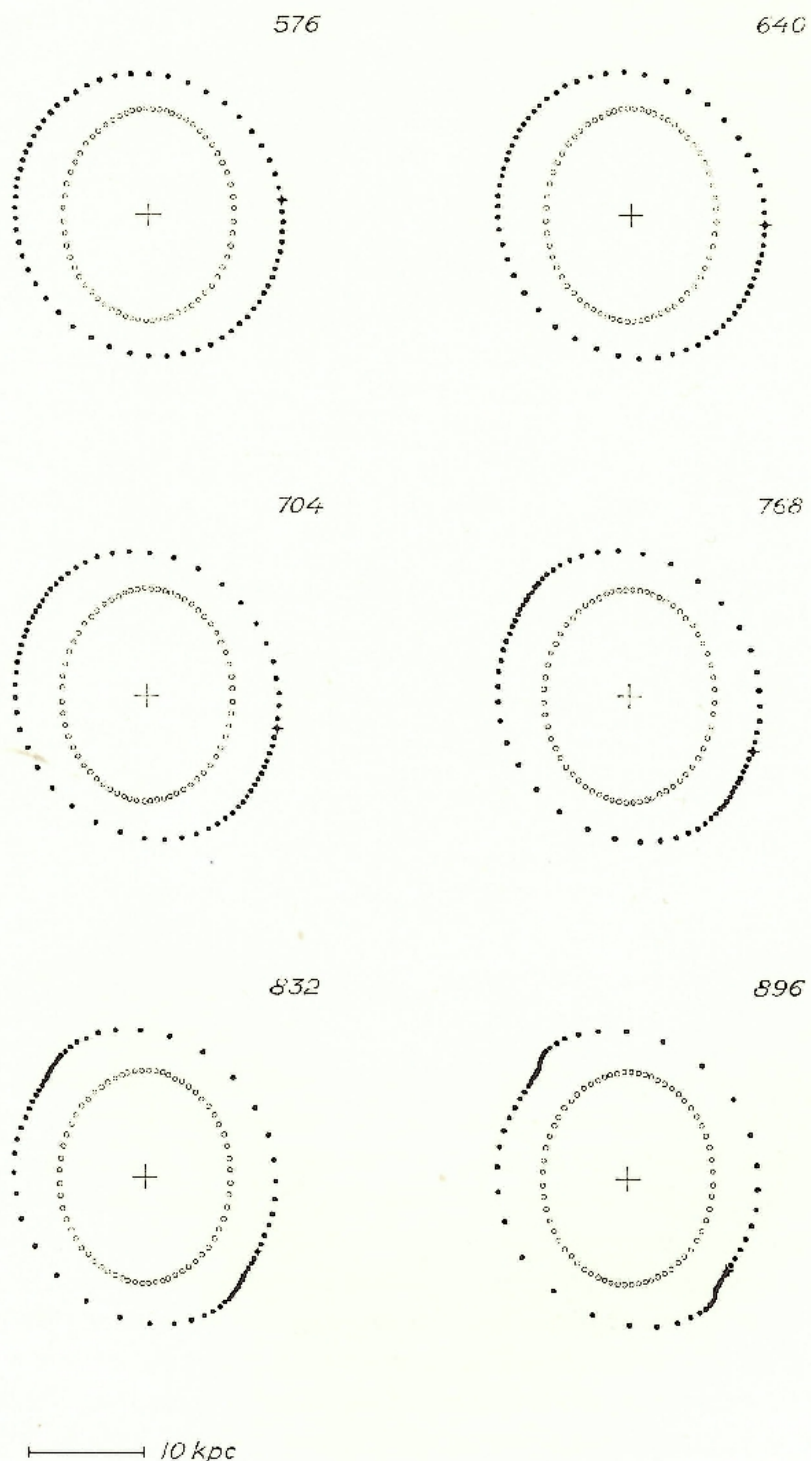
Fig. 13. Dispersion ring I and ring of massless particles with $R_0 = 12$ kpc.

576

640

704

768

832

896

10 kpc
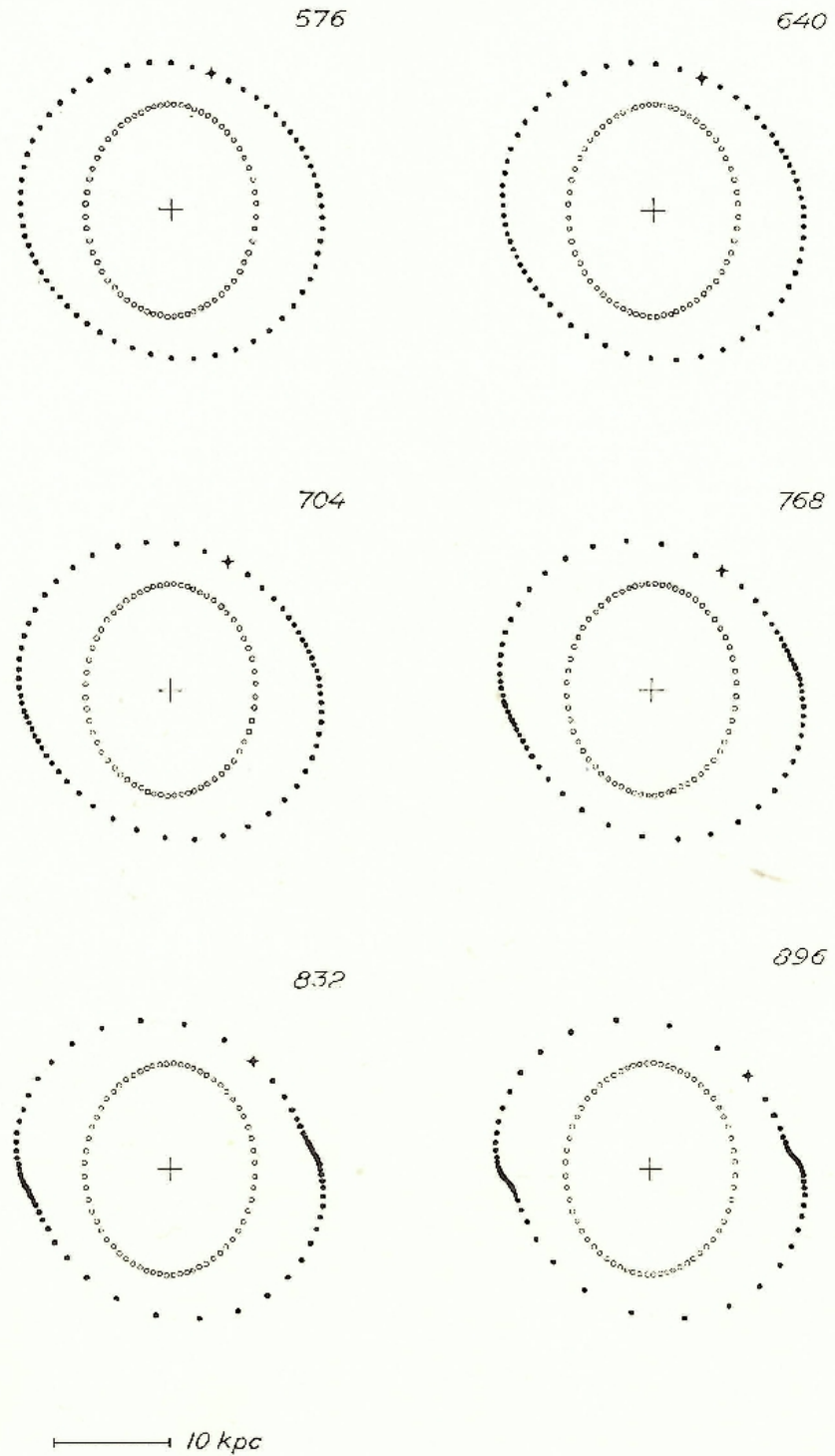
Fig. 14. Dispersion ring I and ring of massless particles with $R_0 = 13$ kpc.
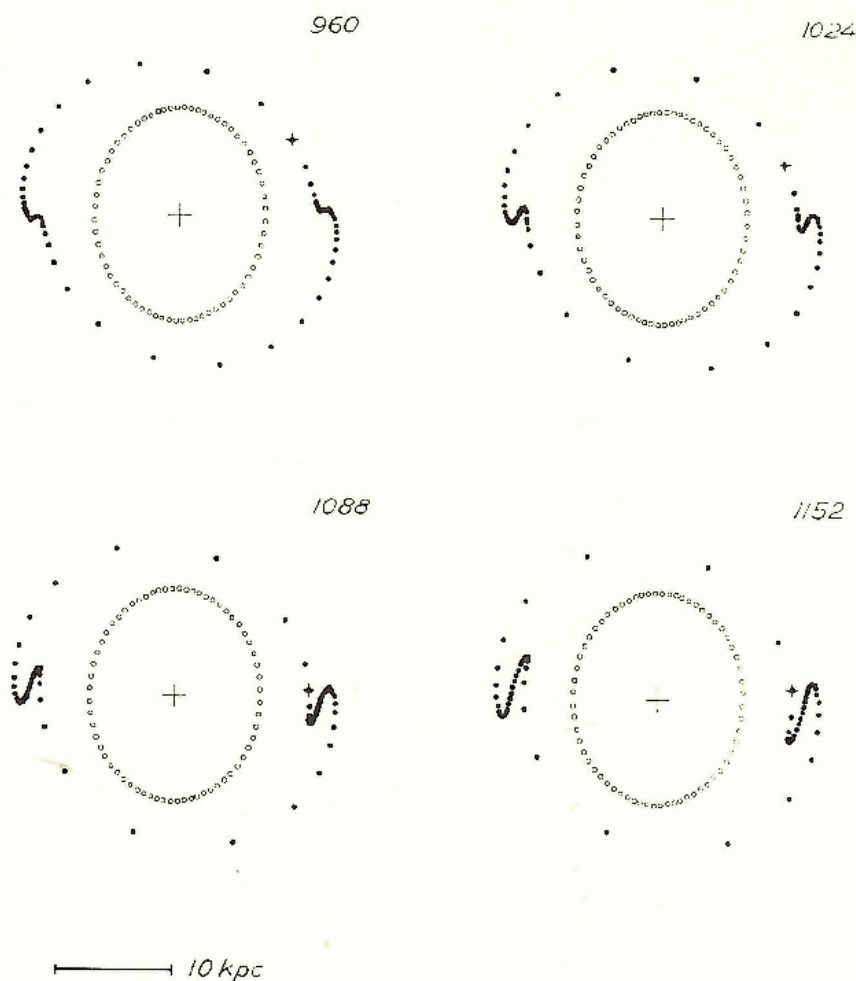
Fig. 14 cont.

a justification of our assumption of an undisturbed development of the dispersion ring. In the treatment of the bar-type wave in the last chapter we will meet a different case.

All rings are combined into one picture in Fig. 18. If we consider a galaxy in an early stage of development to be built up of a number of such discrete, not very massive, almost circular rings, the first effects of a wave of the type considered would be to form a number of leading arms as shown in the figure. Ultimately the arms become more and more concentrated, and each ring breaks down into two aggregates subsequently spread out by differential motion. As the density maxima develop at the major axis of the perturbed ring for $R_0 = 11.25$ kpc and then slide continuously down to the minor axis when R_0 increases to 15 kpc, the radial distribution of these density maxima is minimized. It also appears from Fig. 18 that the final formation of an aggregate, rather independently of the original radius of the ring, tends to occur close to the resonance distance $R = 13$ kpc. Even if the outer region is not built up by discrete rings but forms a more continuous sheet of matter, the result of this first phase of development is likely to be that the disturbing wave in the inner regions will
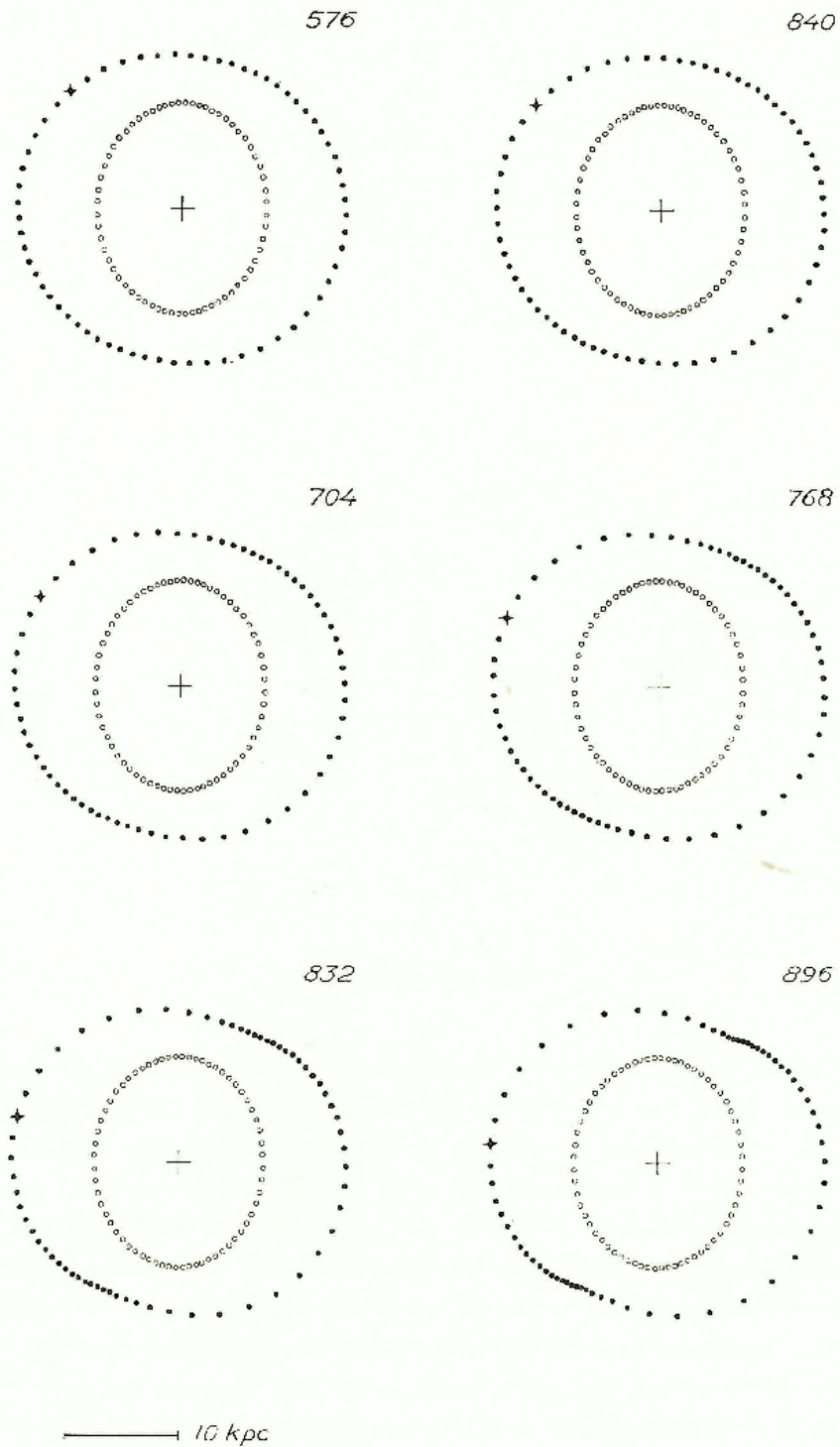
Fig. 15. Dispersion ring I and ring of massless particles with $R_0 = 14$ kpc.
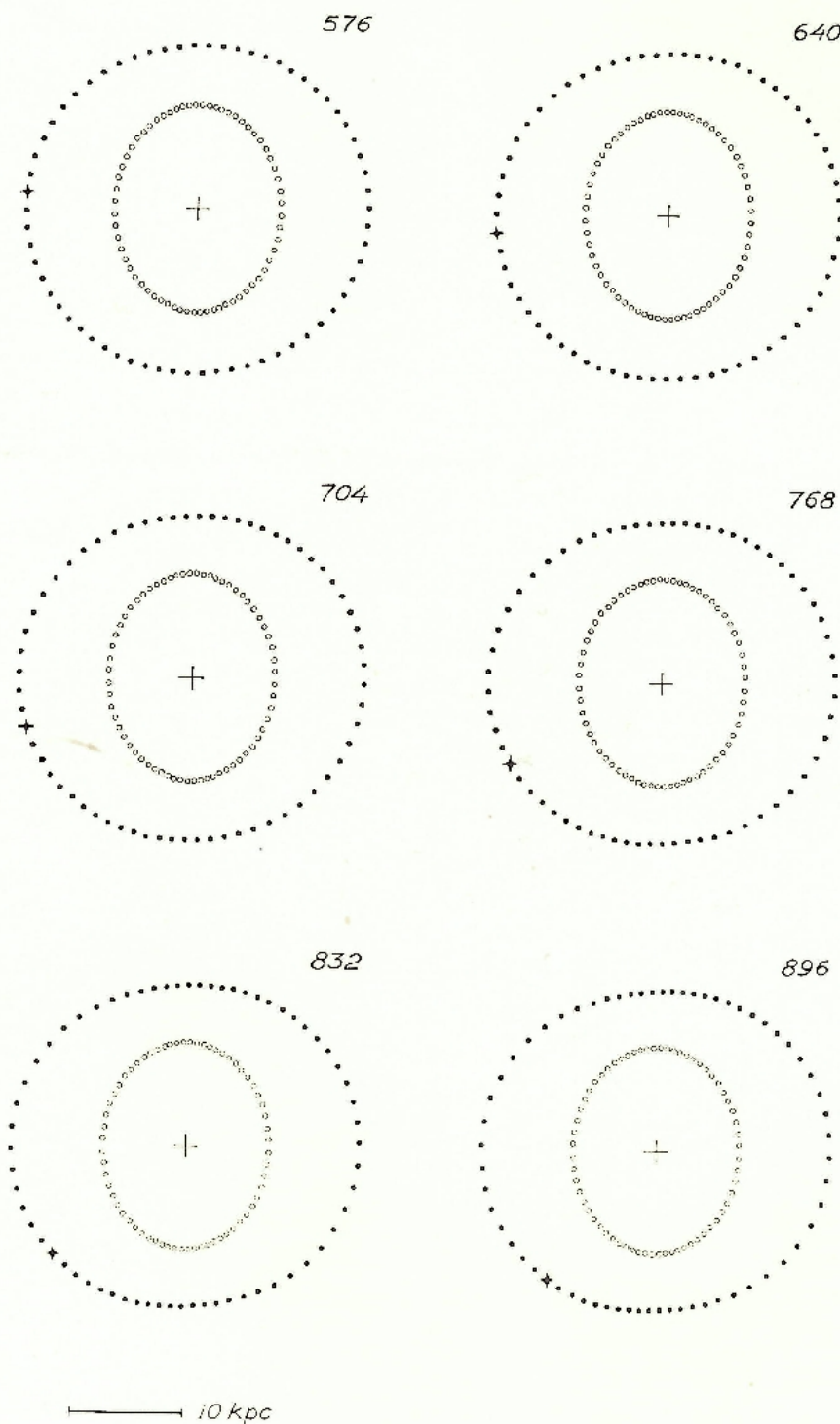
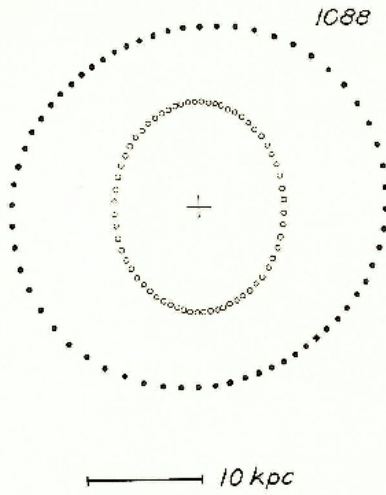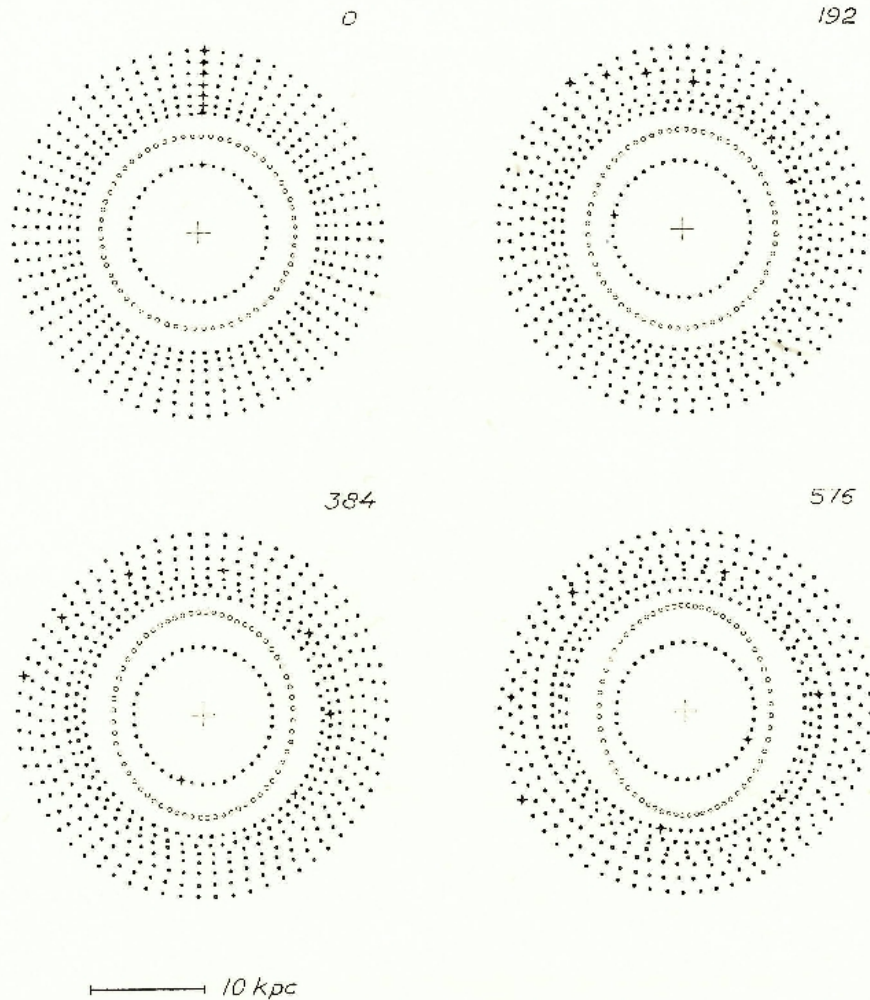Fig. 16. Dispersion ring I and ring of massless particles with $R_0 = 15$ kpc.

1088

|⟶⟶⟶⟶| 10 kpc

Fig. 17. Dispersion ring I and ring of massless particles with $R_0 = 16$ kpc.

0   192

384   576

|⟶⟶⟶⟶| 10 kpc

Fig. 18. Combined picture of the computations of Figs. 12–17 and two additional cases with $R_0 = 10.5$ and 6 kpc. The massive dispersion ring (open circles) develops from a circular ring, and after it has reached its final shape at $T = 576 \cdot 10^6$ years, it rests fixed in the coordinate system that rotates with the angular velocity of the apsidal line.

640

704

768

832

896
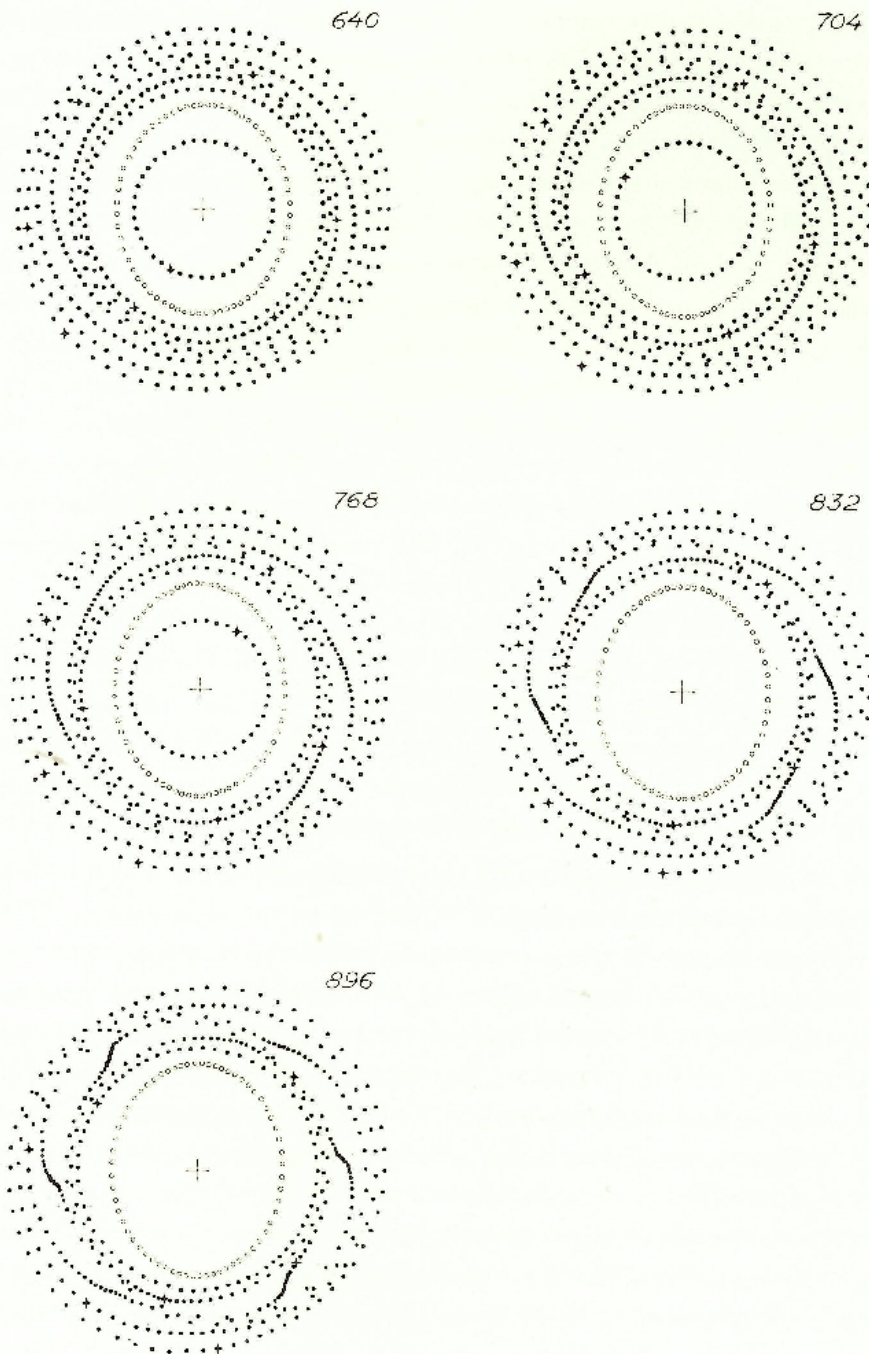
├──────┤ 10 kpc

Fig. 18 cont.

sweep together matter from a region around the resonance distance, where the angular speed of rotation ω is equal to the angular velocity ω' of the perturbing wave, and in the first instance towards this resonance distance. A stable ring cannot exist here and two diametrically opposite aggregates will probably be formed as in the case of Fig. 14 ($R_0 = 13$ kpc), or rather, as these aggregates will be fairly massive, in a way similar to the case of a massive ring at resonance distance to be demonstrated in the next chapter (Fig. 19).

It seems likely that the final result is a re-distribution of matter in the neighbourhood of the resonance distance leaving a zone swept free of matter, except for the two aggregates mentioned, so that the outermost parts of the galaxy are left in a separated, fairly loose ring. The suggestion is that this may be the cause of the annular formations of for instance NGC 4736 (M 94) (Plate I) and NGC 7217 (Plate II). Such outer rings are rather common, according to G. DE VAUCOULEURS (1959), near the transition stage S0 to Sa or SBa, but they appear in later types too, as for example NGC 3344. They are denoted by an (R) in the classification scheme of DE VAUCOULEURS. The outer ring is generally connected with the inner spiral structure in two diametrically opposite points.

It may be pointed out that the distance R for which $\sigma = 0$, i.e. where $\omega = \omega'$ and ω' equals a mean value of $\omega - \frac{1}{2}\varkappa$ for the inner regions, is 14 kpc in the Galaxy (Fig. 3) and 23 kpc in the Andromeda Nebula (Fig. 4). In both cases this is very close to the distance where the hydrogen density drops to zero (VAN DE HULST, RAIMOND and VAN WOERDEN, 1957, Fig. 10), and it may be that the density waves in the interior of the kind discussed are the agents which, by resonance effects, determine the limit of extension in the principal plane of Sa-Sb galaxies.

For the inner dispersion rings II or III the resonance radii for $\sigma = 0$ are about 16 and 13 kpc respectively. The effects here must be of the same kind as for ring I, but much slower, and these rings are of more interest in studies of the effects over regions where $\varkappa \approx \sigma$.

At first the influence of dispersion ring II with mass-points of unit mass was tested. As only very small effects could be traced in outer circular rings with radii 8 and 12 kpc (for $R_0 = 8$ kpc up to the time $T = 1216 \cdot 10^6$ years), dispersion ring III was introduced. This ring has a greater elongation and a more rapid rotation of the apsidal line. m was given the value 4 units so that the total mass was 3 times the mass of dispersion ring I, roughly corresponding to the difference in densities in the galactic plane according to SCHMIDT's model.

This dispersion ring too was successively elongated from a circle in ten steps until it reached its final shape after $576 \cdot 10^6$ years. The motions of outer massless rings with $R_0 = 6$, 8, and 10 kpc were computed up to the epochs $T = 832$, 1216, and $576 \cdot 10^6$ years respectively. However, the deviations from circular symmetry remained very small. For $R_0 = 8$ kpc, where $|\varkappa - \sigma|$ is very small, the difference between maximum and minimum R keeps about 0.08 kpc. The position angle θ of the apsidal line approaches $+45°$ in agreement with the theory. For $R_0 = 10$ kpc, where $\varkappa - \sigma$ is of the order of 4 km/sec·kpc, the full amplitude is 0.21 kpc at $576 \cdot 10^6$ years, and θ approaches $+5°$. In the case $R_0 = 6$ kpc the points scatter more, due to close passages by the massive points, and the small systematic perturbing effects are hidden.

The rapid motions along these rings, i.e. σ large in eqs. (11), thus seem to prevent the appearance of larger resonance effects. This was anticipated already in the case of dispersion ring I and $R_0 - 10.5$ kpc where the perturbing effects were also small. Thus, dispersion rings may not have a great gravitational influence on the motions in the inner parts of a galaxy, but may combine, probably with the aid of gasdynamical forces, as outlined by B. LINDBLAD, into a general wave giving stronger resonance effects in a region far out in the galaxy where σ is small.

It will be seen in Chapter V that the bar-type wave where $\omega' \approx \omega$, i.e. σ small in the neighbourhood of the ring, is of higher importance for the development of the inner parts of the galaxy.

IV. Interactions between a dispersion ring and massive circular rings

In the preceding chapter we have derived by computations with program F a survey of the perturbations from a dispersion ring on the motions in the galactic plane. If the perturbed configurations are rings of sensible mass, it would be of interest to investigate their counteraction on the dispersion ring and their mutual interaction. A number of computations with this aim have been undertaken with program E.

Outer ring at $R = 13$ kpc

As it has been shown in the preceding chapter that the dispersion ring has a tendency in the first phase to sweep together matter from a fairly wide zone to the resonance distance where $\sigma = 0$, it is natural to start with dispersion ring I and a circular ring of $R_0 - 13$ kpc. The initial angular velocities of the mass-points in the dispersion ring are decreased a little corresponding to the attraction of the outer ring, and the velocities are further corrected for self-gravitation by the method of "individual balancing". The circular velocities of the outer ring are corrected for self-gravitation and for the attraction from an imagined circular ring with a radius equal to the mean radius of the dispersion ring. All this is done by programs G and H.

The outer circular ring is built up by 64 points of unit mass, which makes it as massive as the dispersion ring. The motions in this model were computed in a coordinate system at rest, and the result is shown in Fig. 19. Parameters are given in Table A: 2.

The development starts in a manner very similar to the case of Fig. 14. The position angles of the maximal density and of the greatest elongation with respect to the apsidal line of the dispersion ring are in the present case somewhat smaller from the beginning than in the case of Fig. 14, which is due to the fact that we now start with a fully developed dispersion ring. As the density maxima of the outer ring develop, they contract also because of their own gravitation, and as they become more pronounced the aggregates take the shape of a small loop, formed at about $T - 600 \cdot 10^6$ years. The loops are formed roughly in line with
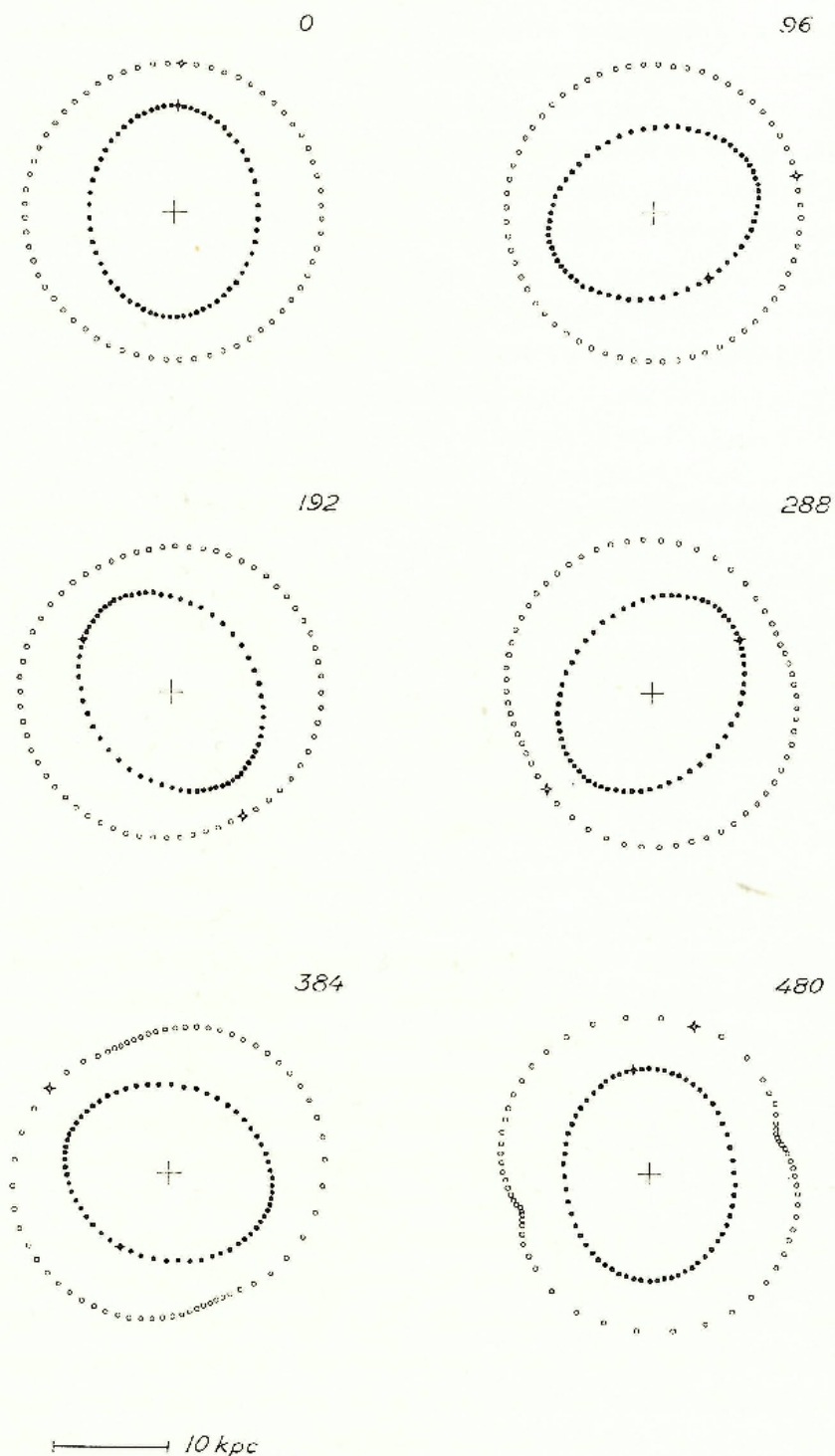
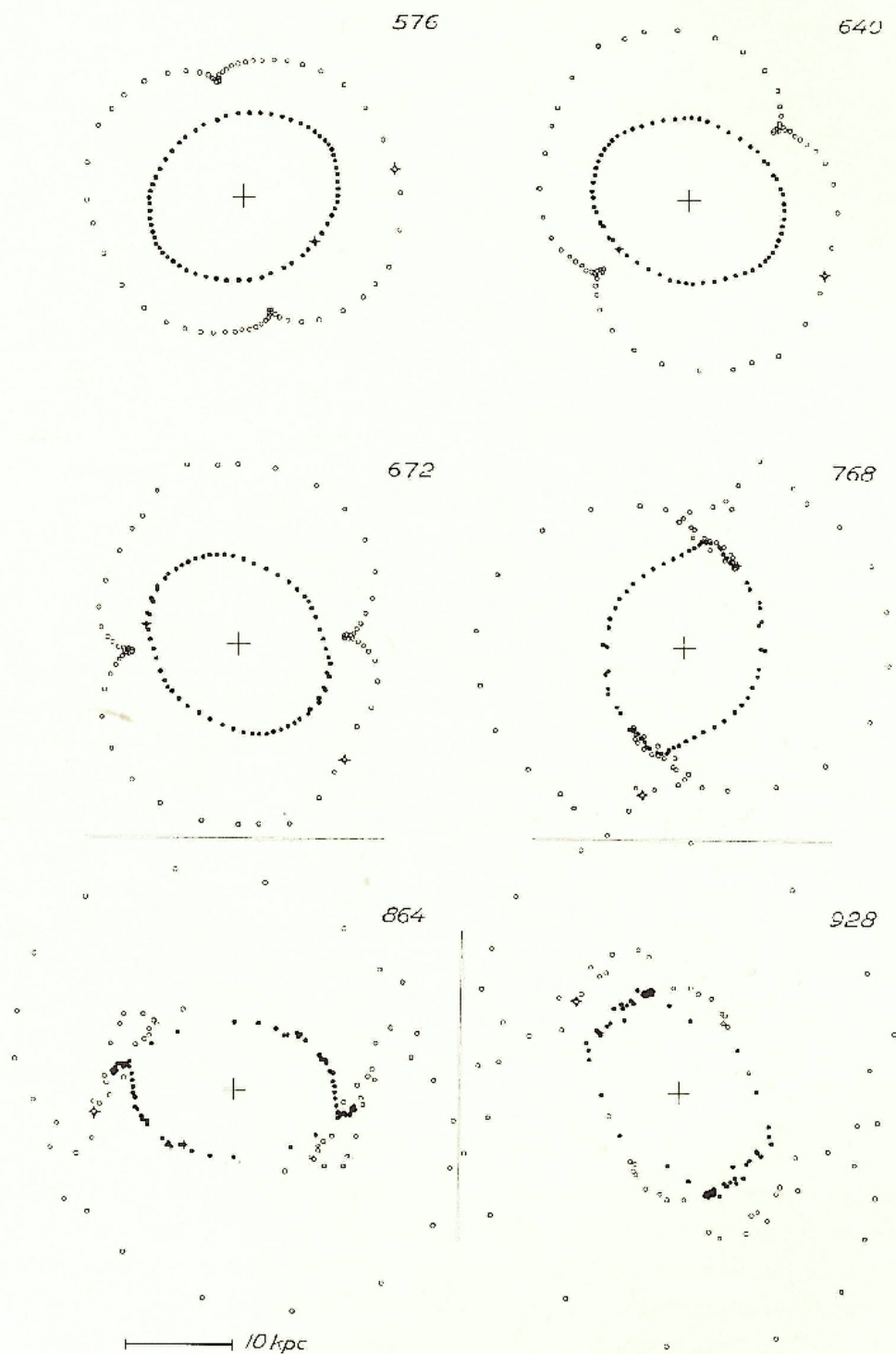Fig. 19. Dispersion ring I and an equally massive ring at $R = 13$ kpc.
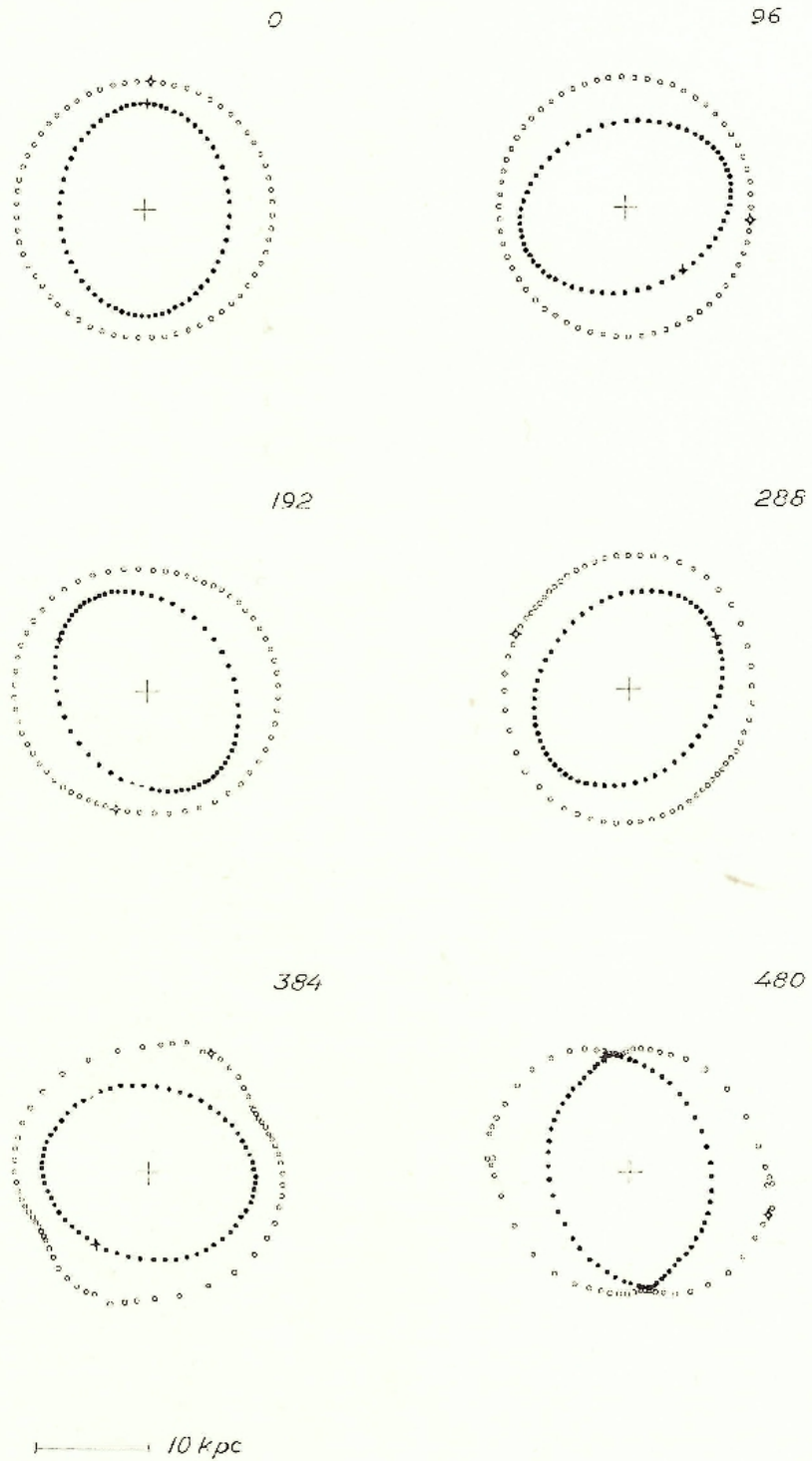
Fig. 19 cont.

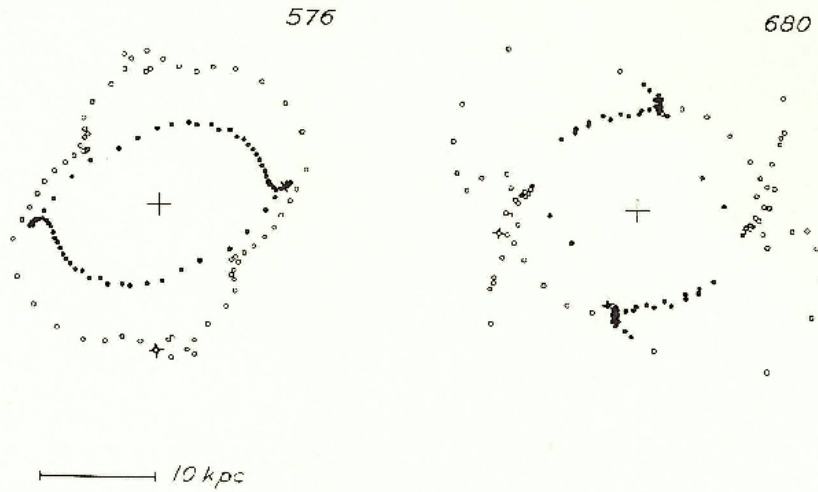Fig. 20. Dispersion ring I and an equally massive ring at $R = 11.25$ kpc.

Fig. 20 cont.

the minor axis of the dispersion ring. As may be seen from the sequence of Fig. 19 the loops are formed from points preceding the loops and decelerated in their motion due to the following concentration of matter. Thus, these aggregates diminish their distances from the centre to about 10 kpc, while the less dense parts of the originally circular ring are formed by particles accelerated in their motion and recede to great distances from the centre. At the same time as the distances of the aggregates decrease, their motion is speeded up and they begin to overtake the apsidal line of the dispersion ring. When the loops come close to the apsidal line a tidal wave is aroused in the dispersion ring, and the loops join the density maxima at the ends of the apsidal line in the dispersion ring ($T - 768 \cdot 10^6$ years). This causes the dispersion ring to break into two halves ($T = 864 \cdot 10^6$ years).

It may be that the aggregates that join and break up the dispersion ring correspond to the diametrically opposite connections between the outer ring and inner spiral structure in the (R)-type galaxies (Plate I–II). Conclusions regarding the direction of winding of spiral arms must, however, be drawn with caution from Fig. 19 as matter inside the dispersion ring has not been free to react.

Outer ring at $R = 11.25$ kpc

From Fig. 3 it is seen that just outside $R - 11$ kpc we have a region where $dx/d\omega = 2$, i.e. a region favourable for the forming of a dispersion ring. Hence the computations of the preceding section were repeated with $R_0 = 11.25$ kpc (Fig. 20). The evolution is similar though faster in the present case. Even now the denser aggregates formed in the outer ring hit the density maxima at the ends of the apsidal line of the dispersion ring, which are lifted out by a tidal wave, and this breaks up the dispersion ring.

Even now the elongation of the outer ring starts in a position angle $\theta \approx 3\pi/2$ ($T - 192$) in contradiction to the theory of the preceding chapter and the computations for a massless outer ring (Fig. 12). This is due to the circumstance that we start with a fully developed
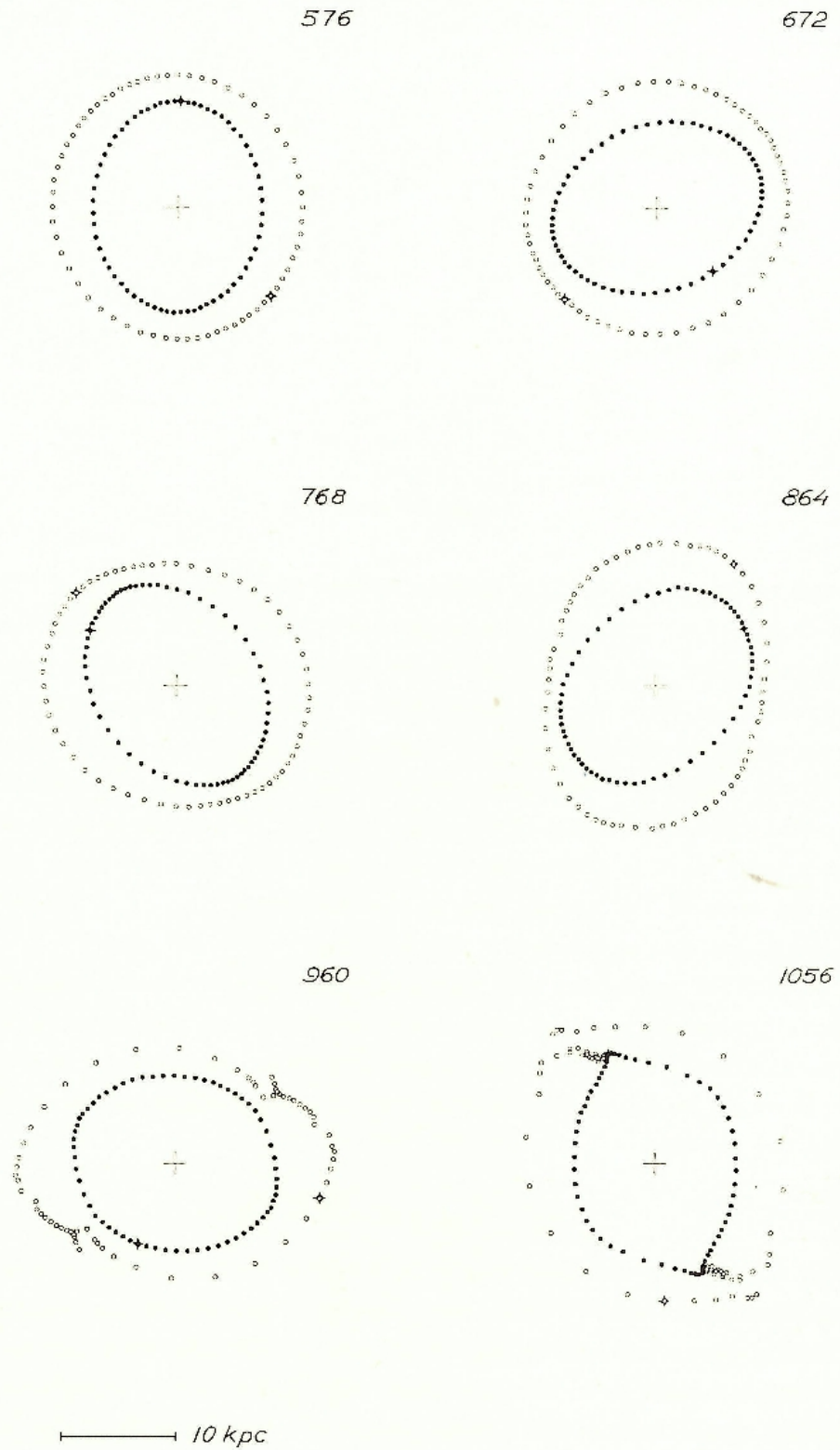
576

672

768

864

960

1056

⊢————→ 10 kpc

Fig. 21. Dispersion ring 1 and an equally massive ring at $R = 11.25$ kpc. The dispersion ring has been successively developed during the first $576 \cdot 10^6$ years.
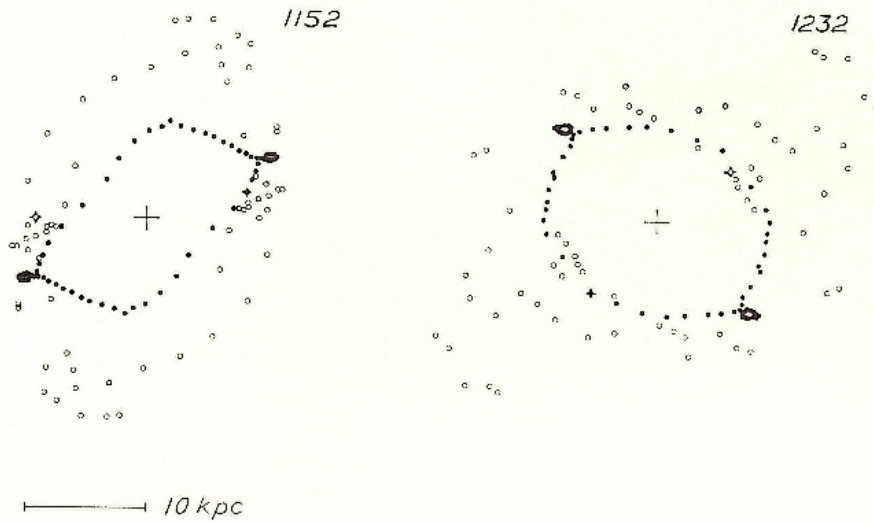
Fig. 21 cont.

dispersion ring that immediately, with full force, decelerates matter preceding and accelerates matter following the apsidal line.

To effectuate a more gentle start, we do not start from a circular outer ring but from the configuration at $T = 576$ million years of Fig. 12, i.e. the case of a massless outer ring at the moment when the dispersion ring is just fully developed. At that very moment all points are given equal mass, the points of the outer ring are given a slightly increased and the points of the dispersion ring a slightly decreased angular velocity to compensate for the addition of mass to the outer ring, and the computations are continued with program E (Fig. 21). The development now takes a slightly different course from the preceding case. The elongation of the outer ring becomes more pronounced ($T - 864$), but the aggregations of higher density ultimately shoot in as tongues of matter, again joining the density maxima of the dispersion ring ($T = 1056$) and cause its break-up.

Several outer rings

Finally, a number of cases with several outer rings simultaneously were computed.

In the case illustrated in Fig. 22 the initial configuration is composed of the dispersion ring I and the rings $R_0 = 11.25$ kpc and $R_0 = 13$ kpc at $T = 576$ million years of Figs. 12 and 14 respectively. Additional angular velocities are applied to the different rings to compensate as far as possible for the assignment of mass $m = 1$ to the points of the two outer ones. The density maxima of the outermost ring are fairly well developed from the start. They enhance the formation of density maxima in the ring of $R_0 = 11.25$ kpc, following the outer ones, by a mechanism similar to the one discussed in the next chapter. The maxima of the two rings join rather violently at $T - 864 \cdot 10^6$ years, and at the same time the rings are each broken up into two separate parts tending to form a pair of longer arms. The aggregates, however, soon spread out in the field of differential rotation, the preceding decelerated parts dive in to-

576

672

768

864

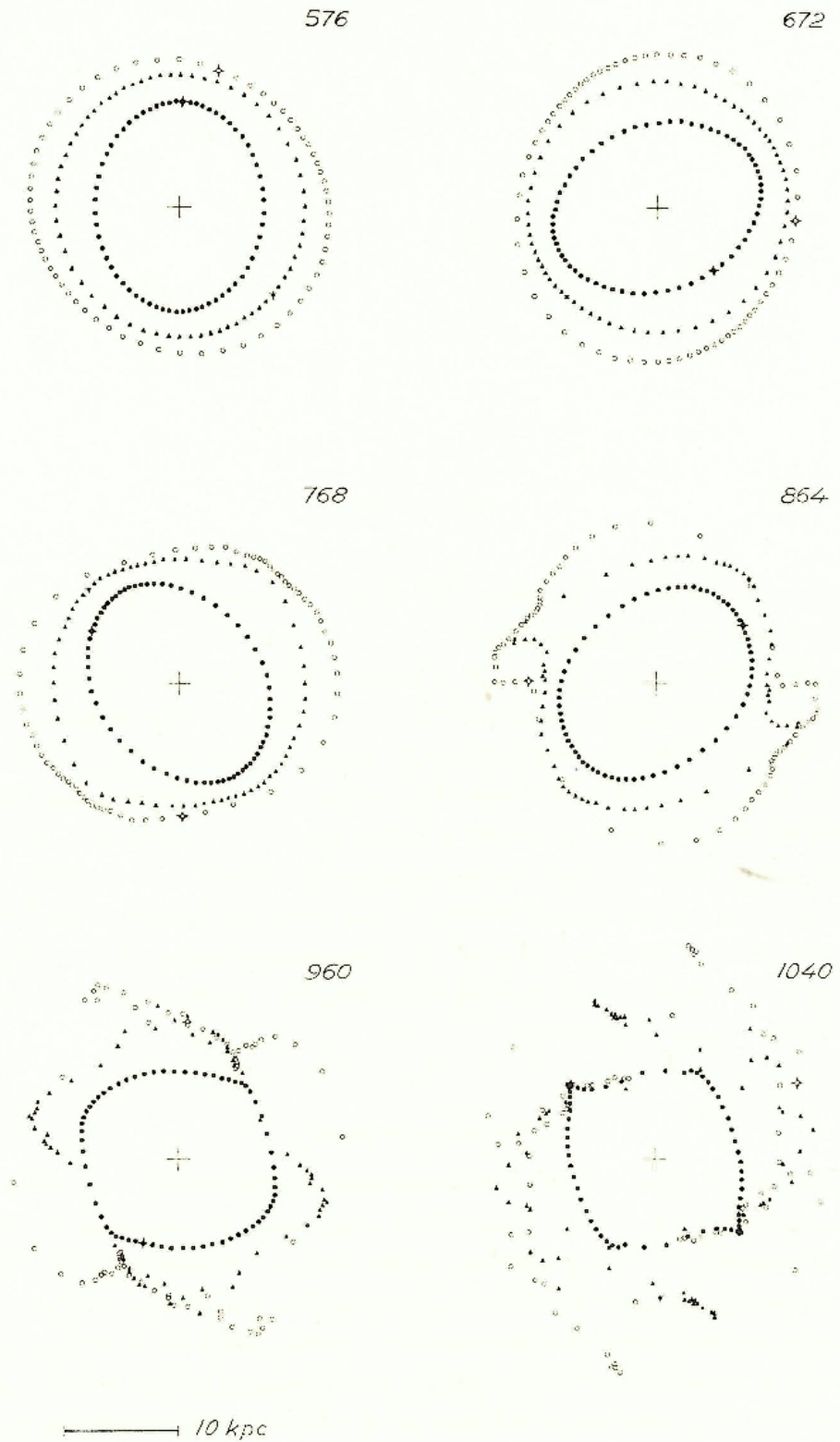960

1040

$\longmapsto$ 10 kpc

Fig. 22. Dispersion ring I and massive rings at $R = 11.25$ (number of mass-points $N = 64$) and 13 kpc. ($N = 64$). The mass of each mass-point $m = 1$ unit.
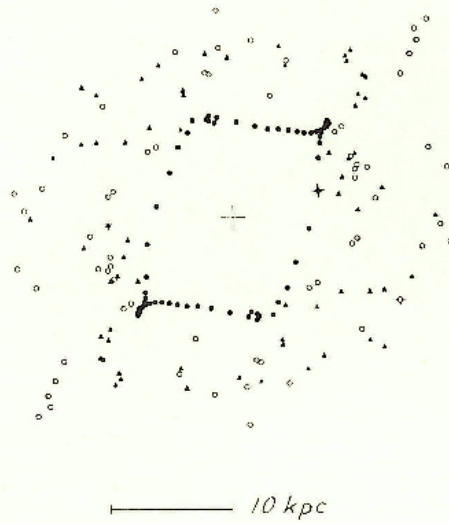
1136

—————— *10 kpc*

Fig. 22 cont.

wards the dispersion ring, and the following accelerated points move out and are left behind ($T = 960-1040$). Thus it seems that the original tightly wound leading arms transform into more open arms trailing against the direction of rotation. These trailing arms are fairly rapidly drawn out by differential rotation and get lost as the scatter of the mass-points increases. The points that dive in towards the dispersion ring break up that ring in a manner similar to that in the cases of the previous sections.

In order to bring about a more gentle combination of the two outer rings the masses of the points were halved, and the number of points in the outer rings decreased so that the ring $R_0 - 11.25$ kpc contains 48 mass-points and $R_0 - 13$ kpc 40 mass-points. The stage during which the outer rings are massless and the dispersion ring is successively formed in ten steps, was extended to 864 million years. The results of the computations are shown in Fig. 23.

The general character of the development is the same as before. The ring at $R = 11.25$ kpc which is not at resonance distance reacts much less violently than in the previous case. The arms that in the beginning have the character of leading spiral arms (up to $T - 1344$), bend in to form two big arcs on both sides of the dispersion ring ($T - 1440$). These arcs soon lose their contact backwards and are transformed into trailing arms, more and more drawn out.

In order to give the outer regions of the model more the character of a continuous layer than of distinct separate rings, an additional ring of 48 mass-points and $R_0 = 10$ kpc was introduced. The number of mass-points of the outermost ring was decreased to 32. The development of this model (Fig. 24) repeats faithfully stage by stage the development of the previous one, as is seen by a comparison between Figs. 24 and 23, although the features are now more concealed. The increasing internal velocity dispersion ultimately gives the figures a somewhat chaotic character.

The computations of the present chapter have shown, exactly as in the "massless" cases of the preceding chapter, that the immediate effect of the action of a perturbing wave
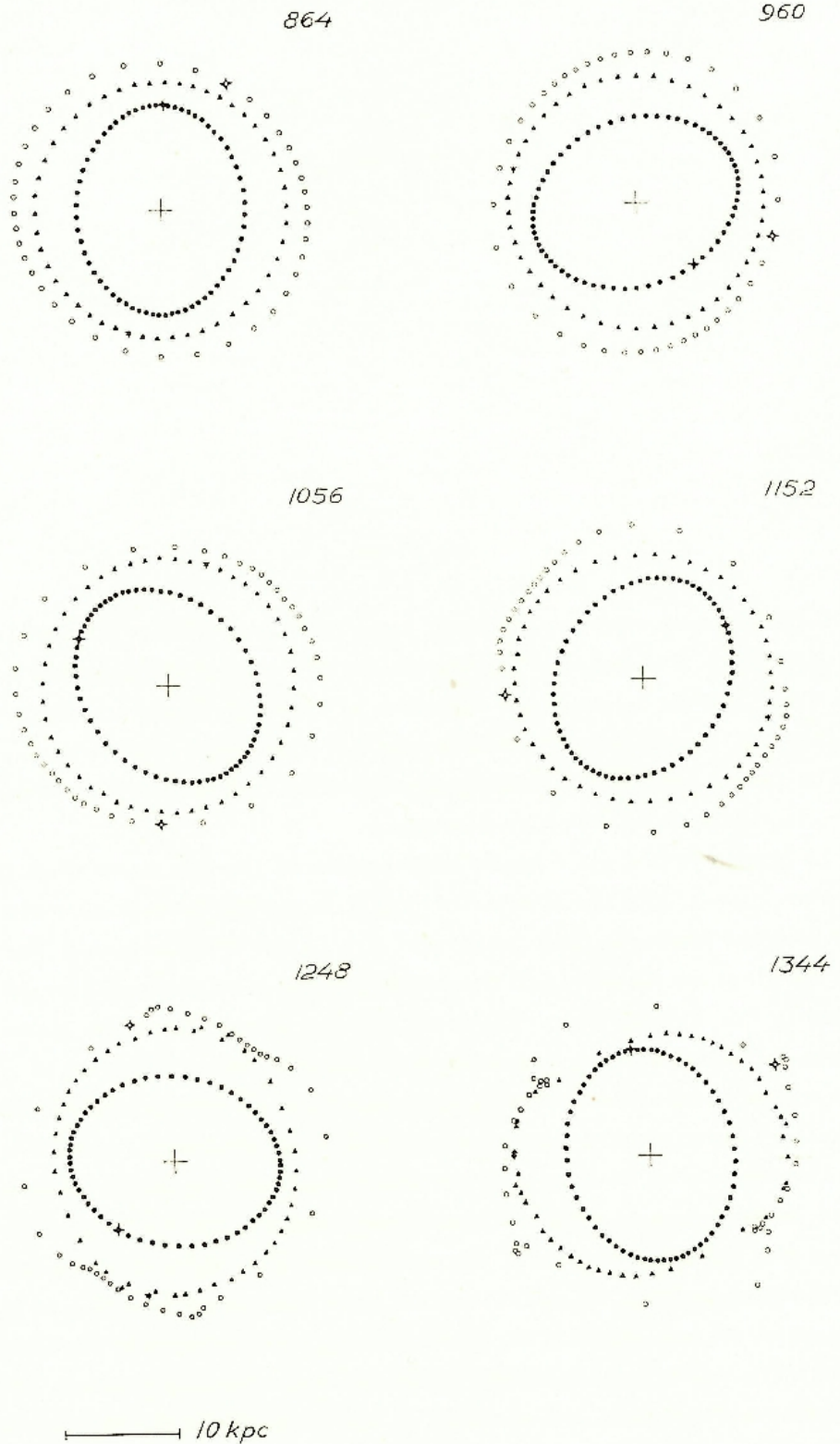
Fig. 23. Dispersion ring I and massive rings at $R = 11.25$ ($N = 48$) and 13 kpc. ($N = 40$). $m = \frac{1}{2}$ unit.
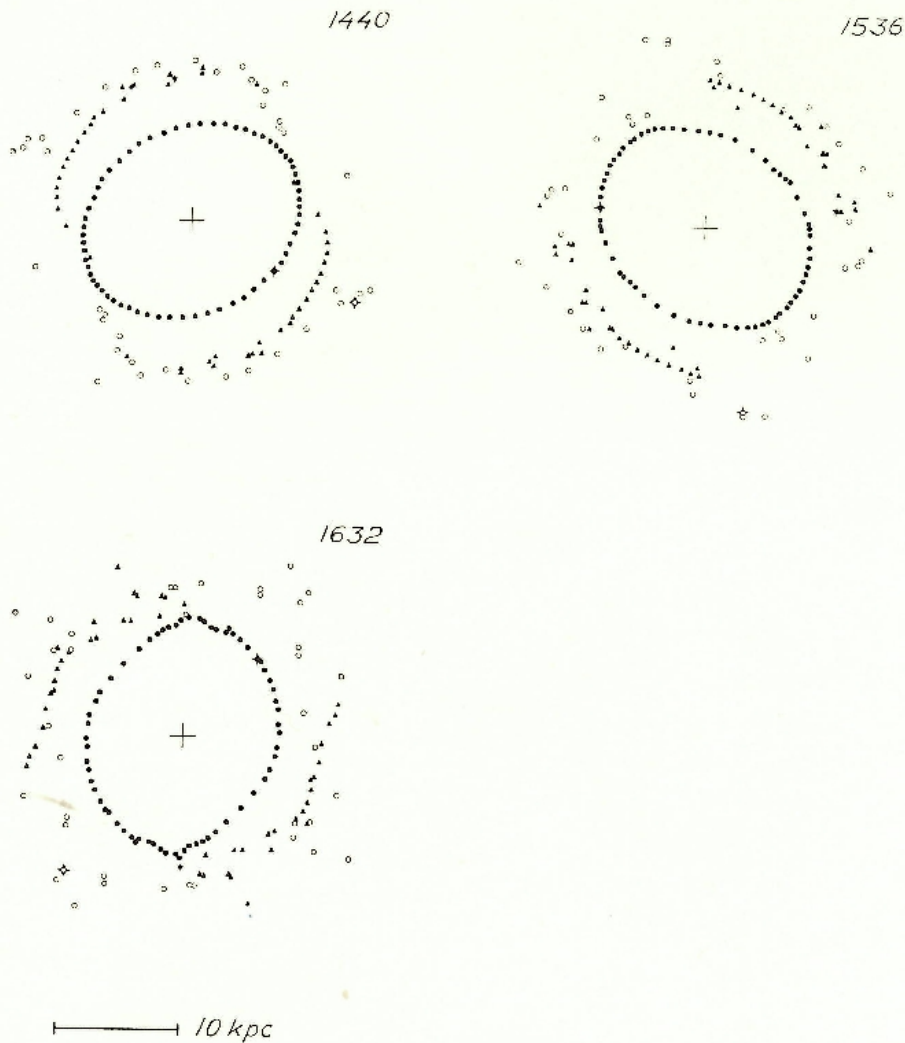
1440

1536

1632

⊢————————⊣ *10 kpc*

Fig. 23 cont.

of the type considered on outer massive rings is to cause an elongation of these rings and a concentration of matter along the branches outgoing in the direction of rotation. If the outer rings are sufficiently massive, and the perturbing wave has the shape of a simple dispersion ring, the concentrations in the outer rings will ultimately break up this dispersion ring.

The kind of leading spiral arms that appear in the beginning of the development (as for instance at $T = 1248$ in Figs. 23 and 24) are not conditioned by the initial ring structure of the outer regions but will appear in a continuous medium as well. Whether the tendency of these arms to transform into trailing arms (after some time) will be found in arms of gas in real galaxies cannot be stated with certainty. The transformation of these arms into trailing ones implies a complete break of the ring and a loss of contact backwards with the dispersion ring (Fig. 23, $T = 1344$–1536), or in a more continuous medium a division into larger or smaller aggregates subsequently drawn out by differential rotation (Fig. 24, $T = 1536$). This evolution may to some extent be counteracted by stabilizing agents as
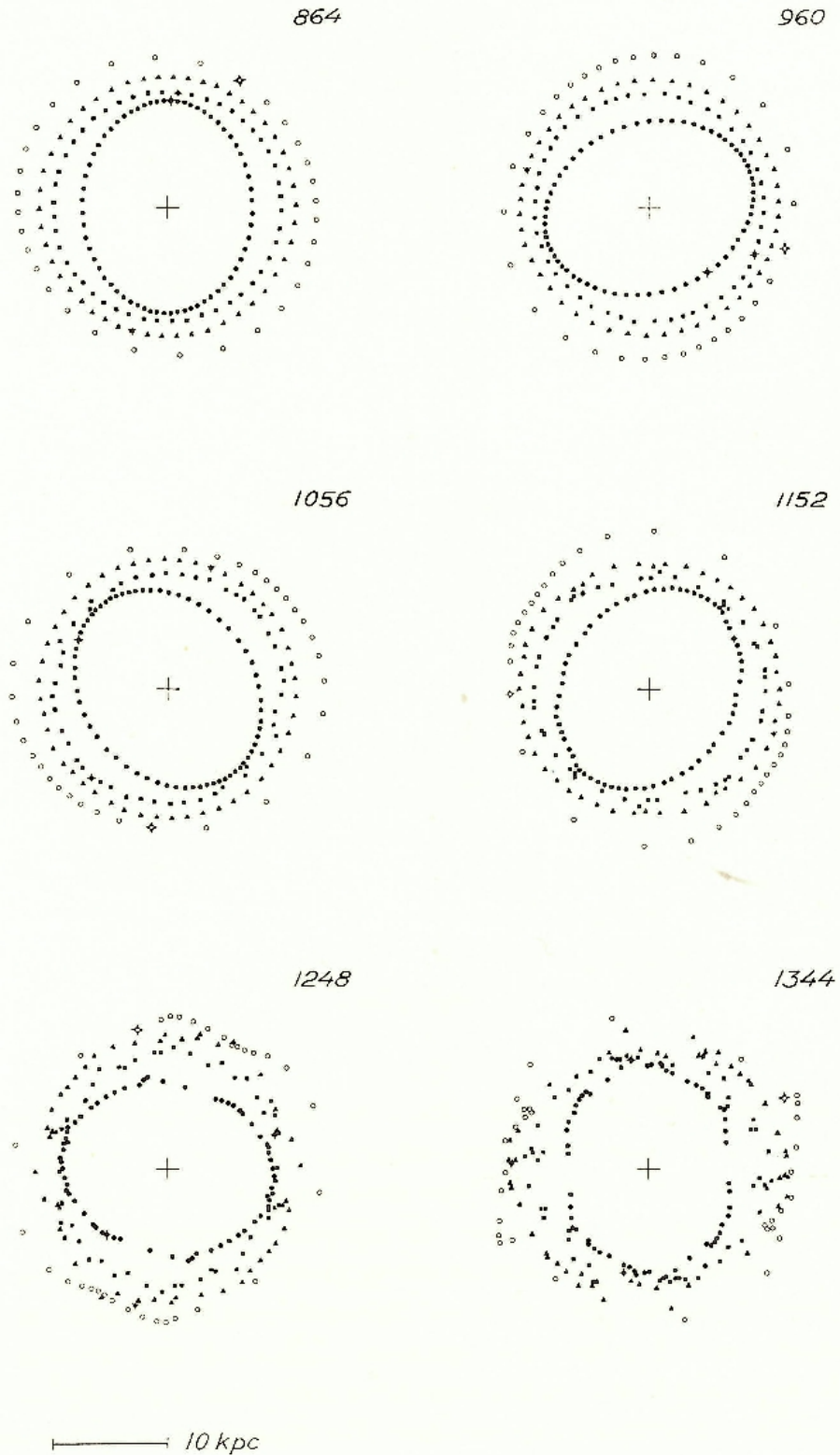
864   960

1056   1152

1248   1344

├────────┤ 10 kpc

Fig. 24. Dispersion ring I and massive rings at $R = 10$ ($N = 48$), 11.25 ($N = 48$) and 13 kpc ($N = 32$). $m = \frac{1}{2}$ unit.

1440   1536

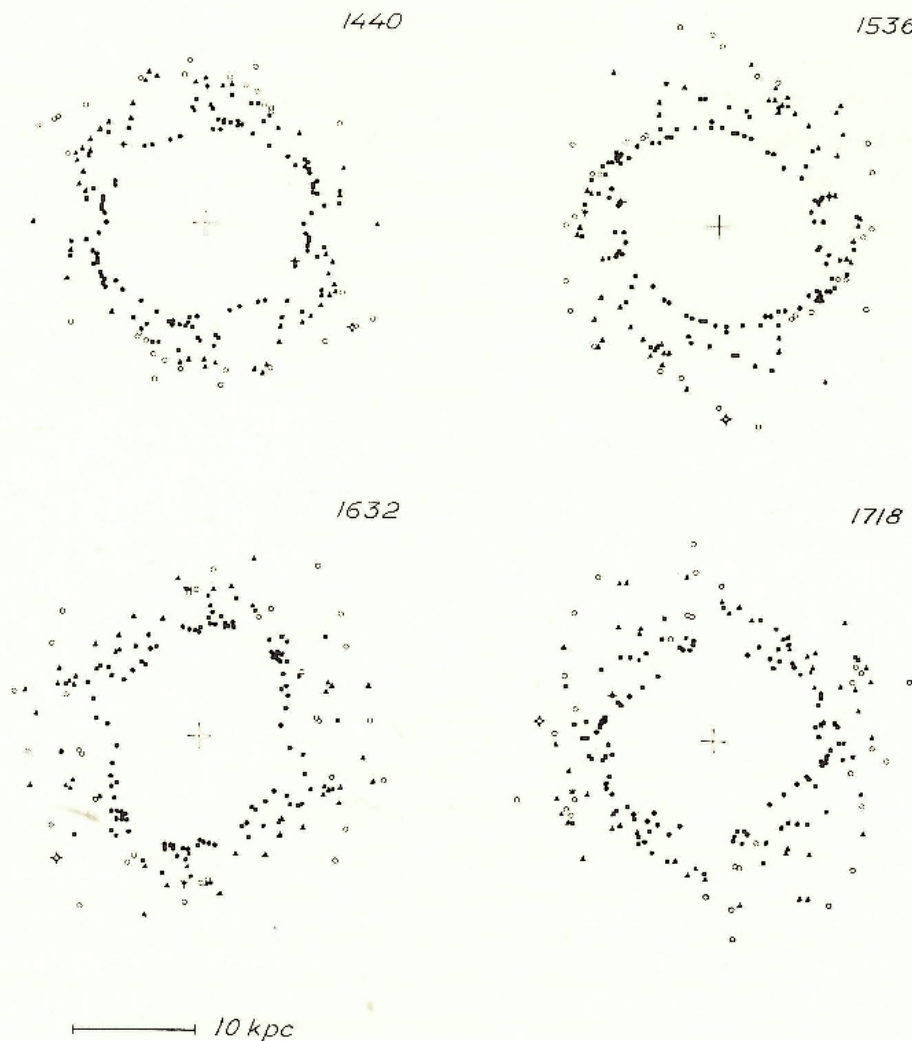1632   1718

⊢———⊣ 10 kpc

Fig. 24 cont.

magnetic fields and viscous forces if the arms are thought to be mainly arms of gas. Other computations that show more clearly a transition from leading to trailing arms will be demonstrated in the next chapter.

V. Bar-type waves

By "bar-type waves" we mean here the kind of bisymmetrical density waves proceeding with approximately the circular velocity of angular motion in the galactic plane as described by B. LINDBLAD and LANGEBARTEL (1953, case $s = 2$) and B. LINDBLAD (1958b, case $\sigma \rightarrow 0$). As shown by LINDBLAD and LANGEBARTEL this wave is the most important in a series of density waves, all travelling with approximately the velocity of circular motion, and with different degrees of asymmetry. In the model computations we let the initial wave be carried by a circular ring of matter. Unlike the dispersion ring type of wave treated in previous chapters this one should have its greatest perturbing gravitational influence on neighbouring matter.

Preliminary computations

In order to find out the amplitude of the density wave necessary to cause a sensible effect on surrounding matter a special kind of artificial steadily growing "bar" was constructed. Starting from a circle with radius 4.31 kpc, which was the mean radius of dispersion ring III, and consisting of 48 evenly distributed mass-points, we let the mass-points slide in steps along the circumference of the ring in such a manner that the ratio of neighbouring intervals between mass-points at any certain moment keeps a constant value when we go along the circumference of the ring from the y-axis to the x-axis. This constant, k, increases with each step, and is given for the sequence of configurations in Table 6. In Fig. 25 configurations 1, 3,

TABLE 6.

Config.	k	Config.	k
1	1.000	5	0.796
2	0.981	6	0.714
3	0.934	7	0.623
4	0.870		

5, 6, and 7 are shown by open circles. To the mass-points are given masses of $\frac{1}{2}$ unit, and the configurations are introduced in turn as the fixed massive configuration of program F. A change from one configuration to the next in the sequence is made every $64 \cdot 10^6$ years.

The influence of this massive growing bar-type wave on two rings of massless points with radii 4 and 5 kpc was tested with program F. The wave was supposed to proceed with circular angular velocity, i.e. the angular velocity of the coordinate system used, in which the wave rests fixed, was chosen to be the circular angular velocity at $R = 4.31$ kpc. The result of the computations is given in Fig. 25. At the start the massless rings were balanced in such a way that the configuration at $T = 0$ would be in equilibrium if the massive ring remained unchanged. As the bar-type wave develops, matter following the density maxima is accelerated and lifted outwards, and matter preceding is decelerated and falls inward (cp. LANGEBARTEL, 1951, Fig. 1). The perturbing force from the bisymmetrical density distribution may be developed in a Fourier series as in eqs. (5). Thus the theory of Chapter III is valid to the first order, and the case σ small that now occurs in the immediate neighbourhood of the wave-carrying ring itself is here of the greatest interest. The approximation (14) and the subsequent reasoning, since D_1 is still a negative quantity, are valid for the first stages of the development. For the outer massless ring with radius 5 kpc, $\sigma < 0$ and the ring becomes elongated in a direction θ slightly exceeding $\pi/2$ with concentrations of matter close to the ends of the minor axis or just in front of the bar. For the inner ring with radius 4 kpc, $\sigma > 0$. The elongation of this ring takes place in a direction between $3\pi/4$ and π, and matter concentrates along the outgoing branches behind the apsidal line. As the bar grows, the effects on the surrounding rings become very pronounced. It should be pointed out that the mass of the fixed ring carrying the increasing bar-type wave is only 1/8 of the mass of dispersion ring III.
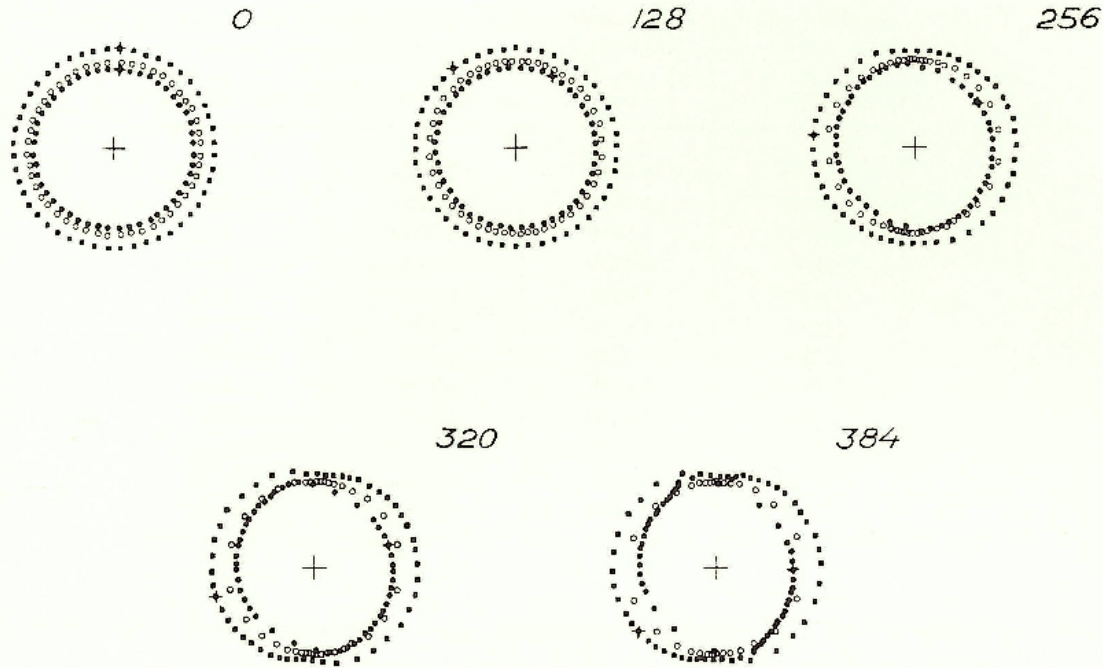
Fig. 25. The influence of a growing bar-type wave (open circles) on neighbouring circular rings of massless particles. The coordinate system rotates with the angular velocity of the wave.

Guided by these computations we now choose as the fundamental structure carrying the bar-type density wave in our computational models, a circular ring of mass-points with a density distribution similar to configuration 3 of the growing artificial "bar", where the ratio of adjoining intervals between neighbouring mass-points is 0.934. This ring is shown by open circles in Fig. 25, $T = 128$, and again in Fig. 26, $T = 0$. The radius of the ring is 4.31 kpc, and the number of mass-points 48. The maximum density at the y-axis is 2.33 times the minimum density at the x-axis.

We now firstly wish to study the behaviour of an isolated ring of that kind. The mass-points are given masses of 4 units, so that the total mass of the ring and its radius are the same as the mass and mean radius respectively of dispersion ring III. We give the mass-points initial angular velocities of 50.25 km/sec·kpc, which would be the circular velocities of equilibrium if the mass distribution along the ring had been even.

The initial positions and velocities are given in Table 7. The motion of the ring was integrated with program E, and the result is shown in Fig. 26.

As we get outgoing motions in the quadrants following and ingoing motions in the quadrants preceding the density maxima, the first effect of the uneven mass-distribution is to cause an elongation of the ring. Along this elongated ring the mass-distribution is fairly uniform. After an interval of about 200 million years the ring has again circular shape with a mass distribution similar to the initial one. The evolution of the ring thus seems to consist in a cyclic oscillation between circular and elongated shape with a period of about 200 million years. This oscillation can be interpreted as the superposition of two interfering waves, one

TABLE 7. *Initial positions and velocities in the first quadrant of the ring of Fig. 26.*

x kpc	y kpc	$\dot{x}$ kpc/32 · 10^6 years	$\dot{y}$ kpc/32 · 10^6 years
0.1818	4.3062	7.0849	− 0.2991
0.5688	4.2723	7.0291	− 0.9358
0.9781	4.1976	6.9062	− 1.6092
1.4067	4.0739	6.7027	− 2.3144
1.8487	3.8934	6.4057	− 3.0416
2.2967	3.6471	6.0005	− 3.7787
2.7396	3.3273	5.4743	− 4.5074
3.1658	2.9247	4.8119	− 5.2086
3.5562	2.4350	4.0063	− 5.8509
3.8912	1.8533	3.0492	− 6.4021
4.1448	1.1820	1.9447	− 6.8193
4.2889	0.4256	0.7002	− 7.0564

travelling with a velocity slightly exceeding that of circular motion and with density maxima at the minor axis, the other proceeding with a velocity slightly less than the velocity of circular motion and with density maxima at the major axis. The mean value of the velocities of the two waves equals the circular angular speed, and the phase difference increases with π in $200 \cdot 10^6$ years. These are the two waves decribed by B. LINDBLAD (1958 *b*, p. 15).

Owing to the oscillation of the ring between circular shape with uneven mass-distribution and elongated shape with more uniform mass distribution the angular velocity ω' of the perturbing wave will appear different from the point of view of a particle inside the ring and a particle outside. The angle θ in eqs. (5) should be counted from the direction of maximum potential along the circle with radius R_0. When the perturbing ring is circular this is the direction of the lines joining the density maxima. When the ring is elongated with uniform mass distribution along the circumference, the direction of maximum potential coincides with the minor axis for an R_0 smaller than, and with the major axis for an R_0 greater than the radius of the perturbing ring. Thus, for an *inner* particle, θ should be counted from the region of maximum density, when the ring is circular, continually shifting over to the region at the end of the minor axis when the ring is elongated (cp. Fig. 26). From the point of view of an inner particle the perturbing wave then seems to travel with the velocity of the faster of the two interfering waves, or in the present case an angular velocity of 57.94 km/sec·kpc. For an *outer* particle, θ should again be counted from the region of maximum density, when the ring is circular, but now shifting over to the end of the major axis when the ring becomes elongated. The perturbing wave now seems to travel with the velocity of the slower wave, or, in the case of Fig. 26, an angular velocity of 43.18 km/sec·kpc.

The action of the ring on neighbouring matter is enhanced by this circumstance, because the resonance region, where $\sigma = 0$, for the wave perturbing inner particles lies inside the ring, and for the wave perturbing outer particles outside the ring.
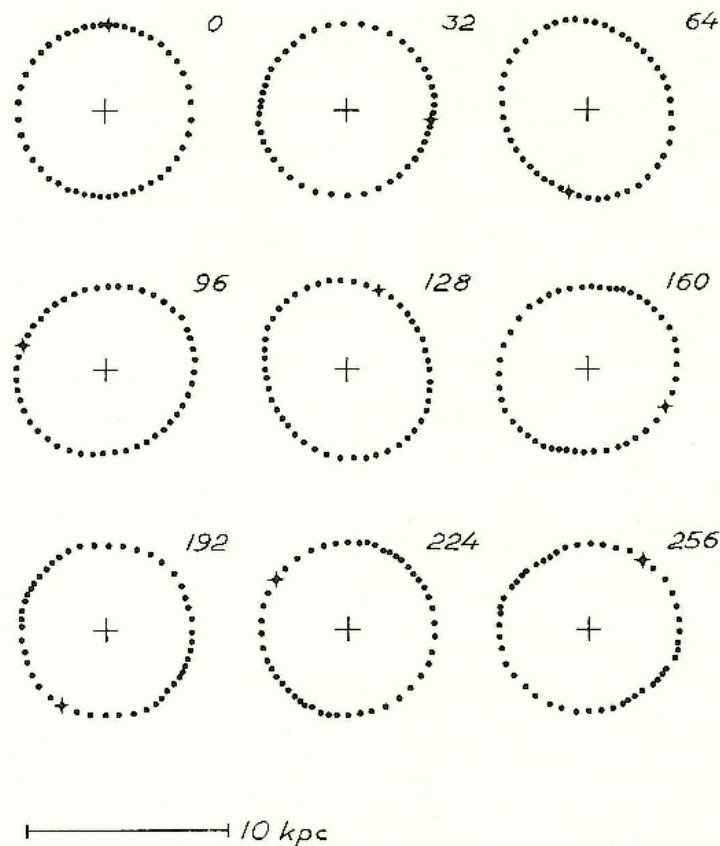
Fig. 26. Bar-type density wave in initially circular ring with radius 4.31 kpc.

The computations were repeated for a mass of the particles of two units. However, the wave then seemed to die out fairly soon, and it appears that the amplitude of the density variation has to be of a certain magnitude for the wave to maintain itself.

In spite of the fact that we cannot consider our ring model of Fig. 26 as a carrier of a simple density wave we will use this kind of ring to give the initial bisymmetrical deviation from rotational symmetry in our models of stellar systems.

The most important difference from the case of the dispersion ring type of wave is that the resonance region $\sigma = 0$ in the present case lies in the immediate neighbourhood of the ring. As, according to eqs. (14), the disturbances on a neighbouring ring of matter give rise to a density variation that travels with the same speed as the perturbing wave, i.e. close to the circular velocity, the secondary perturbations from this perturbed ring are large.

Fig. 27 shows computations with the ring discussed above and an equally massive, initially circular ring with a radius 3.31 kpc and even mass distribution. The initial velocities are adjusted by program H so that the configuration would be in equilibrium if the density distribution of the outer ring had been even. At first the density wave of the outer ring causes an elongation of the inner ring in a direction inclined about 45° to the line joining the density maxima of the outer ring, and concentrations of matter immediately following the vertices of the inner ring in accordance with the theory of Chapter III. This density wave in the inner ring acts back on the outer one in a corresponding manner. The elongation of this
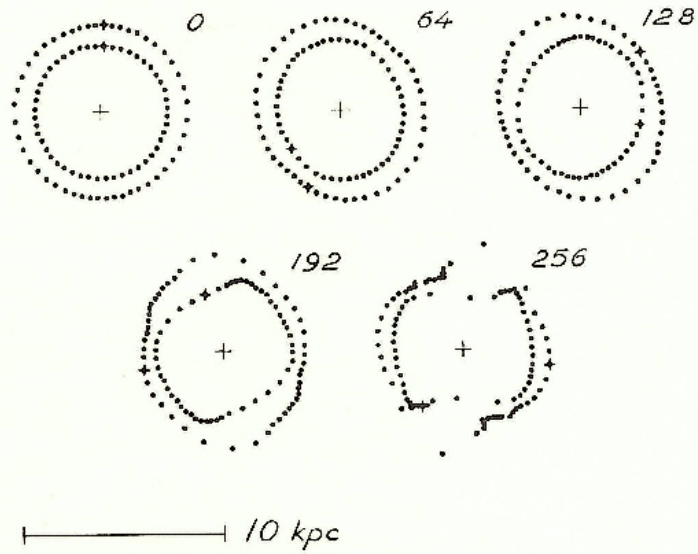
Fig. 27. Bar-type wave as in Fig. 26 and a massive circular ring at $R = 3.31$ kpc.
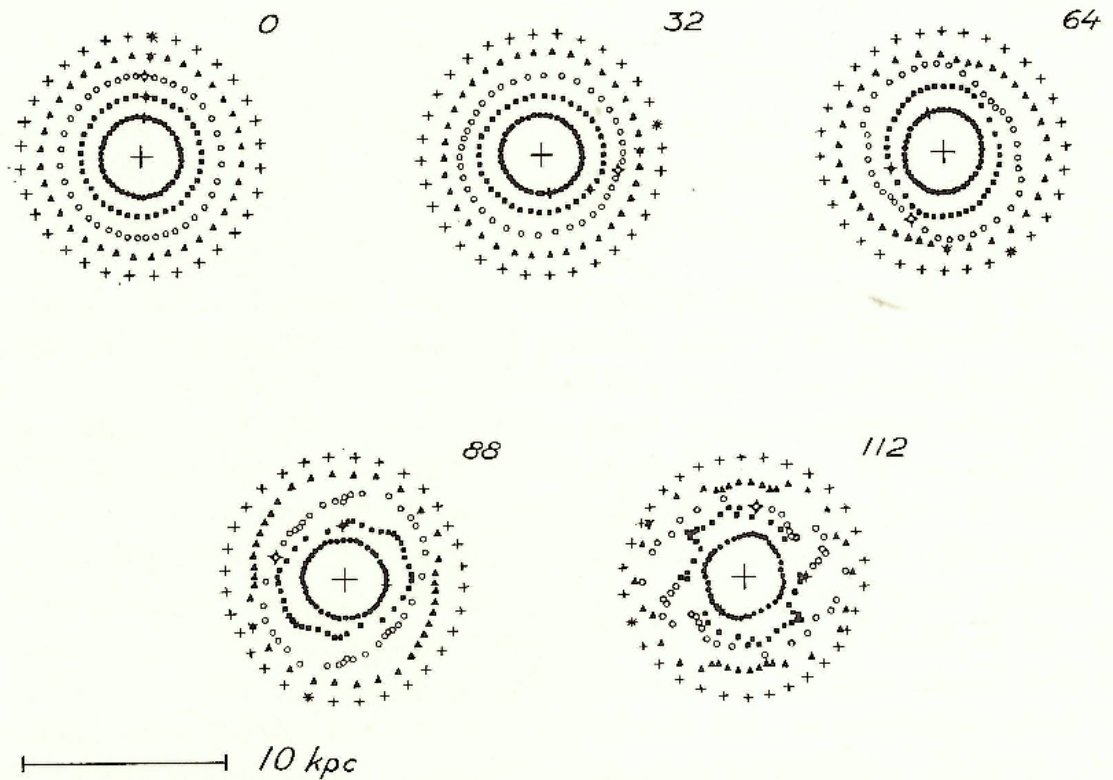
Fig. 28. Massive rings at $R = 2$ ($N = 44$), 3 ($N = 40$), 4 ($N = 40$), 5 ($N = 36$) and 6 kpc ($N = 32$). Bar-type wave in the ring with radius 4 kpc. $m = 4$ units.

ring is increased and the concentration of matter along the outgoing branches enhanced. Ultimately the ring breaks up into two halves. The inner ring too breaks up, but the character of its development is to some extent conditioned by the lack of free matter in the interior. Thus the central layer in a galaxy seems to be unstable for a density variation of the present kind.

Another example is shown in Fig. 28. Here the ring carrying the initial density wave has a radius of 4 kpc and consists of 40 mass-points. The density varies along the ring in the same manner as before, the ratio between neighbouring intervals between the mass-points still being 0.934. This ring is surrounded by four other circular rings with the radii 2, 3, 5, and 6 kpc and even mass distribution. The number of mass-points in these rings are 44, 40, 36, and 32 respectively, and the mass of each point is four units. Again the initial velocities are such that the configuration would be in equilibrium for even mass distribution in all five rings.

It is seen that the development is very rapid, and after only 88 million years the rings of $R_0 = 3$, 4, and 5 kpc tend to break up under formation of a spiral-like pattern. However, this pattern fairly rapidly breaks down, owing to the large masses and the small value 0.7 kpc of Δ_{min} (Table A: 2, No. 33), which gives a large internal dispersion.

Density wave at R = 4 kpc

3-ring model.—After these preliminary computations we are able to construct more carefully prepared models. As a guiding principle we wish to make the initial deviation from rotational symmetry in the density distribution as small as possible, i.e. just as large as is necessary to bring about the instability in the central layer.

We first choose as the agent carrying the inital density wave the ring with radius 4 kpc, consisting of 40 mass-points, used in the computations of Fig. 28. The initial coordinates of the mass-points in the ring are given in Table 8. We begin with a model consisting of three rings, where the other two have radii 2 and 6 kpc and are circular with even distribution of mass (Fig. 30, $T = 0$). The numbers of mass-points in the different rings are, starting from within, 44, 40, and 32. This reproduces roughly the gradient of density in the central layer of SCHMIDT's model as integrated between $z = \pm 0.25$ kpc.

We know from the computations of the preceding section that the density wave in the

TABLE 8. *Initial positions along the first quadrant of the wave-carrying circular rings with radii 4 and 2 kpc.*

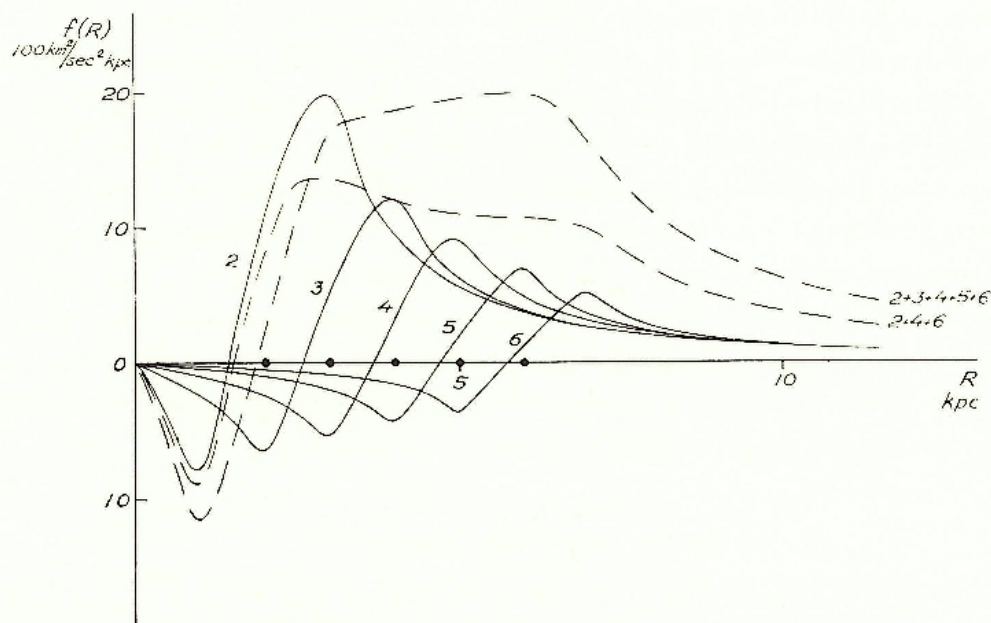| R = 4 kpc		R = 2 kpc	
x kpc	y kpc	x kpc	y kpc
0.2190	3.9940	0.0996	1.9975
0.6843	3.9410	0.3104	1.9758
1.1721	3.8244	0.5308	1.9283
1.6739	3.6329	0.7577	1.8509
2.1772	3.3555	0.9871	1.7394
2.6661	2.9819	1.2134	1.5898
3.1195	2.5037	1.4296	1.3987
3.5109	1.9166	1.6268	1.1634
3.8085	1.2228	1.7944	0.8832
3.9766	0.4320	1.9202	0.5594
		1.9903	0.1967

Fig. 29. Force of attraction from the different circular rings of the models of Figs. 30 and 31 computed for $m - 4$ units and $\Delta_{\min} = 1.133$ kpc.

ring of radius 4 kpc will be able to maintain itself for some length of time if the masses of the points are chosen at 4 units, but that it will probably die out rather soon if the masses are lowered to 2 units. Considering the fairly large distances between the rings we choose the value 4 units for the mass of a mass-point in order to give the model sufficient time to react before the wave dies out. Then the mass-points in the model together represent about $\frac{1}{4}$ of the total mass within the corresponding parts of the central layer. The radius $\Delta_{\min}$ of the non-Newtonian zone around each mass-point we choose at 1.133 kpc.

As the rings of mass-points thus represent a not negligible fraction of the mass, they will noticeably distort the central force function $F(R)$. In order to preserve as far as possible the central force of the Schmidt model also in the present model, we have to correct the tabulated force $F(R)$ for the influence of the rings.

With program G we can calculate the central force $f(R)$ exerted by each ring (the mass distribution in the ring $R_0 = 4$ kpc supposed to be even) at various distances R from the centre. This force is shown in Fig. 29 for the different rings together with the results for similar rings with radii 3 and 5 kpc that will be used in other models. m was 4 units and $\Delta_{\min} = 1.133$ kpc. The figure may be compared with SCHMIDT's (1956, Fig. 7) estimate of the force from the much less massive Orion arm. The broken line $(2 + 4 + 6)$ gives the somewhat smoothed sum of the forces from the rings with radii 2, 4, and 6 kpc. This smoothed force function is then subtracted from the tabulated central force $F(R)$.

Finally, the mass-points are given the appropriate initial circular velocities that would keep the configuration in equilibrium if the mass distribution were even in all rings, and the computations with program E can be started (Fig. 30).

From the beginning the ring at $R_0 = 4$ kpc (open circles in the figure), carrying the density

wave, oscillates in a way similar to the oscillations of the ring in Fig. 26. The ring with radius 6 kpc (filled triangles) lies slightly outside the resonance distance where $\sigma = 0$ for the slower wave. After about 200 million years this ring shows a perceptible elongation in a position angle slightly more than 90° with respect to the perturbing wave, and concentrations of matter along the outgoing branches fairly close to the minor axis, in accordance with the theory of Chapter III for the case σ slightly less than 0. This in turn causes an increased elongation of the ring of small open circles and an ultimate concentration of matter at the ends of the major axis. At T about 350 million years the density maxima of the two rings join. Matter preceding the joint density maxima is decelerated and falls inwards, while matter following is lifted outwards. Thus the two outer rings break in halves that join to form a pair of fairly long leading spiral arms ($T = 416$).

The filled triangles of the outermost ring will move inwards along the arms and the open circles outwards so that the arms get shortened, until practically all matter from these rings is concentrated into the two condensations that together with the central concentration constitute a bar ($T = 512$). The triangles that now have been effectively decelerated in their motions dive in towards the central parts of the sytem, while the open circles that have been accelerated are lifted out and spread out in the field of differential rotation ($T = 544$ 608). Thus we are faced with the somewhat surprising fact that the leading arms have changed over into trailing ones, and that the two outer rings have, in their entirety, changed places. The two configurations at $T = 448$ and $T = 576$ are rather similar, although they are quite opposite as regards the direction of winding and the location of the open circles and filled triangles.

The trailing arms are drawn out more and more by the differential rotation, and after $T = 640$ million years the structure is lost owing to the increasing velocity dispersion.

The inner ring with radius 2 kpc (filled circles) lies far inside the resonance distance for the faster wave and takes little part in the development. During the interval $T = 128$–320 it shows a distinct elongation in the direction of the density maximum or minor axis of the perturbing ring, with concentration of matter towards the vertici in agreement with the theory of Chapter III for σ positive and fairly large. When the outer structure becomes more complicated, several waves arise, and the ring keeps a more or less circular form.

5-ring model.—In order to obtain a more continuous model we add two new rings, one with a radius 3 kpc consisting of 40 mass-points and one of 36 mass-points with a radius 5 kpc (Fig. 31, $T = 0$). As the distances between the rings are now decreased, the radial transfer of a density variation is made much easier, and we can lower the mass of all mass-points to two units in order to make the surface density of the present model comparable to that of the preceding one, and at the same time follow the guiding principle of smallest possible initial density variation. The mass-points then together represent about $\frac{1}{5}$ of the mass of the corresponding parts of the central layer.

The sum of the attraction from all five rings as a function of distance from the centre is shown as the line $(2 + 3 + 4 + 5 + 6)$ in Fig. 29 for $m = 4$ units and $\Delta_{min} = 1.133$ kpc. This
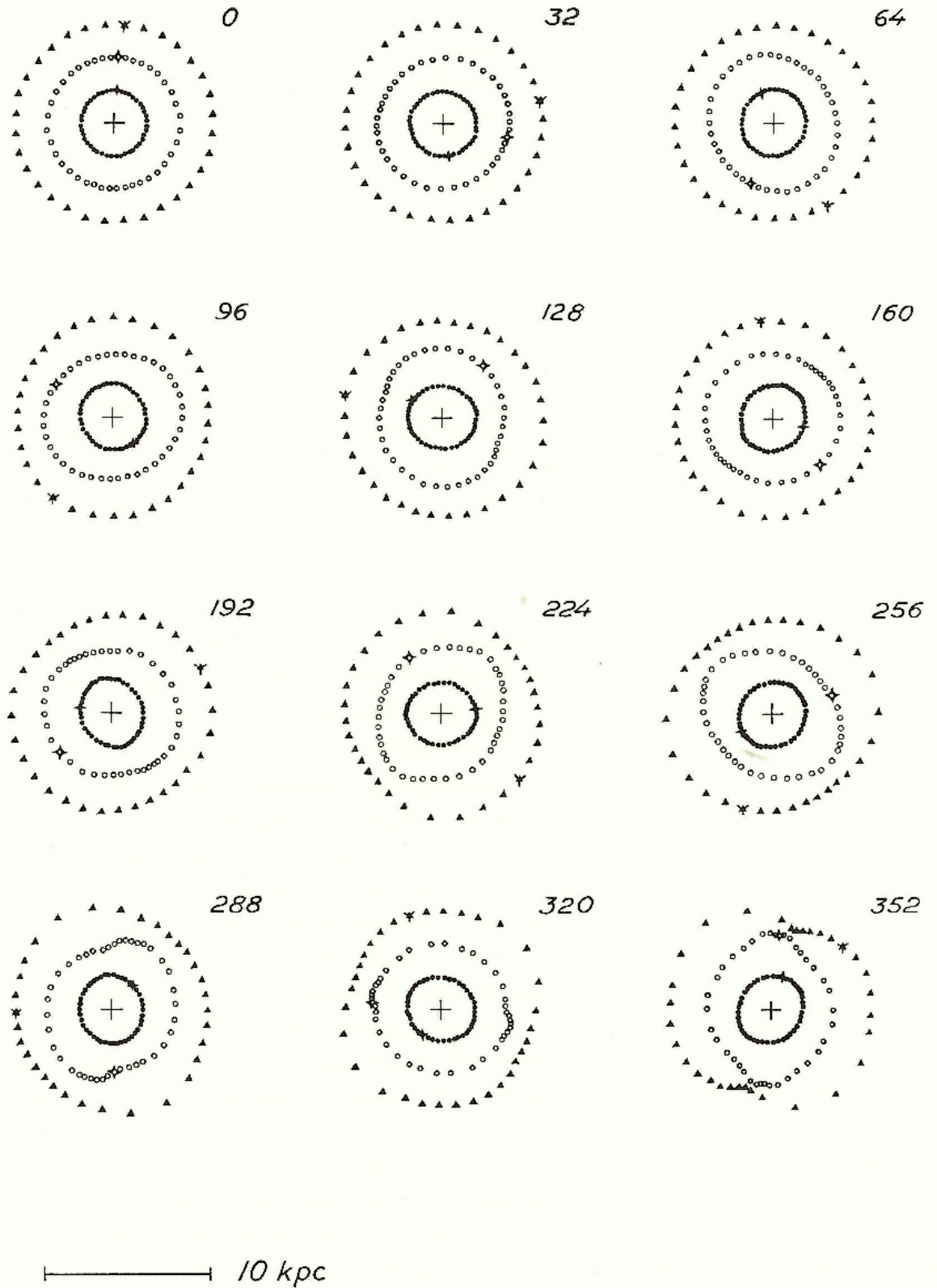
Fig. 30. Massive rings at $R = 2$ ($N = 44$), 4 ($N = 40$) and 6 kpc ($N = 32$). The ring at 4 kpc (open circles) carries the bar-type density wave. $m = 4$ units.
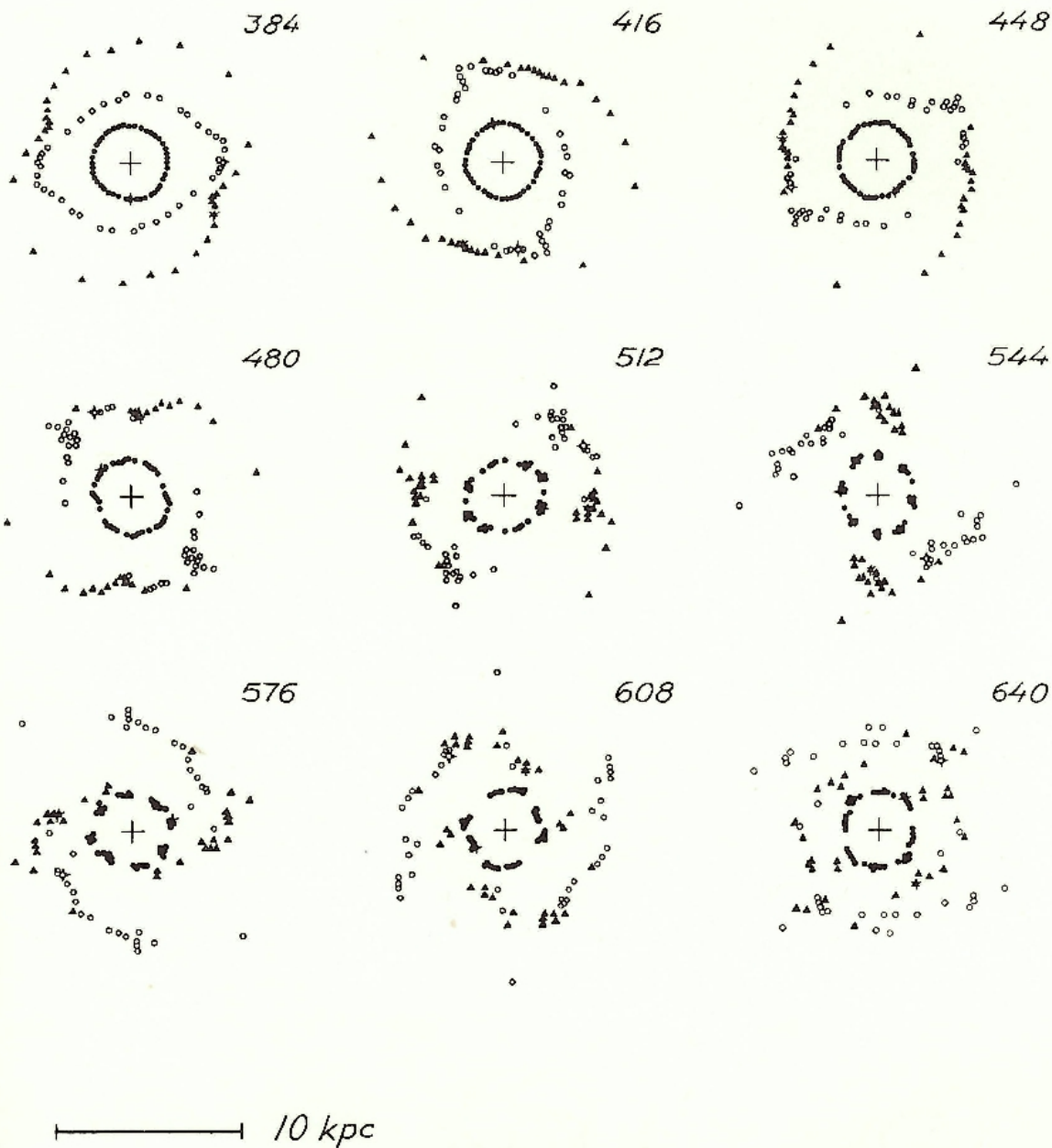
Fig. 30 cont.

force, divided by 2, is subtracted from the tabulated force $F(R)$. Finally the mass-points are given the appropriate circular velocities, and the computations can be started.

In this more continuous model the reaction of the neighbouring rings on the density wave is more rapid. At $T = 176$ million years we see how the ring at 5 kpc from the centre (filled triangles in Fig. 31) has formed two concentrations of density, immediately preceding the major axis of the ring carrying the initial density wave (open circles), and the ring at 3 kpc (filled squares) has formed concentrations immediately following the density maxima of the original wave. The concentrations of matter thus aroused cooperate in their turn to increase furthermore the elongation of the ring of open circles and concentrate its matter to
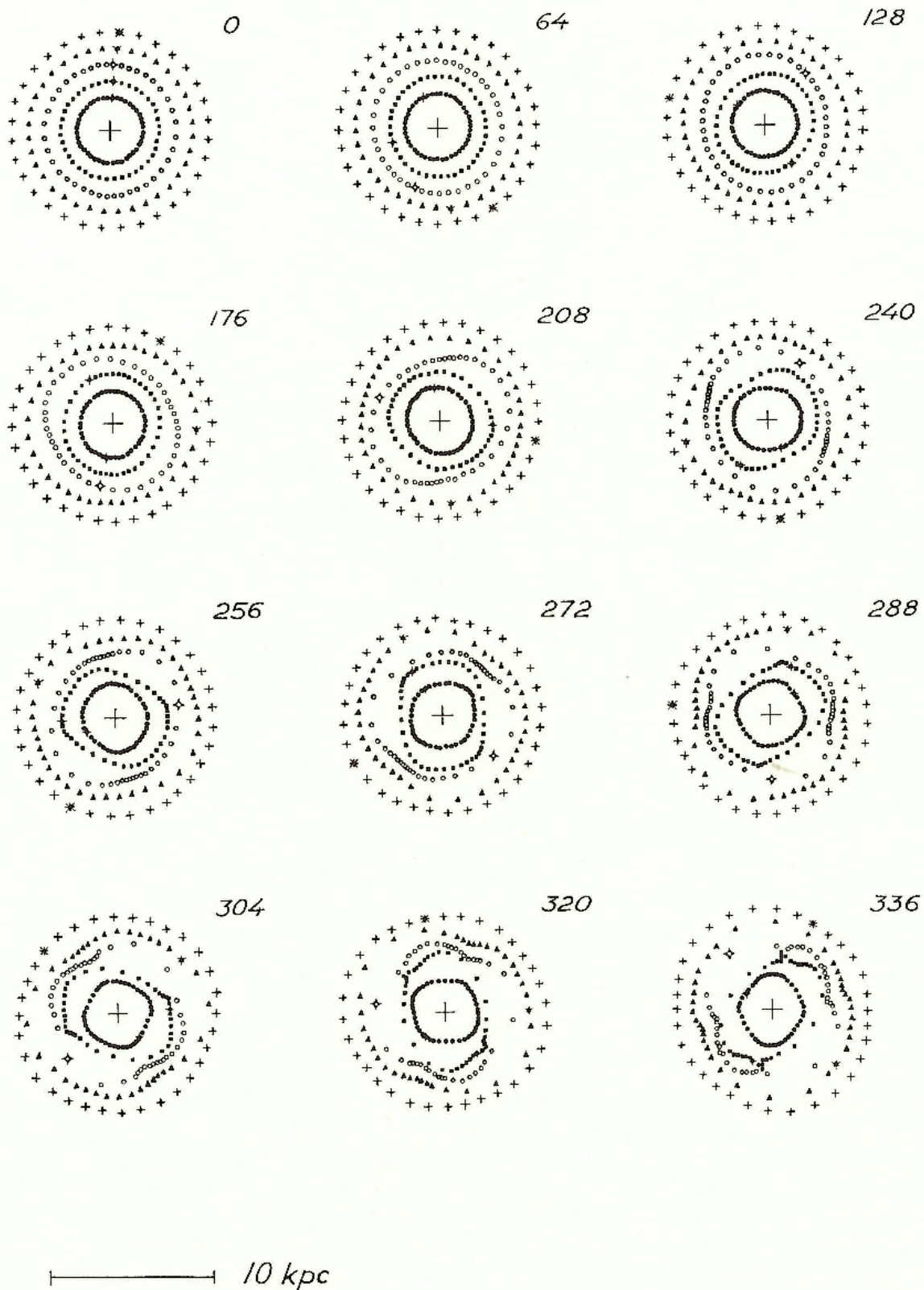
Fig. 31. Massive rings at $R = 2$ ($N = 44$), 3 ($N = 40$), 4 ($N = 40$), 5 ($N = 36$) and 6 kpc ($N = 32$). The ring at 4 kpc (open circles) carries the initial density wave. $m = 2$ units.

352

360

376

392

408

424

440

456

472

⊢——————⊣ 10 kpc
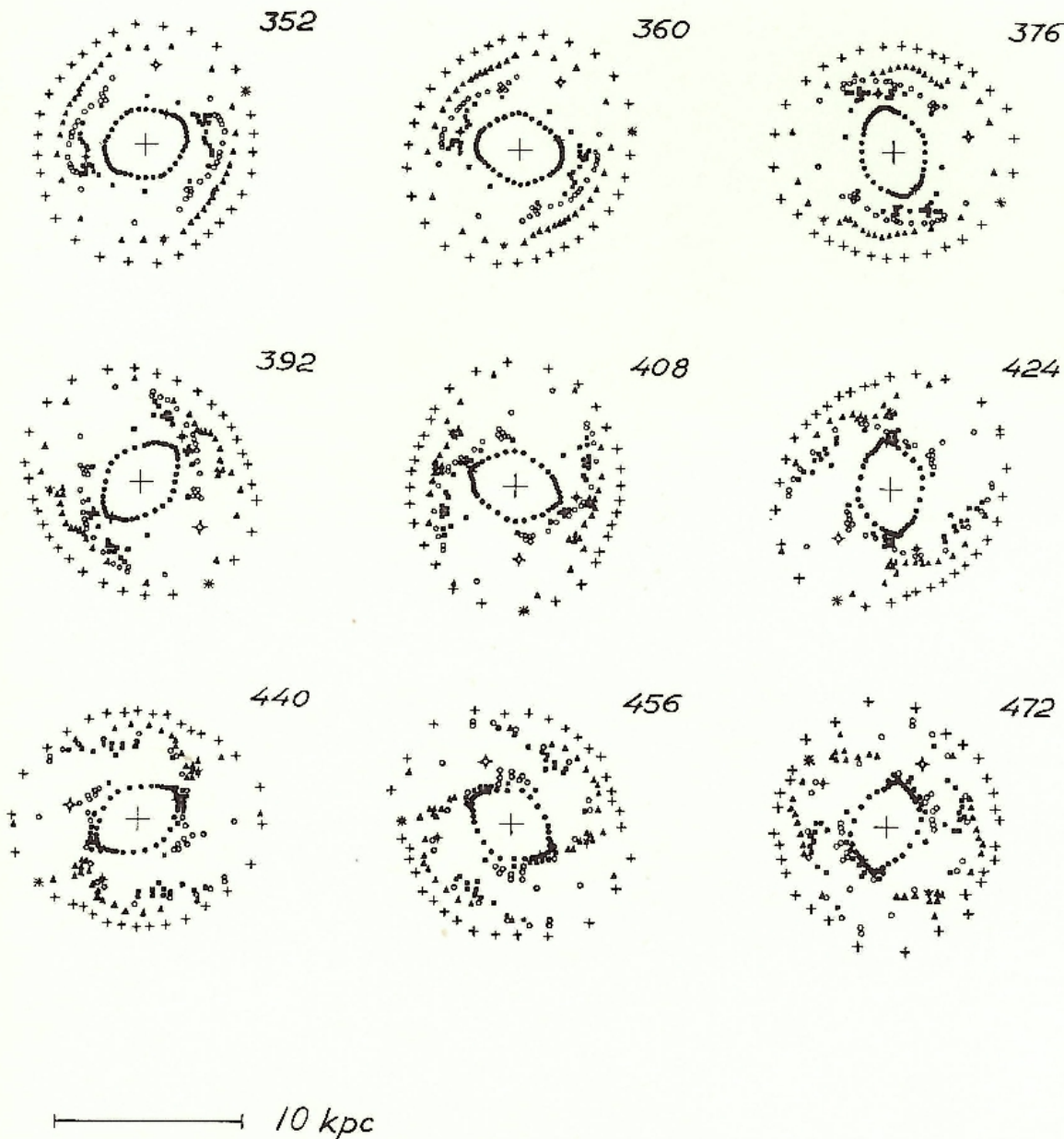
Fig. 31 cont.

the outgoing branches ($T = 176–256$). In this way the instability sets in, the rings more or less break up and form together a pair of leading spiral arms in a system that resembles a barred spiral ($T = 272–360$). The bar increases in strength as the density wave grows inwards. This growth of the bar is made much easier in the present model than in the previous one. At $T = 352$ the innermost ring has developed two very marked condensations along the bar that remain throughout the computations. The matter in the leading arms, as in the earlier model, slides back into the bar, and after a transition stage ($T = 376–392$) the system develops a pair of trailing arms ($T = 408–456$). The arms are drawn out as the spiral winds itself up. In the end the velocity dispersion has grown large, and the true structure is difficult
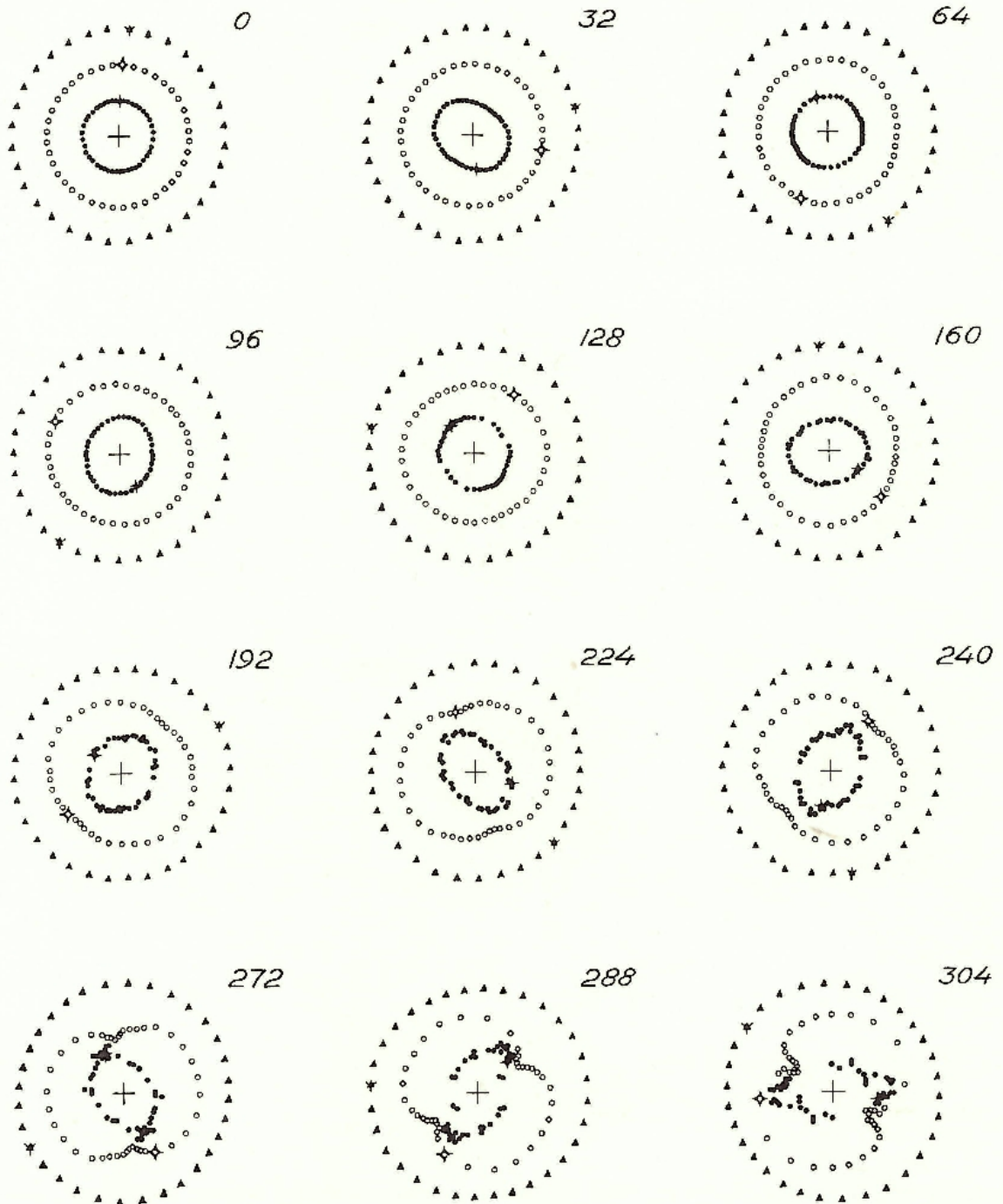
Fig. 32. Rings at $R = 2$ ($N = 44$), 4 ($N = 40$) and 6 kpc ($N = 32$). The initial bar-type density wave is now in the ring at $R = 2$ kpc (filled circles). $m = 4$ units. $\Delta_{min} = 0.7$ kpc.
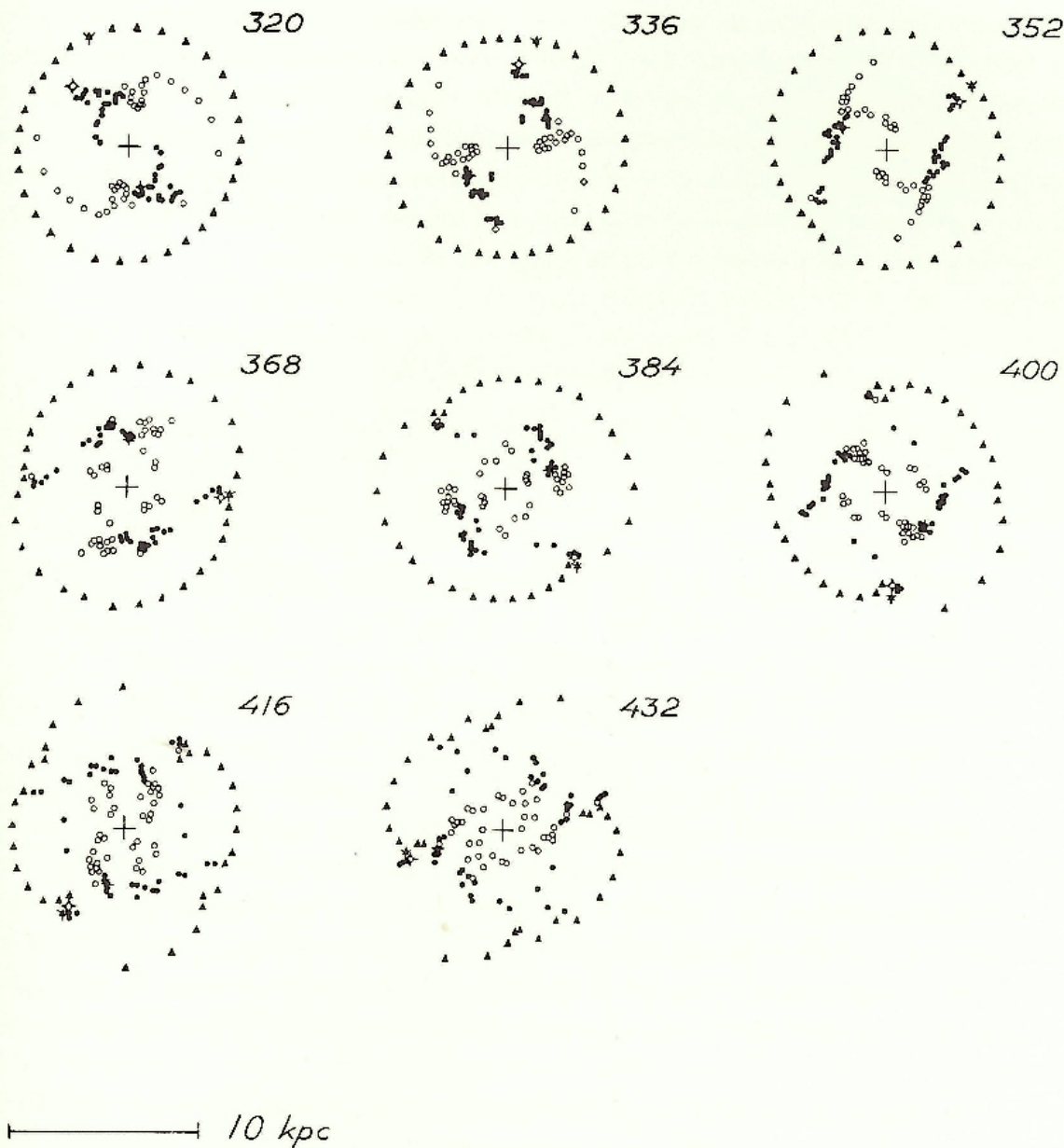
Fig. 32 cont.

to follow. There may be, however, in the stage $T - 472$ a hint that the spiral in the idealized case may change back to leading arms again, and thus the change of the sense of winding in the model be a periodic phenomenon.

A comparison between the stages with leading and trailing arms shows that, in the former case, the bar seems to be fairly long and straight while in the latter case, when the arms are drawn backwards owing to differential rotation, the bar is shorter, and the model resembles more an S-shaped spiral. In the process of shifting from leading to trailing arms the branches from the different rings slide along each other, and the mixing of matter from different rings along the arms is much more complete than in the preceding less continuous model

with fewer rings. It is possible that this shifting process would be still somewhat modified in a model with free matter still closer to the centre. Considering that the main difference between the models of Figs. 31 and 28 is that the mass-points are twice as massive in the latter, and the main difference between the models of Figs. 31 and 30 is the difference in the homogeneity of the distribution of matter in radial direction in the galactic plane, one may get an idea of the importance of total mass and density distribution in the central layer for the time-scale and character of the development of the system.

Density wave at $R = 2$ kpc

3-ring model.—As it appears from the preceding computations that the bar forms inwards from the region of the initial density wave, it may be of interest to make some complementary computations with the initial density wave in the innermost ring, which will then represent a fairly short bar.

We choose the same model as in Fig. 30 with the diffence that the original density wave now lies in the ring with $R_0 = 2$ kpc (Fig. 32, $T = 0$). The density variation is of the same kind as before, but the ratio between neighbouring intervals between mass-points is now 0.94. The coordinates of the points in the innermost ring are given in Table 8. The mass-points are given masses of 4 units as in the former model, but Δ_{min} is decreased to 0.7 kpc. As before, the tabulated force function $F(R)$ is modified to compensate for the attraction of the ring, and the mass-points are given the appropriate initial circular velocities. (The force function $F(R)$ has a slightly different shape for $R < 2$ kpc than in the two previous models with a higher maximum than in Fig. 1. This originated in a somewhat different and less satisfactory way of performing the numerical differentiation of SCHMIDT's potential function in this critical region at the time of the present computations that were actually carried out before the ones described in the preceding section.) The computations are illustrated in Fig. 32.

From the beginning, the ring carrying the density wave oscillates between circular and elongated form in a manner similar to the case of Fig. 26. The ring at 4 kpc lies outside the resonance distance where $\sigma = 0$ for the slower wave. From T about 96 million years this ring shows a perceptible elongation, increasing with time, in a position angle in agreement with the theory for σ rather large, with maxima of density close to the minor axis and just preceding the perturbing wave. As the ring at $R = 4$ kpc becomes more and more elongated the innermost ring seems to establish a more steady elongated shape, with the apsidal line rotating with nearly the same angular velocity as the former slower wave, and following closely the density maximum of the ring $R_0 = 4$ kpc. The most regular shape of this inner elongated ring is shown at $T = 224 \cdot 10^6$ years. The density maxima of the small open circles seem at the same time to form an extension of this "bar". This has a very strong perturbative effect on the ring of open circles. The particles preceding the bar are decelerated and drawn in. The dense part becomes more pronounced and contact is established between

the two rings at about $T = 272$. The effects of the bar and its elongation ultimately cause the ring of open circles to break up into two leading arms. These arms are drawn backwards into the bar, the relative motion of matter being inwards along the arms, as is seen in the stages $T = 304-352$. When the matter from the ring meets the bar, the motion is very much slowed down, and the particles are pumped inwards in front of the bar ($T = 352$). The innermost ring breaks too at the same time as the other. Some of its mass-points move out owing to the acceleration by the bar and get left behind as kinds of trailing arms ($T = 336-416$). At this time the outermost ring begins to break up similarly to the ring of open circles and to form kinds of leading arms, and the spiral structure becomes somewhat confused.

It is seen how, at the end of the computations, the filled and open circles have completely changed regions of occupation in the system in a way similar to the case of Fig. 30.

The corresponding computations were repeated for a mass of the points of 2 units. However, with this small mass the perturbing wave of the innermost ring had not sufficient time to cause any effects in the outer rings before the wave died out, and when the computations ended at $T = 784$ million years, all rings showed perfect circular symmetry.

Equally, the computations were repeated after a change of Δ_{min} to 1.133 kpc, and even now the effects were too small for the instability to come about. Thus it seems that the conditions of Fig. 32 are just above the level where the instability sets in.

Conclusions

It has been shown in the last chapter how the central layer of a galaxy with ordered circular motions is gravitationally unstable to a bisymmetrical density wave of a certain minimum amplitude, proceeding with the angular velocity of the circular motion. As the instability sets in, the regular structure of the central layer breaks down under formation of a spiral pattern. The arms of this spiral structure will at first be leading, in agreement with the theoretical discussion by B. LINDBLAD as to the most probable path of evolution of the barred spirals. The original density wave that increases in strength will grow into a bar extending through the centre over a certain region of the system. The character of this bar depends on the original distribution of matter in the plane, as will appear by a comparison between Figs. 30 and 31. The matter in the arms will move towards the bar, and after some time the spiral structure will, as a rule, be changed into one with trailing arms. In connection with this change of direction of winding there is, at least in the less continuous models of few rings, a general exchange of matter between inner and outer regions.

A comparison with photographs of typical barred spirals shows several main features in common with the computed models (Plate III). However, as we do not know anything about the relative motion of matter in the observed systems, it is very difficult to attribute a certain stage of development of the numerical models to a certain observed galaxy. In particular, since two quite different stages of development of the models, one with leading and one with trailing arms, may look very similar, it appears difficult, so far, even to tell with any certainty if the arms should be leading or trailing in the observed system.

We have seen in the first chapters of the present work that in the case of disturbances due to the potential field of a dispersion ring on an outer ring structure, situated close to the resonance distance, we obtain as the first result a spiral structure with tightly wound leading arms. In fact, the principles of the development are similar, as in both cases the potential wave travels with an angular velocity close to the speed of the circular motion in the perturbed region. The main difference is that in the case of the dispersion ring the perturbing wave itself is not subject to a perceptible counter-action from the perturbed mass until possibly at a more advanced stage in the development. If the outer structure is sufficiently massive, the rings perturb each other and may join to form more coherent spiral arms. These arms too show a tendency to change over from leading into trailing ones, but the cause of this change lies in the gravitational action of the mass in the arms themselves and not in the perturbing wave. The importance of this perturbing wave as the cause of the formation of an outer ring in a galaxy has already been discussed in Chapter III, where a comparison has been made between Figs. 18 and 19 and the photographs of M 94 in Plate I and NGC 7217 in Plate II.

Thus the present computations show that gravitational actions are able to reproduce several characteristic features of spiral galaxies. This does not imply that gas-dynamical forces are outruled, as the structure consisting of a number of concentric rings in a very flattened central layer of circular motions which makes the initial configuration in all of our computations, will come into being with the cooperation of gas-dynamical forces. Thus the arms formed will consist, in the first place, of population I. The action of gas-dynamical and magneto-hydrodynamic forces in the course of the development of spiral arms is difficult to predict. However, it is evident from the present computations that gravitation, and gravitational resonance effects in particular, will play a major rôle in delineating the main features of spiral galaxies.

APPENDIX

Description of computing programs

The numerical computations of the present work were carried out by means of a series of machine programs. There are two main programs (E, F) that integrate the equations of motion of the mass-points of the models and a number of auxiliary programs. These either compute a defined portion of the problem and may be included in the other programs (A, B), or their task is to provide the proper initial positions and velocities for programs E and F (C, D, G, H).

Program A

This is an auxiliary program that computes, for given R, the central force $F(R)$ in the galactic plane. This is done by interpolation to the second order with the Newton-Bessel formula in a table that is contained in the program. The table is essentially Table 1 which
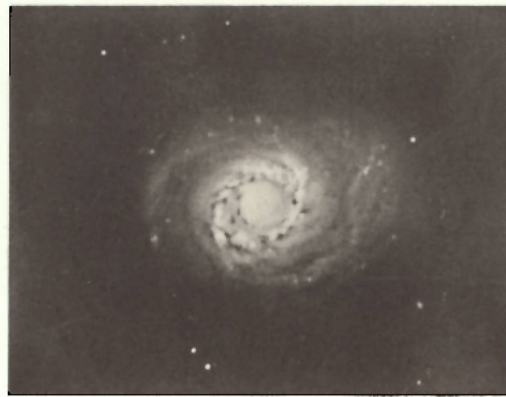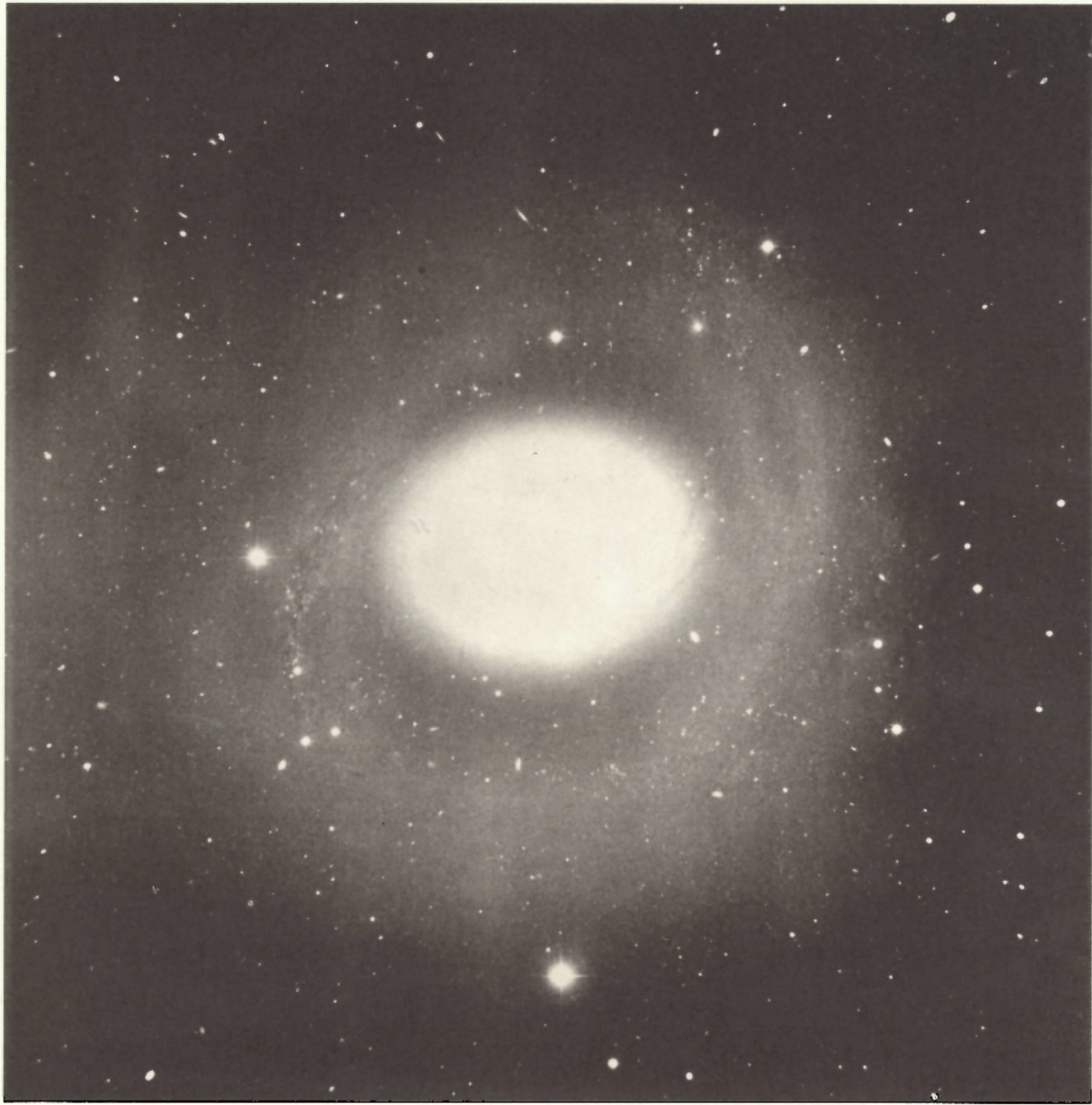
M 94. (NGC 4736). Left: Mount Wilson photograph of the central region. Right: Outer ring structure. Palomar 200-inch photograph.

NGC 7217. Mount Wilson 60-inch photograph.

NGC 1300. Photograph by G. van Biesbroeck with the 82-inch reflector, Mc Donald Observatory.

NGC 1097. Radcliffe 74-inch photograph.   NGC 613. Radcliffe 74-inch photograph.

was derived from the potential in the galactic plane as given by SCHMIDT (1956). For $R \geqslant 40$ kpc the force is computed by

$$F(R) = \frac{3012}{R^2} \qquad (100 \text{ km}^2/\text{sec}^2 \cdot \text{kpc})$$

again in accordance with SCHMIDT.

The time required by the program for computing the force is on the average $78A$ ($A =$ the operation time of one addition) or 3 msec.

Program B

Given a system of N mass-points of equal masses m, symmetrically placed with reference to both coordinate axes (N a multiple of 4), the program computes the gravitational attraction of this system on a particle in an arbitrary position in the plane. If the distance Δ between the particle and one of the mass-points is less than a pre-fixed Δ_{min}, the force of attraction will be made proportional to Δ as is explained in Chapter I.

The computing time is about $100 \, N \cdot A$ or $4 \, N$ msec.

Program C

The program computes the orbit of a particle in the central field $F(R)$. The particle is supposed to start in the apocentre, the apocentric distance and the initial velocity perpendicular to the radius vector being parameters at choice. The program computes successive positions along the orbit by the Runge-Kutta method of integration (see program E) with constant step-size, until the radius vector, which is first decreasing, starts to increase (i.e. $R_{i+1} \geqslant R_i$). Then the step is halved and the direction of integration in time converted, and this is repeated as soon as the radius vector increases again. Thus the particle is brought to oscillate closer and closer to the pericentre. The position of the pericentre and the time spent by the particle in the orbit between the apocentre and the pericentre can be computed in this way with desired accuracy.

The program includes program A for computing $F(R)$.

Program D

Similarly to program C this program too computes the orbit of a particle in the field $F(R)$ starting from the apocentre, but now in a rotating coordinate system. The apocentre is supposed to be situated on the positive y-axis. The aim of the program is to print positions and velocities in the first quadrant of an idealized dispersion ring of N particles with infinitely small masses. Hence the angular velocity of the coordinate system must be chosen in such a way that the orbit will be closed. This angular velocity can be computed from data given by program C.

If T is the time, according to program C, in which the particle moves from the apocentre to the pericentre, positions and velocities are first printed after a time $\frac{1}{2} 4T/N$ and subse-

quently with intervals of $4T/N$, until the y-coordinate becomes negative, and the computing stops. The integration step can be chosen as small as is desirable but must be an integral part of $\frac{1}{2} 4T/N$.

The program includes program A.

Program E

This is the main program of the present work. It computes the motions of N mutually attracting particles of equal mass in the central field of forces $F(R)$. The initial positions and velocities of the N particles are supposed to be symmetrical with regard to the centre so that a particle of position and velocity $(x_i, y_i, \dot{x}_i, \dot{y}_i)$ is always corresponded to by one of $(-x_i, -y_i, -\dot{x}_i, -\dot{y}_i)$.

If m is the mass of a particle and G the constant of gravitation, the equations of motion are

$$\left. \begin{aligned} & \frac{d x_i}{d t} = \dot{x}_i ; \qquad \frac{d y_i}{d t} = \dot{y}_i \\[2mm] & \frac{d \dot{x}_i}{d t} = -F(R_i) \frac{x_i}{R_i} - \sum_{j \neq i} \frac{G m (x_i - x_j)}{[(x_i - x_j)^2 + (y_i - y_j)^2]^{\frac{3}{2}}} \\[2mm] & \frac{d \dot{y}_i}{d t} = -F(R_i) \frac{y_i}{R_i} - \sum_{j \neq i} \frac{G m (y_i - y_j)}{[(x_i - x_j)^2 + (y_i - y_j)^2]^{\frac{3}{2}}} \\[2mm] & R_i^2 = x_i^2 + y_i^2 ; \qquad i, j = 1, 2, 3, \dots, N \end{aligned} \right\} \quad \text{(A:1)}$$

On account of the symmetry we need only calculate motions for one half of the configuration, and the equations of motion may be transformed into

$$\left. \begin{aligned} & \frac{d x_i}{d t} = \dot{x}_i ; \qquad \frac{d y_i}{d t} = \dot{y}_i \\[2mm] & \frac{d \dot{x}_i}{d t} = -F(R_i) \frac{x_i}{R_i} - \frac{G m}{4 R_i^2} \frac{x_i}{R_i} - \sum_{j \neq i} \frac{G m (x_i - x_j)}{[(x_i - x_j)^2 + (y_i - y_j)^2]^{\frac{3}{2}}} - \sum_{j \neq i} \frac{G m (x_i + x_j)}{[(x_i + x_j)^2 + (y_i + y_j)^2]^{\frac{3}{2}}} \\[2mm] & \frac{d \dot{y}_i}{d t} = -F(R_i) \frac{y_i}{R_i} - \frac{G m}{4 R_i^2} \frac{y_i}{R_i} - \sum_{j \neq i} \frac{G m (y_i - y_j)}{[(x_i - x_j)^2 + (y_i - y_j)^2]^{\frac{3}{2}}} - \sum_{j \neq i} \frac{G m (y_i + y_j)}{[(x_i + x_j)^2 + (y_i + y_j)^2]^{\frac{3}{2}}} \\[2mm] & i, j = 1, 2, 3, \dots, \frac{N}{2}. \end{aligned} \right\} \quad \text{(A:2)}$$

Starting from a given set of initial positions and velocities, this system of $2N$ linear differential equations of the first order is numerically integrated by the Runge-Kutta method (see, for instance, L. COLLATZ, 1955). In the course of the Runge-Kutta integration the right-hand members of eqs. (A:2) are computed at four approximated points within the interval of one integration step—one at the beginning, two around the middle and one close to the end of the interval—and certain mean values are taken to give the increase of the dependent variables. $F(R_i)$ is computed by program A which is included in the code. Each term under

the summation symbols reappears, except for the sign, also in the expressions for $d\dot{x}_j/dt$ or $d\dot{y}_j/dt$. The number of such terms to be computed is thus $\frac{1}{2} N(N-2)$. The singularities of the differential equations are avoided by an exchange of the Newtonian force of attraction for another force function at close encounters between particles as is explained in Chapter I. When the mutual distance $\Delta_{i,j} = [(x_i \mp x_j)^2 + (y_i \mp y_j)^2]^{\frac{1}{2}}$ becomes less than a certain $\Delta_{\min}$, the attractive force, which we will call δf, should be proportional to $\Delta_{i,j}$ and the constant of proportionality such that the force is equal to the Newtonian one for $\Delta_{i,j} = \Delta_{\min}$, or

$$\delta f = \frac{G\,m}{\Delta_{\min}{}^2} \cdot \frac{\Delta_{i,j}}{\Delta_{\min}} \qquad \text{for } \Delta_{i,j} < \Delta_{\min}.$$

This is achieved by the program simply by replacing $\Delta_{i,j}$ by $\Delta_{\min}$ for $\Delta_{i,j} < \Delta_{\min}$. No particles ever came so close to the centre during the computations that special treatment had to be given to the second term in the expressions for $d\dot{x}_i/dt$ and $d\dot{y}_i/dt$ that represent the attraction between a particle and its symmetrical counterpart.

The Runge-Kutta method is, in the present case, an integration procedure of the fourth order, i.e. if the increase of a variable is developed as a power series of the step size h, the coefficients are identical with that of the Taylor series up to the term containing h^4. In other words, the truncation error is of the fifth power of h. Now, in order to exercise control over this error, each integration step was immediately re-integrated in two steps of half the size. We call the two values of the variable arrived at in one step and in two steps $q_i^{(1)}$ and $q_i^{(2)}$ respectively. If we assume that, in the latter case, the error after the second step is twice as large as after the first, an assumption that is not proved but that in view of the estimates of the δ_i:s of eq. (A: 3) made in test computations (see below) appears to be approximately right, then the error of the more accurate $q_i^{(2)}$ should be 1/16 of the error of $q_i^{(1)}$.

If

$$\delta_i = q_i^{(2)} - q_i^{(1)} \tag{A:3}$$

the set of values
$$q_i = q_i^{(2)} + \frac{1}{15}\delta_i \tag{A:4}$$

is accepted for the new configuration.

Thus in one full integration step all the right members of (A: 2) are computed 12 times.

One of the advantages of the Runge-Kutta method is that the size of the integration step can easily be changed during the computations. Thus the δ_i:s for *positions* were used for an automatic control of the step size. Two parameters D and d are given to the machine. If any $\delta_i > D$ the step size is divided by two and the step repeated. If all $\delta_i < d$ the size of the next step is doubled. The maximum full step is the machine-unit of time that was $32 \cdot 10^6$ years.

After each step the final coordinates and velocities are punched to 0.1 pc and 0.1 pc/$32 \cdot 10^6$ years respectively. If the computation is interrupted, these values may be read into the machine again as starting values for new computations.
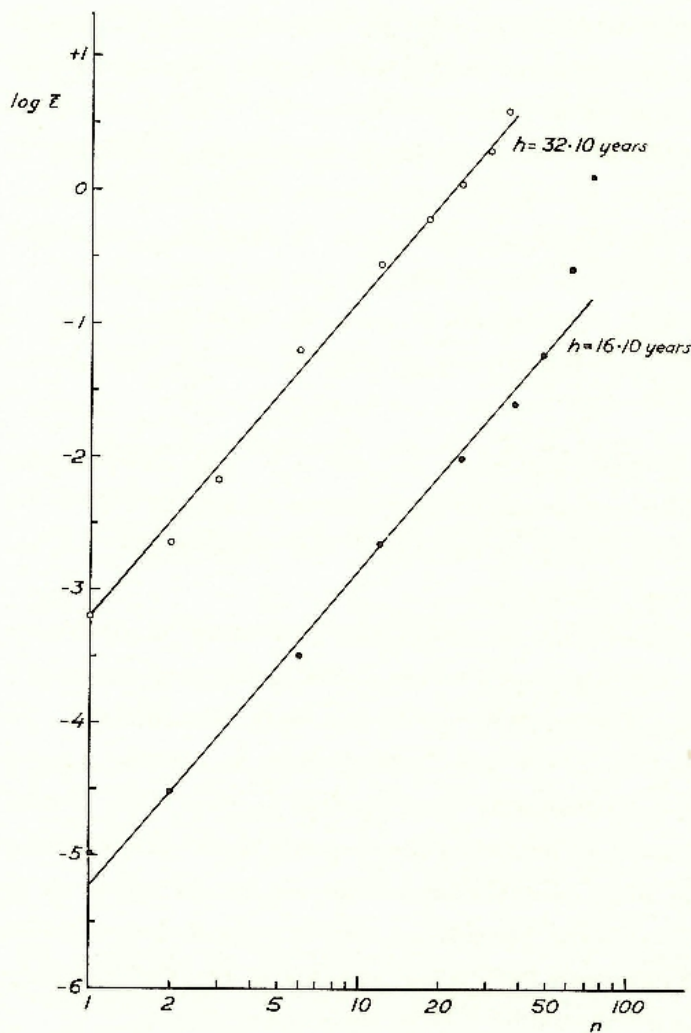
Fig. A: 1. The run of the mean progressive error $\bar{\varepsilon}$ (expressed in kpc) as a function of the number of full integration steps n in integrations of the motion of dispersion ring I with two different step-sizes h.

As an independent check on the accuracy of the computations the sum of the areal velocities

$$c = \sum_i (y_i \dot{x}_i - x_i \dot{y}_i)$$

is printed. It can be shown that, for a central force, this sum must be monotonously increasing, the increase in one integration step, h, being proportional to h^6, and the rate of increase with time thus proportional to h^5.

The maximum number of mass-points handled in the present computations is $N = 192$. The computing time for one step, provided that the step need not be decreased, may be estimated by

$$t = 0.\!^{m}0063 \, N + 0.\!^{m}000508 \, N^2.$$

Thus it is 2.5 min for $N = 64$ and 20 min for $N = 192$. About 10 % of this time is spent in extracting square roots of numbers and about $0.\!^{m}0028 \cdot N$ in printing the results.

The progressive error.—In order to investigate the progressive error three integrations (Nos. 2, 3 and 4) of the dispersion ring I were made with three different step-sizes. Parameters

for the computations are given in Table A: 2, and the results are illustrated in Fig. 7. In the run 4, D was given the value 0.15 kpc, which permitted the integration step h to keep its maximum value of $32 \cdot 10^6$ years. In run 3 the maximum permitted value of h was lowered to $16 \cdot 10^6$ years, and finally in run 2, D was given a very large value and $d = 0$ so that the program kept throughout a given initial $h = 8 \cdot 10^6$ years.

The computations Nos. 3 and 4 were then compared with No. 2 at a number of different epochs, and the mean values $\bar{\varepsilon}$ of the differences in position between corresponding particles were computed. Table A: 1 gives the epoch T, the number of steps n and the mean deviation

TABLE A: 1.

$h = 16 \cdot 10^6$ years			$h = 32 \cdot 10^6$ years		
T 10^6 years	n	$\bar{\varepsilon}$ kpc	T 10^6 years	n	$\bar{\varepsilon}$ kpc
16	1	0.0000104	32	1	0.00064
32	2	0.0000305	64	2	0.0023
96	6	0.00032	96	3	0.0067
192	12	0.0022	192	6	0.062
384	24	0.0098	384	12	0.28
608	38	0.025	576	18	0.60
776	48.5	0.059	768	24	1.11
984	61.5	0.25	976	30.5	1.96
1176	73.5	1.27	1152	36	3.88

$\bar{\varepsilon}$. In Fig. A: 1 log $\bar{\varepsilon}$ is plotted against log n, and it is seen that the points adhere fairly well to straight lines up to $n = 50$. If $\bar{\varepsilon}$ varies with the same power of n in the two cases, the two lines should be parallel. This condition seems to be well fullfilled up to the time when the error is of the same order as the dimensions of the configuration, and the equations of the lines may be approximated by

$$\log \bar{\varepsilon}_{h=32} = 0.81 - 4 + 2.36 \log n \qquad (A: 5)$$

$$\log \bar{\varepsilon}_{h=16} = 0.78 - 6 + 2.36 \log n. \qquad (A: 6)$$

As $n = T/h$, we find that, if the integration step is halved, the progressive error at a certain epoch becomes about 20 times smaller. To allow for the progressive errors of the run with $h = 8 \cdot 10^6$ years, $\bar{\varepsilon}_{h=16}$ should be increased 5 %, i.e. the constant in eq. (A: 6) be $0.80 - 6$

Special test-runs with different D showed that a change from $h = 32 \cdot 10^6$ to $h = 16 \cdot 10^6$ in the first step occurred at a value of D between 0.09 and 0.1 kpc, and from $h = 16 \cdot 10^6$ to $h = 8 \cdot 10^6$ somewhere around $0.0015 < D < 0.0075$ kpc. These facts compared with the maximum values of ε in the first step, which are $1 \cdot 10^{-3}$ for $h = 32 \cdot 10^6$ and $3 \cdot 10^{-5}$ for $h = 16 \cdot 10^6$, suggests that the δ_i of eq. (A: 3) is of the order of 100 ε_i. Thus the minimum value of D to ensure a sufficiently small step-size should be about 200 times the permissible average error ε_1 of the first step, if we assume that $\varepsilon_{1\,max} \approx 2\bar{\varepsilon}_1$. $\bar{\varepsilon}_1$ can be estimated from

TABLE A:2. *Catalogue of computations.*

Col. 1: Consecutive numbers.

2: Number of figure where the computation is illustrated.

3: Machine program.

4: Initial configuration of the mass-points. A Roman number stands for the dispersion ring with the same number. An Arabic number stands for a circular ring with a radius equal to the number with the kpc as unit. The word "bar" preceding such a number within parenthesis means that the circular ring carries a bisymmetrical density variation.

5: The number of free mass-points.

6: The mass m of the massive points.

7: The radius of the "non-Newtonian" zone around each mass-point.

8: The parameter D of the step-size control.

9: The average integration step in the earlier part of the computation.

10: The relative increase of areal velocity during 10^9 years with 10^{-4} as unit.

11: Time interval covered by the computation.

1 No.	2 Fig.	3 Progr.	4 Configuration	5 N	6 m	7 Δ_{min} kpc	8 D kpc	9 h 10^6 years	10 $\Delta c/c$ 10^{-4}	11 T 10^6 years
1	6	E	I	64	1	0.8	.15	32	45	768
2	7	E	I	64	1	1.133	—	8	0.05	1192
3	7	E	I	64	1	1.133	—	16	1.8	1176
4	7	E	I	64	1	1.133	.15	32	54	1264
5	8	E	I	64	1/2	1.133	.15	32	58	864
6	9	E	II	48	1	1.133	.15	16	17	1168
7	—	E	II	48	4	1.9	.15	16	17	352
8	10	E	III	48	4	1.5	.15	16	84	1168
9	(18)	F	Fixed I+10.5³	64	1	1.133		16		960
10	12	F	Fixed I+11.25	64	1	1.133		16		896
11	13	F	Fixed I+12	64	1	1.133		16		896
12	14	F	Fixed I+13	64	1	1.133		16		1152
13	15	F	Fixed I+14	64	1	1.133		16		896
14	16	F	Fixed I+15	64	1	1.133		16		960
15	17	F	Fixed I+16	64	1	1.133		16		1088
16	—	F	Fixed II+8	48	1	1.133		16		1216
17	—	F	Fixed II+12	48	1	1.133		16		960
18	—	F	Fixed III+6	48	4	1.5		16		832
19	—	F	Fixed III+8	48	4	1.5		16		896
20	—	F	Fixed III+8	48	4	1.5		8		1216
21	—	F	Fixed III+10	48	4	1.5		8		576
22	19	E	I+13	128	1	1.133	.15	32	23	1104
23	20	E	I+11.25	128	1	1.133	.15	32	304	680
24	21	F, E	I+11.25¹	128	1	1.133	.15	32	23	1328
25	22	F, E	I+11.25+13¹	192	1	1.133	.15	32	16	1184
26	23	F, E	I+11.25+13²	152	1/2	1.133	.15	32	23	1664
27	24	F, E	I+10+11.25+13²	192	1/2	1.133	.15	32	18	2448
28	25	F	Artific. "bar" (4.31)+4+5	96	1/2	1.133		16		576
29	—	E	"Bar" (4.31)	48	4	1.133	.15	16	78	224
30	26	E	"Bar" (4.31)	48	4	1.133	.01	8	2.8	312
31	—	E	"Bar" (4.31)	48	2	1.133	.01	8	2.3	168
32	27	E	"Bar" (4.31)+3.31	96	4	1.133	.15	16	151	320
33	28	E	"Bar" (4)+2+3+5+6	192	4	0.7	.15	8	94	168
34	30	E	"Bar" (4)+2+6	116	4	1.133	.01	8	14	848
35	31	E	"Bar" (4)+2+3+5+6	192	2	1.133	.03	8	8.9	496
36	32	E	"Bar" (2)+4+6	116	4	0.7	.25	16	36	440
37	—	E	"Bar" (2)+4+6	116	2	0.7	.25	16	256	784
38	—	E	"Bar" (2)+4+6	116	4	1.133	.002	4	≤2	480

[1] The dispersion ring was successively formed out of a circular ring during the first $576 \cdot 10^6$ years.

[2] The dispersion ring was successively formed out of a circular ring during the first $864 \cdot 10^6$ years.

[3] The configuration Fixed I+6 was computed with a slightly different program where the dispersion ring was fully developed from the start.

$$\log \bar{\varepsilon}_1 = \log \bar{\varepsilon}_T - 2.36 \log \frac{T}{h} \qquad\qquad (A:7)$$

where $\bar{\varepsilon}_T$ is the average error to be permitted after the time T and h is the larger of the two most probable step-sizes that, in practice, it is always possible to guess. As the error of one step is divided by a factor of about 100 when the step is halved, d ought to be about $D/100$.

The relative increase $\Delta c/c$ of the sum of the areal velocities during 10^9 years is shown too in Table A: 2. It is seen that this increase varies very closely as h^5 in accordance with the statement on p. 68.

Program F

This program integrates what may be called the restricted version of the preceding problem. It computes the motions of N particles of negligible mass under the influence of a central force $F(R)$ and a fixed configuration of n mass-points in a rotating coordinate system.

$F(R)$ is computed by program A and the force from the fixed configuration by program B, which are included in the code. The positions of the n mass-points thus have to satisfy the same conditions as in program B. The maximum of n is 76. In reality there is no upper limit to the number of free particles N, as they move entirely independently, and the results from several runs may be combined. The integration step is kept constant, and each step computed just once. The computing time t of one step is

$$t = 0\overset{m}{.}00029 \cdot n \cdot N.$$

As this program works much faster than program E, it is especially suited for making surveys of first order effects of perturbations from configurations that have proved to possess a certain degree of stability.

Program G

Given the parameters r, N, n and R the program computes the force of attraction from a circular ring with radius r, consisting of N evenly distributed mass-points of mass m, on a particle at distance R from the centre. This particle is always supposed to be situated on a line that bisects the line joining two neighbouring mass-points in the ring.

The program includes program B.

Program H

The task of this program is to produce balanced initial configurations (positions and velocities) for programs E and F. The configuration may either be a circle, in which case only the radius, the number of points and the angular velocity have to be read into the machine, or a dispersion ring, in which case the results from program D are read in, or any other configuration read into the computer.

In order to balance the configuration as far as possible for its own gravitation and for the attraction of other rings, the program can add to the velocities an additional angular velocity. This angular velocity can be derived from data delivered by program G. A special possibility to compensate for the self-gravitation of a configuration is available and has been used generally for dispersion rings. In this case the velocity v for each particle is increased by the amount $dv - (\bar{\varrho} \cdot f_n)/2v$ where f_n is the component at right angles to v of the combined attraction from all other points of the ring, and $\bar{\varrho}$ is the mean radius of curvature of the true orbit. This procedure we will call "individual balancing".

Any combination of such configurations, balanced in different ways, into a larger model may be made.

Acknowledgements

References

Collatz, L., 1955, *Numerische Behandlung von Differentialgleichungen*, 2. Ed., Springer-Verlag, Berlin–Göttingen–Heidelberg.

Elvius, Aina and P. O. Lindblad, 1959, Numerical computations on the ejection of stars into spiral arms from gas rings containing magnetic fields, *Arkiv f. astronomi* 2, No. 36 = *Uppsala Medd.* No. 126.

Hubble, E., 1940, Problems of nebular research, *Sci. Monthly* Nov. 1940, 391.

van de Hulst, H. C., E. Raimond and H. van Woerden, 1957, Rotation and density distribution of the Andromeda Nebula derived from observations of the 21-cm line, *B.A.N.* 14, 1; No. 480.

Kwee, K. K., C. A. Muller and G. Westerhout, 1954, The rotation of the inner parts of the Galactic System, *B.A.N.* 12, 211; No. 458.

Langebartel, R. G., 1951, On the motion in barred spirals, *Stockholm Ann.* 17, No. 3.

Lindblad, B. and R. G. Langebartel, 1953, On the dynamics of stellar systems, *Stockholm Ann.* 17, No. 6.

Lindblad, B. and F. Nahon, 1954, On the theory of star-streaming, *Stockholm Ann.* 18, No. 2.

Lindblad, B., 1955, Star-streaming and spiral structure, *Stockholm Ann.* 18, No. 6.

—— 1956, Contributions to the theory of spiral structure, *Stockholm Ann.* 19, No. 7.

—— 1957, Differential motions in dispersion orbits in the Galaxy, *Stockholm Ann.* 19, No. 9.

—— 1958a, Dispersion orbits and spiral structure in the Galaxy, *Stockholm Ann.* 20, No. 4.

—— 1958b, On the dynamics of the central layer in the Galaxy, *Stockholm Ann.* 20, No. 6.

—— 1959, Galactic dynamics, *Handb. d. Physik* 53, 21, Springer-Verlag, Berlin–Göttingen–Heidelberg.

Münch, G., 1959, The mass-luminosity ratio in stellar systems, *Publ. A.S.P.* 71, 101.

Oort, J. H., 1958, Dynamics and evolution of the Galaxy, in so far as relevant to the problem of the populations, *Stellar populations* (ed. O'Connell), *Ric. Astron.* 5, 415, Specola Vaticana.

—— 1960, Note on the determination of K_z and on the mass density near the sun, *B.A.N.* 15, 45; No. 494.

Randers, G., 1940, A note on the evolution of extragalactic nebulae, *Ap.J.* 92, 235.

Schmidt, M., 1956, A model of the distribution of mass in the Galactic System, *B.A.N.* 13, 15; No. 468.

—— 1958, *I.A.U. Draft reports*, Commission 33, p. 310.

Spitzer, L. Jr. and M. Schwarzschild, 1953, The possible influence of interstellar clouds on stellar velocities. II, *Ap.J.* 118, 106.

de Vaucouleurs, G., 1959, Classification and morphology of external galaxies, *Handb. d. Physik* 53, 275, Springer-Verlag, Berlin–Göttingen–Heidelberg.